Colloidal Suspensions in Temperature Gradients with Mesoscopic Simulations

I n a u g u r a l - D i s s e r t a t i o n

zur

Erlangung des Doktorgrades

der Mathematisch-Naturwissenschaftlichen Fakultät

der Universität zu Köln

vorgelegt von

Daniel Lüsebrink

aus Köln

Köln

2011

Berichterstatter:	Prof. Dr. Gerhard Gompper
(Gutachter)	Prof. Dr. Joachim Krug

Tag der mündlichen Prüfung: 26.05.2011

Contents

Abstract

A temperature gradient applied to a fluid system produces not only a transport of energy but also a transport of mass. This mass transport is known as thermodiffusion or Soret effect. This effect was first found more than 150 years ago in salt water solutions, where it was observed that the salt concentration was higher towards the cold side of the system, which was realized as a diffusive effect. This non-equilibrium effect is commonly described by the Soret coefficient, which is phenomenologically defined as the ratio of the mass transport due to the temperature and to the concentration gradients. Different substances may drift to the cold or to the warm areas, and mixtures may display a relative accumulation in any of the two areas. These reverse behaviors translate into positive or negative signs of the Soret coefficient.

Nowadays this effect is being studied actively in a wide range of systems, including binary liquids, colloidal and polymer solutions, and emulsions with droplet formation. Nonetheless, a general theoretical explanation of the quantitative values of the Soret coefficient does not yet exist for liquid systems, nor for complex fluids, and it is a matter of strong debate. Industrial applications of thermodiffusion range from crude oil refinement to microfluidic devices for DNA sequencing.

In this work, we investigate the thermodiffusion of colloidal suspensions. The term 'colloid' embraces a large class of systems in which the constituent elements are small enough to diffuse in the solvent, but still large enough to experience the fluid as a continuous medium. Examples of colloidal particles are spherical particles, polymers, proteins, or vesicles. The behavior of colloidal suspensions in temperature gradients is especially challenging due to the large number of biological and technological applications, and also due to a very rich spectrum of interactions with other colloids or with the solvent, that dramatically change the thermophoretic properties of the suspensions.

Our investigations are based on a state-of-the-art mesoscopic simulation technique known as multi-particle collision dynamics (MPC). This method gives a

description of the solvent in which by construction mass, momentum, and energy are conserved quantities, including as well the effect of thermal fluctuations. Hydrodynamic interactions, diffusive behavior, and temperature inhomogeneities can therefore be properly taken into account in a straightforward manner.

The properties of the MPC solvent in the presence of a temperature gradient are first analyzed in detail. We study different implementations regarding mainly bulk suspensions and systems in confinement. The MPC solvent adapts linearly to the temperatures imposed at the boundaries, in case the employed parameters belong to the liquid-like regime of MPC solvent. The transport of energy can also be properly quantified and compared with existing analytical predictions.

The thermophoretic behavior of colloidal suspensions has been explained as the sum of two main contributions. These are given by collective and single particle effects. First, collective effects are investigated in concentrated solutions, where the influence of different inter-colloidal interactions is analyzed. The concentration dependence found in our simulations agrees qualitatively with experimental results. With increasing concentration, colloids are found to accumulate more effectively than the solvent in the warm areas. Moreover, the accumulation of colloids in the cold areas is more effective the more attractive the interactions are. This is for stronger or longer ranged attractions.

Single particle effects to the thermodiffusion of colloidal particles are studied for dilute colloidal suspensions, varying the interactions between the colloid and the surrounding solvent. Simulation results for repulsive interactions show that the colloids diffuse to the warm area, and that this tendency is weakened with increasing temperature. Conversely, colloids with attractive interactions diffuse to the cold areas. Increasing temperatures also weaken the trend and, in this case, they can revert the trend. We present a thermodynamic argument that is able to qualitatively explain these results. Some of the trends observed in our results are in agreement with experimental findings, although we also observe some other trends that are different or even opposite. The origin of these deviations still needs to be elucidated.

1 Introduction

Thermodiffusion is a phenomenon which is found in multi-component systems with inhomogeneous temperature. It is a non equilibrium phenomenon, in which a temperature gradient induces a mass flux. This temperature gradient is externally imposed to the system and drives the components in the system appart. The resulting concentration gradients again produce a mass flux leading to a final stationary state. This demixing of the components is a cross effect of a mass flux which is induced by the heat flux driven by the temperature gradient and is an interference of two irreversible transport processes. The nonequilibrium phenomenon of thermally inhomogeneous diffusion is described in the framework of irreversible thermodynamics. However, the transport coefficients describing the mass fluxes are, up to now, not generally understood and difficult to determine. They are determined by all microscopic mutual interactions of the components.

In systems of macromolecular particles suspended in a fluid, the diffusion under influence of an inhomogeneous temperature is referred to as thermophoresis. In this case it is phenomenologically similar to sedimentation of particles in a suspension which are small enough to be subjected to Brownian motion. The gravitational field acts as an external field and drives the particles to the lower region of the system. This leads to an inhomogeneous distribution of the particles and builds up a concentration gradient. The concentration gradient internally induces a diffusion flux which counteracts the flux of particles due to the external force. In the case of thermophoresis the temperature gradient has the same effect as an external force, driving the particles to one region of the system. The difference to sedimention is that the driving force due to the temperature gradient is internally induced by particle interactions. The interactions among the suspended particles and between the fluid and the dissolved particles are decisive for the response of the particles to the temperature gradient. Very different responses are observed which are dependent on a variety of parameters and it can be found that the particles build up a concentration gradient up- or downhill the temperature gradient. It is therefore very interesting to study such

systems and it is still not clear how in general the microscopic properties of the suspension influence its response to a temperature gradient.

1.1 Historical background

The effect of thermodiffusion has been found by the physiologist Ludwig [65] in 1856. Ludwig observed the effect of diffusion under influence of a temperature gradient with a solution of sodium-sulfate (also known as Glauber salt) and water. He found that after several days of heating the system from one side and cooling it on the other side, that there was a higher salt concentration on the cold side, than on the warm side. He also realized that this phenomenon is related to diffusion. The first systematic study of this effect was done by physicist and chemist Soret in 1879 and the following years [108, 109, 110]. He performed experiments with electrolyte solutions in which he found that the salt ions are found with higher concentrations on the cold side. Nowadays the measure to quantify the separation of different components in solutions under influence of temperature gradients is generally called Soret coefficient. A large Soret coefficient indicates a strong separation of the components. The sign of the Soret coefficient for one of the components denotes if its mass fraction increases towards the cold (thermophobic) or warm region of the system (thermophilic).

A first theoretical understanding of thermodiffusion arose from the work of Enskog [28] and Chapman [13] in the 1910s, which was developed for mixtures of gases. It was found that the Soret coefficient depends on the mass and size of the respective species and the composition of the mixture. Their results could be confirmed experimentally by Chapman and Dootson [15].

Later Enskog extended this kinetic theory to describe dense hard sphere liquid mixtures [14]. The theory is able to describe some general trends. A general trend is that for example in binary mixtures the species with heavier mass and larger size moves towards the cold. This theory however, is no longer valid if soft interactions are present [129]. In the 1930's Onsager proposed his famous phenomenological linear equations in the framework of irreversible thermodynamics that relate the generalized thermodynamic forces with their conjugated fluxes. In the case of inhomogeneous systems the forces are the gradients in temperature and density or concentration. The equations contain the complementary cross relations of mass muss flux induced by a temperature gradient (Soret effect) and of heat flux induced by a concentration gradient (Dufour effect), which can be

described by the same transport coefficient.

First experimental studies of liquid mixtures (cyclohexanol-cyclohexane) have been carried out by Prigogine *et al.* in 1950 [90]. They explained their results with a free energy/entropy concept that accounts for orientational arrangements of the molecules within the fluid (formation of complexes with the loss of free energy upon disruption).

One important experimental improvement has been the use of thermogravitational columns introduced by Clusius and Dickel [16], which enhances the thermodiffusive effect due to gravitationally induced convection. Due to the improvements in experimental techniques and especially the use of optical methods, a large variety of systems has been investigated experimentally and various effects have been studied up to now. Studies range from isotope separation, liquid and gaseous mixtures to complex fluids, such as colloidal or polymeric mixtures. Despite the wide range of interesting observations, it was until recently that mutually consistent results for applying different measurement techniques for the same substance were achieved (benchmark test on organic binary mixtures dodecane, isobutyl benzene and tetralin [123]).

1.1.1 Simulation studies

The first simulation of dense Lennard-Jones mixture in a liquid state was performed in 1986 by MacGowan and Evans [67, 32]. Simulations have been mainly focused on the study of binary fluid mixtures by means of Molecular Dynamics [38, 55, 40, 96], where they are applied to Lennard-Jones mixtures or to molecules with a more precise microscopic structure modelled with the help of force field simulations [75, 76, 130, 88, 87]. Simulations of binary Lennard-Jones fluids [96, 6, 35, 3, 62] have found that, as in the case of hard spheres, the heavier species prefers the cold side of the system. Upon changing the interaction strength, they observed that the species with stronger attractions prefers the cold side. Regarding the size ratio, the larger component tends to accumulate in the hot region.

Recently Galliero and Volz [34] have applied MD to a system with nanoparticles. This simulation study has been performed with LJ fluids and macroscopic particles composed of atoms with the same molecular parameters as the solvent, which are arranged in a fcc crystal and are connected through a finite extensible nonlinear elastic (FENE) bonding potential. Similar model was em-

ployed by Vladkov and Barrat [114] to study thermal conduction. Colloidal systems however, have not been studied in simulations, apart from the mentioned works. MD simulations of colloidal systems with explicit solvent are very demanding due to the larger separation of length and time scales and so far no mesoscopic hydrodynamic simulations have been performed. Simulations on polymers have been performed by Luettmer-Strathmann [66] with a coarse grained two chamber model, and with MD simulations by Zhang and Müller-Plathe [131].

1.1.2 Thermodiffusion in colloidal systems

One aspect of studying dilute colloidal suspension is the dependence of the Soret effect on the size of the colloidal particles, which was studied by Braibanti *et al.* [7] and by Duhr and Braun [22]. It was found that there is a characteristic dependence on the temperature in the case of dilute dispersions which was also found for micellar solutions by Piazza and Guarino [86]. There the surfactant concentration, which forms the interface between the micelles and solvent, also plays an important role. Würger studies theoretically the size dependence and the effects of the boundary conditions on the colloid surface [71]. In general, it is observed that the interactions of colloids and solvent molecules are decisive for the thermodiffusive behavior of macromolecular suspensions. A comprehensive overview of thermodiffusion in colloidal systems is given Ref. [125]. Theoretical and experimental aspects of colloidal suspensions are discussed by Piazza and Parola [84].

The effect of intercolloid interactions is studied by Ning *et al.* [77] in experiments with concentrated colloidal solutions. A theoretical description of concentration effects is given by Dhont in Refs. [19, 20].

1.1.3 Main influences on the Soret coefficient

A summary of the influences that affect the thermodiffusive behavior of liquids is shown in Fig. 1.1. The first three contributions regard "mechanic" properties of the particles or molecules. One influence on the Soret coefficient arises from different masses of the components. In gases this can be understood from an entropic argument. Since the heat conductivity is more effective for substances with a lower mass, the lighter component will tend to have a larger concentration on the warm side. In this way the flux of heat is minimized, which also

lowers the entropy production rate which is proportional to the flux of heat and the temperature difference. The particle size has the influence that in binary mixtures, the larger particles will be found with a higher concentration on the cold side. The moment of inertia is studied with mixtures in which the shape of the suspended molecules can not be regarded as spherical, which is the case in many organic mixtures, for example benzene rings.

The other three contributions regard chemical effects. An important influence in macromolecular suspensions is the chemical interaction between the surface of the suspended particles and solvent. Similar to this are contributions due to charges on the surface of the macromolecules and the ions in the solvent. A further contribution comes from the mutual interactions between the macromolecular particles and collective contributions.

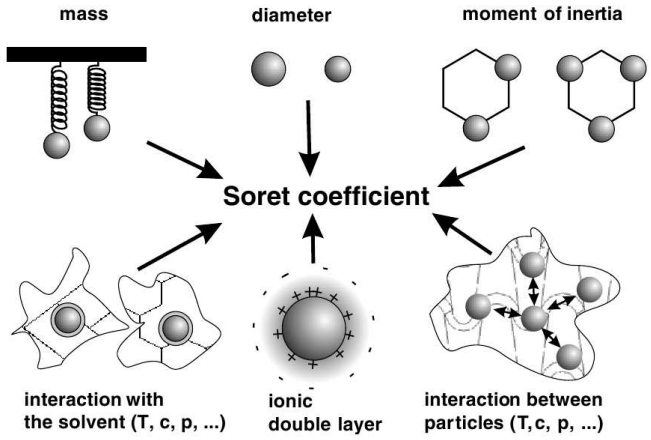

Figure 1.1: Different properties that influence thermodiffusion. Fig. from the topical review of Ref. [118].

1.1.4 Thermodiffusion applications

Thermodiffusion plays a role or is used in the following context: crude oil refinement, isotope separation [51] , technical instruments like thermal flow field characterization of colloids [106, 107] and for polymers [104, 92, 17], origin of life [22], magic dust (dirty walls close to heater), salt concentration in different layers of oceans and in convective processes in the earth mantle [10].

Other interesting systems are solutions of biological macromolecules which have been studied by Duhr and Braun where they constructed a trap for DNA

in a microchannel with ambient flow [21]. This device can be used to obtain highly concentrated spots of biological molecules and it is speculated that this could be responsible for the origin of life enabled in mineral pores close to oceanic heat sources. In their experiments they could also use thermodiffusive effects to modify DNA solutions with a laser and write the letters DNA in a bio-organic solution [23].

1.2 Irreversible thermodynamics

Phenomenologically thermodiffusion of a multi-component mixture is described by two opposing mass fluxes that cancel each other in a stationary state. One flux stems from the temperature gradient and the other flux from the resulting concentration gradient. The coefficients that relate the fluxes to their driving forces are the thermal diffusion coefficient and the mass diffusion coefficient. The ratio between them is called Soret coefficient and characterizes the demixing response of the system to the temperature gradient. How the coefficients are derived will be explained in the following derivation of a phenomenological expression for the Soret coefficient. The derivation follows and summarizes the route of the book by de Groot and Mazur [18]. A similar summary can also be found in [67, 129].

Thermodiffusion is a non equilibrium phenomenon and is described in the framework of irreversible thermodynamics. Systems out of equilibrium are characterized by their entropy production rate. The local formulation of the second law of thermodynamics has the form of a balance equation for the entropy

$$\rho_m \frac{ds}{dt} = \nabla j_s + \sigma_s, \tag{1.1}$$

where

$$\sigma_s \geq 0. \tag{1.2}$$

Here ρ_m is the mass density, s is the entropy per mass unit in a small volume element and $\frac{ds}{dt}$ the change of entropy with time. j_s is the entropy flux through the volume element and corresponds to the external entropy exchange of the volume element. σ_s is the internally rate of entropy production within the volume element. In mechanical equilibrium and for vanishing total net flux the Gibbs fundamental relation for the entropy is $Tds = du + pd\mathrm{v} - \sum_k \mu_k dw_k$, where p the pressure, $\mathrm{v} \equiv \rho^{-1}$ is the specific volume, T is the local temperature and u

is the specific internal energy. μ_k the chemical potential of component k and $w_k = \rho_{m,k}/\rho_m$ the mass fraction of component k; with the mass density $\rho_{m,k}$ of component k. Under the assumption of local equilibrium the time-dependent form for a small volume element is

$$T\frac{ds}{dt} = \frac{du}{dt} + p\frac{d\mathrm{v}}{dt} - \sum_k \mu_k \frac{dw_k}{dt}. \tag{1.3}$$

If one regards isotropic liquids and neglects viscous effects, the rate of change of the specific internal energy can be expressed as

$$\frac{du}{dt} = \frac{dq}{dt} - p\frac{d\mathrm{v}}{dt}, \tag{1.4}$$

where q is the specific heat which changes according to

$$\rho_m \frac{dq}{dt} = -div\boldsymbol{j}_q. \tag{1.5}$$

The change of mass fraction of component k with time is

$$\rho_m \frac{dw_k}{dt} = -div\boldsymbol{j}_k. \tag{1.6}$$

With Eq. (1.1) one obtains for the rate of entropy production

$$\sigma_s = -\frac{1}{T^2}\boldsymbol{j}_q \nabla T - \sum_{k=1}^{n} \boldsymbol{j}_k \nabla\left(\frac{\mu_k}{T}\right), \tag{1.7}$$

where n is the number of components in the system. With the heat flux $\boldsymbol{j}_q = \boldsymbol{j}_s + \sum_{k=1}^{n} \mu_k \boldsymbol{j}_k$ and $\boldsymbol{j}'_q = \boldsymbol{j}_q - \sum_{k=1}^{n} h_k \boldsymbol{j}_k$, where h_k is the specific enthalpy of component k, and by use of the thermodynamic relation $T\, d\left(\frac{\mu_k}{T}\right) = (d\mu_k)_T - \frac{h_k}{T} dT$ this can be reformulated (for details see [18], chapter 3) in

$$\sigma_s = -\frac{1}{T^2}\boldsymbol{j}'_q \nabla T - \frac{1}{T}\sum_{k=1}^{n-1} \boldsymbol{j}_k \nabla\left(\mu_k - \mu_n\right)_{T,p}, \tag{1.8}$$

where the index T, p denotes that the gradient of the chemical potential has to be taken at constant temperature and pressure. This equation is the basis for the phenomenological equations that describe thermodiffusion. From the equation for the entropy production one can obtain the generalized thermodynamic forces and their conjugated fluxes. Between the fluxes and their respective forces exist linear relations in the form of $\boldsymbol{j}_i = \sum_i L_{ik}\boldsymbol{X}_k$, where $\boldsymbol{X}_k$ are the generalized forces and L_{ik} the related coefficients. The fluxes and forces appear in

the entropy production as $\sigma_s = \sum_i \boldsymbol{j}_i \boldsymbol{X}_i = \sum_{ik} L_{ik} \boldsymbol{X}_i \boldsymbol{X}_k$. It was shown by Onsager [80] that there exist reciprocal relations between the coefficients L_{ik}, which follows from time reversal invariance , see e.g. [105]. The reciprocal relations describe cross effects of coupled irreversible processes, such as appear in thermodiffusion, where diffusive mass flux is coupled to heat flux and vice versa. Furthermore, by Onsager's variational principle [80, 81] it follows that the rate of entropy is minimal if the fluxes are stationary.

In the case of thermodiffusion the linear Onsager relations for a two component system are

$$\begin{aligned} \boldsymbol{j}_1 &= L_{11} \boldsymbol{X}_1 + L_{1q} \boldsymbol{X}_q \\ \boldsymbol{j}_q &= L_{q1} \boldsymbol{X}_1 + L_{qq} \boldsymbol{X}_q, \end{aligned} \tag{1.9}$$

where as consequence of the reciprocal relations $L_{1q} = L_{q1}$, describing the physically complementary cross effect of heat and diffusive mass flux. In the case of a temperature gradient L_{1q} describes the Soret effect, which is that a temperature gradient induces mass transport; and L_{q1} the Dufour effect, which is that a concentration gradient induces a heat transport.

From Eq. (1.8) follow the generalized thermodynamic forces for a two component system

$$X_q = -\frac{1}{T^2} \nabla T \tag{1.10}$$

$$X_1 = -\frac{1}{T} \nabla (\mu_1 - \mu_2). \tag{1.11}$$

By use of the Gibbs-Duhem relation with the mass fraction w_i

$$\sum_i w_i \mu_i = 0 \quad (p \quad \text{and} \quad T \quad \text{constant}), \tag{1.12}$$

it follows that,

$$\nabla (\mu_1 - \mu_2) = \frac{1}{1 - w_1} \frac{\partial \mu_1}{\partial w_1} \nabla w_1 \tag{1.13}$$

Then the fluxes in Eq. (1.9) are

$$\begin{aligned} \boldsymbol{j}_1 &= -\frac{L_{11}}{T} \frac{1}{1 - w_1} \frac{\partial \mu_1}{\partial w_1} \nabla w_1 \quad - \quad L_{1q} \frac{1}{T^2} \nabla T \\ \boldsymbol{j}_q &= \qquad -L_{q1} \frac{1}{T^2} \nabla T \qquad - \quad \frac{L_{qq}}{T} \frac{1}{1 - w_1} \frac{\partial \mu_1}{\partial w_1} \nabla w_1. \end{aligned} \tag{1.14}$$

With D_m, the mutual diffusion coefficient, which is given by

$$D_m = \frac{1}{\rho_m}\frac{L_{11}}{T}\frac{1}{1-w_1}\frac{\partial \mu_1}{\partial w_1} \tag{1.15}$$

and D_T, the thermal diffusion coefficient or "thermophoretic mobility", defined as

$$D_T = \frac{1}{\rho_m T^2}\frac{1}{w_1(1-w_1)}L_{1q}, \tag{1.16}$$

the mass flux is given in the typical form

$$\boldsymbol{j}_1 = -\rho_m D_m \nabla w_1 - D_T \rho_m w_1(1-w_1)\nabla T. \tag{1.17}$$

Here, ρ_m is the mass density. Eq. (1.17) can be rewritten as

$$\boldsymbol{j}_1 = -\rho_m D_m \left[\nabla w_1 + S_T w_1(1-w_1)\nabla T\right], \tag{1.18}$$

where the definition of the Soret coefficient S_T as

$$S_T = \frac{D_T}{D_m} \tag{1.19}$$

has been employed.

In the stationary state total mass flux vanishes, i. e. $\boldsymbol{j}_1 = \mathbf{0}$. In this case the Soret coefficient (with the temperature gradient along the z-direction) can be expressed with the gradients of the mass fraction and the temperature as

$$S_T = -\frac{1}{w_1(1-w_1)}\frac{\nabla_z w_1}{\nabla_z T}. \tag{1.20}$$

Here ∇_z corresponds to $\partial/\partial z$. The Soret coefficient is a quantity that depends on the constance of the transport coefficients in Eq. (1.15) and Eq. (1.16). On the basis of the phenomenological Eq. (1.9) it is therefore defined in a volume in which these quantities have small changes. This implies small temperature and density gradients in the regarded volume. Also the mass fraction w_1 in Eq. (1.20) can be regarded as the constant average mass fraction in the volume.

1.3 Hydrodynamics and diffusion of a colloidal particle

Colloidal particles are macroscopic particles in the range of several nm up to 20 μ m. The lower limit is determined by the fact that colloids can be very small

particles, but are still large compared to the fluid molecules. In this range the fluid can be regarded as a continuous medium so that the flow fields around the colloid can be described by hydrodynamics and the discreteness of the fluid molecules does not play a role. The upper limit is the size at which particles still perform Brownian motion arising from thermal "kicks" of the fluid particles. A spherical particle propagating with a velocity $\boldsymbol{v}$ in a liquid experiences an opposing frictional force, which is given by the Stokes law

$$\boldsymbol{F} = 6\pi\eta R_{coll}\boldsymbol{v}, \tag{1.21}$$

where η is the (dynamic) viscosity and R_{coll} the radius of the particle. The prefactor is altered from 6π to 4π when the surface of the particle obeys slip instead of stick boundary conditions.

The diffusion coefficient is given by the Einstein relation [25]

$$D_s = \frac{k_B T}{\xi_S}, \tag{1.22}$$

where ξ_S is the friction coefficient. For a colloidal particle it can be obtained from the Stokes equation for slip boundary conditions as

$$\xi_S = 4\pi\eta R. \tag{1.23}$$

and for stick boundary conditions as

$$\xi_S = 6\pi\eta R_{coll}. \tag{1.24}$$

Here η is the viscosity of the solvent and R_{coll} the radius of the colloid.

The description of single colloid diffusion in inhomogeneous systems is discussed in section 5.1.2.

2 Simulation method

The main objective of this work is to study the behavior of colloidal suspensions in the presence of a temperature gradient by computer simulations. The simulation model has three main components. These are the method to simulate the colloids and their interactions, the model to simulate the solvent, and the technique to implement the interactions between solvent and colloids. The employed solvent should include hydrodynamic interactions, thermal fluctuations, and be able to sustain temperature gradients. Hydrodynamics have a macroscopic character and determine viscous forces on the colloids as well as transmitting interactions through the flow fields generated by them. Thermal fluctuations become apparent in the diffusive character of the colloid motions, namely the Brownian motion. In order to simulate hydrodynamic interactions, the solvent needs to have local conservation of linear momentum, while the inclusion of temperature inhomogeneities requires local conservation of energy.

2.1 Molecular Dynamics

The simulation of colloids allows the use of standard molecular dynamics models, where interaction between colloids can be modified. Molecular dynamics (MD) considers a set of N particles described by their masses m_i, positions $\boldsymbol{r}_i$, velocities $\boldsymbol{v}_i$, and applied forces $\boldsymbol{F}_i$. The particle dynamics is determined by solving the corresponding Newton's equations of motion

$$m_i \ddot{\boldsymbol{r}}_i = -\frac{\partial U}{\partial \boldsymbol{r}_i} = \boldsymbol{F}_i. \tag{2.1}$$

For solving the discretized equations of motion and updating the positions and velocities we have used the velocity Verlet algorithm

$$\boldsymbol{r}_i(t + \Delta t_{MD}) = \boldsymbol{r}_i(t) + \Delta t_{MD} \boldsymbol{v}_i(t) + \frac{\Delta t_{MD}^2}{2m_i} \boldsymbol{F}_i(\boldsymbol{r}_i(t)), \tag{2.2}$$

$$\boldsymbol{v}_i(t + \Delta t_{MD}) = \boldsymbol{v}_i(t) + \frac{\Delta t_{MD}}{2m_i} \left[\boldsymbol{F}_i(\boldsymbol{r}_i(t)) + F_i(\boldsymbol{r}_i(t + \Delta t_{MD})) \right]. \tag{2.3}$$

An important aspect is the choice of the discrete time step Δt_{MD} which is used for updating positions and velocities. How to evaluate sensible choices for the time step in the case of colloids is described for example in a recent publication of Padding and Louis [82]. The choice of parameter for our simulations is depends on the particular studied aspect and it will discussed in the corresponding chapters.

The system under study is determined by specifying the applied forces. To reproduce the properties of a colloidal system with repulsive and eventually also attractive interactions, pair non-bonded potentials are considered. Colloids with purely repulsive interactions are simulated by considering a shifted Lennard Jones potential [116, 61]

$$U(r_{ij}) = 4\epsilon \left[\left(\frac{\sigma}{r_{ij}} \right)^{2n} - \left(\frac{\sigma}{r_{ij}} \right)^{n} \right] + \epsilon, \quad r_{ij} < r_c, \tag{2.4}$$

where $r_{ij} = |\boldsymbol{r}_i - \boldsymbol{r}_j|$ is the distance between the interacting particles, ϵ the strength of the potential, σ the size of the colloid and n determines the steepness. The potential is cut of at a distance $r_c = 2^{\frac{1}{n}}$ at the minimum of the full potential.

For additional attractive interactions we have used the full Lennard Jones [61] potential

$$U(r_{ij}) = 4\epsilon \left[\left(\frac{\sigma}{r_{ij}} \right)^{2n} - \left(\frac{\sigma}{r_{ij}} \right)^{n} \right], \quad r_{ij} < r_c, \tag{2.5}$$

where the cut off radius for a rLJ 12-6 potential is $r_c = 2.5\sigma$. The cut of radius is chosen at a distance where the interaction strength is very small for numerical reasons to have less interaction partners. Other potentials are cut off at a radius so that

$$U(r_c) = U^{12-6}_{\epsilon=1}(2.5\sigma). \tag{2.6}$$

Then the resulting cut off radius is

$$r_c = 2^{\frac{1}{n}} \left(\frac{1}{1 - \sqrt{1 + \frac{U^{12-6}_{\epsilon=1}}{\epsilon}}} \right)^{\frac{1}{n}} \sigma_{cs}. \tag{2.7}$$

Another option would be to choose a smooth truncation, such as for example in [60].

In the following we use the notation LJ 2n-n for the full potential and rLJ 2n-n for the repulsive one, where n denotes the exponent. Throughout this work we have used Lennard-Jones potentials of type 2n-n.

Since the computational cost for MD of colloidal particles with explicit solvent is large, effective ways for computation of the mutual forces and updates of the particle positions are required. In our case we have calculated the forces using cell lists for the macroscopic particles and Verlet lists for fluid-solute interactions. These procedure are described in detail literature, for example the book of Allen and Tildesley [2].

2.2 Mesoscopic methods

2.2.1 Mesoscopic length and time scales

Colloidal suspensions are subjected to effects that span the large range of length and time scales dictated by their components. The size of a colloidal particle is in the range of ca. 10 nm to 1 μm, whereas a solvent molecule is usually smaller than 1 nm. The size ratio is then of 10^2 to 10^5. In order to estimate the related time scale, we use the Stokes formula given by Eq. (1.24) and the Einstein relation in Eq. (1.22). The characteristic time for a colloid to diffuse a length of its own diameter can be calculated as

$$t = a^2/2D = a^3 3\pi\eta/k_B T \approx 2 \text{ s} ,$$

with $a = 0.1$ μm, $\eta_{H_2O} = 1$ Pas and $T = 20^\circ$ C. The diffusive timescale for a colloidal particle is therefore in the order of seconds. The timescale for the movement of the solvent molecules, without considering internal degrees of freedom, is in the order of 10^{-12} s [128].

Furthermore, the timescale for observing macroscopic phenomena like a particle drift or establishment of a stationary concentration gradient are much larger than the diffusive timescale. Hydrodynamic interactions are of long ranged character since they decay as $1/r$, where r is the distance from the source, and require simulation systems much larger than the regarded particles.

Therefore, a hypothetical full simulation that would intend to cover timescales from atomistic movement to long time behavior of macroscopic objects would be computationally gigantically costly. Moreover, most of the computational effort would be devoted to the simulation of the solvent, which detailed motion is the less interesting part of the system dynamics.

In a different approach, a continuum description of the hydrodynamic flow fields can be achieved by solving the Navier Stokes equations. However, this

has proven to be at least equally demanding due to the complex nature of the boundary conditions at the liquid-solid interfaces in the system given by the moving colloids.

Mesoscopic methods arise then as a necessary tool for the simulation of complex systems like colloidal suspensions. Most of these methods start conceptually from a microscopic description of the solvent in which the molecules degrees of freedom are considered in an averaged manner.

2.2.2 Previous mesoscopic methods

The development of techniques to coarse grain the solvent effects have been in constant development from a very early stage of the history of computer simulations. Brownian Dynamics (BD) takes the solvent effect into account by including a dissipative and a stochastic contributions to the movement of the particles. Mass is then a conserved quantity, but not the momentum, what describes a diffusive macroscopic behavior in which hydrodynamic interactions are not included. Now we introduce two of the major and still widely employed methods.

Lattice Boltzmann

The Lattice Boltzmann method (LB) uses particle density distribution functions instead of particle coordinates and velocities. LB has been used successfully for flows in complex geometries, like porous media, colloidal suspensions, or multicomponent systems. A restriction of LB is the absence of thermal fluctuations, which can be accounted for by additionally including a noise term on the basis of fluctuating hydrodynamics [57]. Another intrinsic problem is that energy conservation is not fulfilled, so that LB is restricted to isothermal applications, but which has been recently accounted for in an energy conserving generalization of the model.

Dissipative particle dynamics

Dissipative particle dynamics (DPD) was introduced by Hoogerbrugge and Koelman in 1992 [42] and refined by Español and Warren in 1995 [29]. This method enables effective hydrodynamic simulations in complex geometries on large spatial and temporal scales, which can also be applied to out or equilibrium systems. Essentially DPD is a MD simulation with particles interacting by conservative forces, friction forces and thermal noise [30]. The fluid is represented by particles which are not regarded as molecules but rather as clusters of

fluid particles, which enables a hydrodynamic description with a much smaller number of particles than in MD. Interactions among the particles consist of: (i) frictional forces proportional to the velocities, (ii) a random force which corresponds to the rapid, microscopic forces that are eliminated in this coarse grained model and (iii) a weak repulsive conservative force. DPD conserves momentum and has a hydrodynamic macroscopic behavior. Nevertheless, DPD does not conserve energy and lacks a thermal transport equation. A subsequent extension of the technique has been developed in which energy is global and locally conserved [4, 31, 97].

2.2.3 Multiparticle Collision Dynamics

Multiparticle collision dynamics (MPC) is one the most recent mesoscopic model in order to describe solvent dynamics. It was introduced by Malevanents and Kapral in 1999 [68] and since then has received several alternative names, like stochastic rotation dynamics (SRD). Comprehensive reviews about the method are given by Gompper *et al.* in [36] and by Kapral in [53]. It uses a synchronous discrete time-dynamics with continuous velocities and stochastic local multiparticle collisions. This procedure is related to an earlier method called Direct Simulation Monte Carlo (DSMC) which only considers two-particle collisions. In MPC the fluid is represented by point particles, which do not correspond to the molecules of the fluid, but describe the spatial time evolution of mass, momentum and energy of the fluid medium. This fluid particle have positions and velocities given by $\boldsymbol{r}_i$ and $\boldsymbol{v}_i$, that are updated with a discrete time step.

In the streaming step, particle evolve freely and the particle positions are updated by

$$\boldsymbol{r}_i(t+h) = \boldsymbol{r}_i(t) + h\boldsymbol{v}_i(t), \tag{2.8}$$

with h the collision time. The simulation box is decomposed into Wigner-Spitz cells, which are mostly chosen to be cubic cells with a length a. In the collision step, the particles are sorted into the cells, in which the respective center of mass velocities are calculated

$$\boldsymbol{v}_{cm}(t) = \frac{1}{n} \sum_{j|\boldsymbol{r}_j \in Cell} \boldsymbol{v}_j(t), \tag{2.9}$$

where n is the number of particles in the cell. For simplicity, no extra notation for distinguishing the different center of mass velocities in each cell is employed.

The relative velocity $\boldsymbol{\Delta v}_i(t)$ is then

$$\boldsymbol{\Delta v}_i(t) = \boldsymbol{v}_i(t) - \boldsymbol{v}_{cm}(t). \tag{2.10}$$

The subsequent collision operation consists of choosing a random rotation axis and rotating the relative velocity of each particle by an angle α. In the collision step, the particle velocities are updated by

$$\boldsymbol{v}_i(t+h) = \boldsymbol{v}_{cm}(t) + R(\alpha)\boldsymbol{\Delta v}_i(t), \tag{2.11}$$

where $R(\alpha)$ is a rotation matrix around the random rotation axis. The rotation axis is the same for each particle in the cell, but for each cell a different rotation axis is chosen a each simulation step. The construction of $R(\alpha)$ for rotation axes with arbitrary direction can be found in [1]. An alternative model, in which only the axes of a Cartesian coordinate system are employed is introduced in Ref. [112], where the effects of this rotation in the transport coefficients is also studied. The angle α is the same for all particles and is a simulation parameter which determines the amount of momentum and energy exchange in a collision event. For small α the individual particles are less affected by the collision than for large α.

The mean free path of the fluid particles between subsequent collision events is determined by the collision time h and the system temperature T

$$\frac{\lambda}{a} = h\sqrt{\frac{k_B T}{m}}. \tag{2.12}$$

Here k_B is the Boltzmann constant which is set to $k_B = 1$ when dimensionless units are used.

The streaming and collision operations fulfill the conservation laws for mass, momentum and energy. For the streaming operation this is trivial and for the collisions it can be understood from a simple argument. The sum of the relative velocities in one cell with respect to its center of mass is zero per construction. A rotation of all relative velocities by the same angle does not change this, which

means that the momentum is conserved.

$$\begin{aligned}
\sum_{i|\boldsymbol{r}_i\in Cell} \boldsymbol{v}_i(t+h) &= \sum_{i|\boldsymbol{r}_i\in Cell} [\boldsymbol{v}_{cm}(t) + R(\alpha)\boldsymbol{\Delta v}_i(t)] \\
&= \sum_{i|\boldsymbol{r}_i\in Cell} \boldsymbol{v}_{cm}(t) + \sum_{i|\boldsymbol{r}_i\in Cell} R(\alpha)\boldsymbol{\Delta v}_i(t) \\
&= \sum_{i|\boldsymbol{r}_i\in Cell} \boldsymbol{v}_{cm}(t) + R(\alpha) \sum_{i|\boldsymbol{r}_i\in Cell} \boldsymbol{\Delta v}_i(t) \\
\text{with } \sum_{i|\boldsymbol{r}_i\in Cell} \boldsymbol{\Delta v}_i(t) = 0, \qquad &= \sum_{i|\boldsymbol{r}_i\in Cell} \boldsymbol{v}_{cm}(t) \\
&= \sum_{i|\boldsymbol{r}_i\in Cell} \boldsymbol{v}_i(t) \qquad (2.13)
\end{aligned}$$

Separating the total kinetic energy into the contribution from the center of mass and one from the relative velocities, it is clear that the first part does not change if the total momentum in the cell is conserved. The second contribution, which can be regarded as a cell thermal energy does not change, because the magnitude of the relative velocities is not affected upon rotation.

Local energy conservation (norm conservation upon rotations of the relative velocities):

$$\begin{aligned}
\sum_{i|\boldsymbol{r}_i\in Cell} v_i^2(t+h) &= \sum_{i|\boldsymbol{r}_i\in Cell} [\boldsymbol{v}_{cm}(t) + R(\alpha)\boldsymbol{\Delta v}_i(t)]^2 \\
&= \sum_{i|\boldsymbol{r}_i\in Cell} v_{cm}^2(t) + \sum_{i|\boldsymbol{r}_i\in Cell} [R(\alpha)\boldsymbol{\Delta v}_i(t)]^2 \\
&= \sum_{i|\boldsymbol{r}_i\in Cell} v_{cm}^2(t) + \sum_{i|\boldsymbol{r}_i\in Cell} [\Delta v_i(t)]^2 \\
&= \sum_{i|\boldsymbol{r}_i\in Cell} v_i^2(t) \qquad (2.14)
\end{aligned}$$

By comparing the second and third line it can be seen that the center of mass energy $\propto \sum_{i|\boldsymbol{r}_i\in Cell} v_{cm}^2(t)$ and thermal energy $\propto \sum_{i|\boldsymbol{r}_i\in Cell} (R(\alpha)\boldsymbol{\Delta v}_i(t))^2 = \sum_{i|\boldsymbol{r}_i\in Cell} (\Delta v_i(t))^2$ are respectively not altered by the collision operation.

Conservation of momentum shown in Eq. (2.13) ensures hydrodynamic interaction between particles, while conservation of energy at the collision box level in Eq. (2.14) ensures the proper description of energy transport such that temperature gradients can be sustained.

Random shift

Ihle and Kroll [46] found that for small mean free paths the fixed collision grid originally employed by Malevanents and Kapral [68, 69] introduces artificial correlations and breaks Galilean invariance. In cases where the mean free path λ is significantly smaller than the cell size, particles will stay in the same cell for many subsequent simulation steps, so that correlations between them will arise and the assumption of molecular chaos is not valid, which is essential for the validity of the Boltzmann equation. A situation where this becomes apparent is the presence of an external flow field. It was shown that the self-diffusion coefficient of the fluid particles is not longer isotropic anymore since the component parallel to the flow field is significantly larger than the perpendicular component. This meant first that MPC with fix collision grid does not fulfill the Galilean invariance requirement. Moreover, the unwanted correlations can lead to anomalies in the shear viscosity measured from vorticity correlations.

To avoid these problems a random shift operation of the collision grid has been introduced to ensure Galilean invariance and avoid correlations. The idea is to shift the grid for the collision boxes in each simulation step by a random vector with its components in the interval $[-a/2, a/2]$. In this way neighboring particles will more likely have different collision partners in subsequent simulation steps and artificial correlations are avoided.

Furthermore, this procedure does not only restore Galilean invariance, but also accelerates momentum transfer between the cells, leading to an additional contribution to the collisional transport coefficients what enhances the fluid like behavior of the MPC solvent.

Transport coefficients

When Malevanets and Kapral introduced this method, they showed that from the streaming and collision rules, the particle distributions and their time evolution can be described. The stationary particle distribution is Maxwellian as a consequence of the semi-detailed balance in the collision operation. It can also be shown that the time evolution is described by the Boltzmann equation. From the Boltzmann equation, using an expansion of the reduced probability distribution for slowly varying density fields, (Chapman-Enskog procedure) the hydrodynamic equations can be derived as a consequence of mass, momentum and energy conservation. Furthermore, it was shown that an H-theorem exists

for this algorithm.

The transport coefficients for mass, momentum, and energy of the solvent have been analytically calculated for the MPC algorithm. These are the self-diffusion coefficient for the fluid molecules, the shear viscosity for momentum transport, and the thermal conductivity for energy transport. Malevanets and Kapral derived the first approximations for the viscosity and thermal conductivity [68, 69] with a fixed collision grid. In following work Tüzel, Ihle and Kroll have derived Green-Kubo relations for the transport coefficients using a projection operator technique, which have been proven to agree very well with simulation results [45, 46, 47, 48, 49, 112]. A summary of the results is given in Ref. [111]. Yeomans *et al.* [54, 89] employ alternatively a non-equilibrium kinetic approach to derive similar results. More recently Winkler and Huang obtain the shear viscosity from an analytical calculation of the stress tensor [120]. The transport coefficients have a kinetic contribution which in MPC arises from the streaming of particles to other cells. Additionally, there is a collisional contribution which in MPC is due to the random shift of the lattice, as first explained in Ref. [45]. The shear viscosity is then

$$\nu = \nu_{kin} + \nu_{col}. \tag{2.15}$$

In three dimensions the kinetic contribution is

$$\nu_{kin} = \frac{k_B T h}{2m} \frac{5\rho}{(\rho - 1 + \exp(-\rho))\,(2 - \cos(\alpha) - \cos(2\alpha))} - 1. \tag{2.16}$$

The collisional contribution is

$$\nu_{col} = \frac{a^2}{h} \frac{1}{6d\rho} (\rho - 1 + \exp(-\rho))\,(1 - \cos(\alpha))\,, \tag{2.17}$$

where d the dimension.

The transport of mass is characterized by the self-diffusion coefficient of the fluid particles and has only a kinetic contribution which is given by

$$D_{fluid} = \frac{d\rho}{(1 - \cos(\alpha))\,(\rho - 1 + \exp(-\rho))} - 1. \tag{2.18}$$

For the transport of energy the reader is referred to Chapt. 3 where the analytical expression for the thermal conductivity is compared to simulation results.

2.3 Boundary conditions

The choice of the boundary conditions is determined by the characteristics of the problem under study. The boundary conditions for the simulation box can

be periodic and/or include solid walls. For the effect of periodic boundary conditions on MPC system properties the reader is refereed to a recent work of Winkler and Huang [120]. Also the embedded macroscopic objects, like for example colloids, may work as boundaries for the fluid and can have similar implementations and effects on the fluid.

The different procedures to implement impenetrable walls can be classified in those resulting in slip and stick boundary conditions. If the particles next to the wall are imposed or allowed to have a different velocity than the wall, we refer to slip boundary conditions. Conversely, if particles are enforced to have the same velocity as the neighbouring walls, we refer to stick boundary conditions. Stick boundary conditions describe rough surfaces at which the fluid velocity, parallel as well as perpendicular, vanishes. This is a good estimation in most cases for real systems. In turn, slip conditions would correspond to (super) hydrophobic surfaces (for water).

Slip boundary conditions are for instance obtained with specular reflection of the particles at the wall, this is when just the normal component of the velocity is inverted and the parallel component remains unchanged. Stick boundary conditions can be implemented by applying the bounce-back rule upon which the relative velocity to the wall is reversed, i.e. $\boldsymbol{v}_i - \boldsymbol{v}_{wall} = -(\boldsymbol{v}_i - \boldsymbol{v}_{wall})$. In MPC this has also been achieved by using a stochastic reflection method, used by Inoue *et al.* [50] and Hecht *et al.* [41], in which the velocity after a wall collision is generated stochasticly from a Maxwell-Boltzmann distribution.

Furthermore, one can use any type of potential for wall interactions and treat the dynamics of the particles with standard MD, which can be easily incorporated into the MPC algorithm. Also interactions of the fluid with embedded particles and interactions among these particles with each other can be treated in this way.

2.3.1 Stick boundary conditions in MPC

The implementation of bounce back conditions in MPC simulations has shown a mismatch between the wall and the fluid velocity at the wall. A constant force applied parallel to two confining walls normally leads to a parabolic flow profile; this is the so-called *Poisseuille flow*. In the MPC simulation the parabolic velocity profile does not reach zero directly at the wall surface, but rather at a distance inside the wall, $b = \left|\left(1/\frac{dv}{dz}\right) v\right|_{z=0}$, which is referred to as slip-length

(Fig. 2.1).

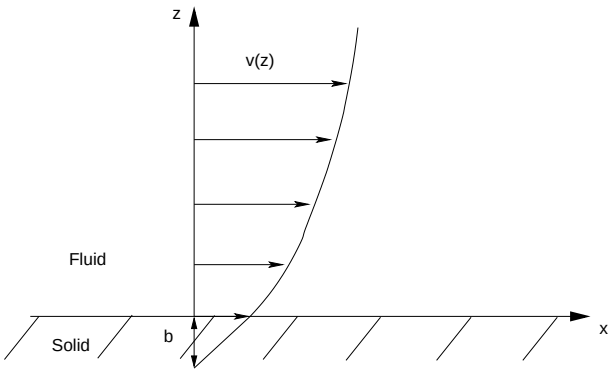

Figure 2.1: Definition of the slip length [74]. The relative velocity of the fluid to the surface at $z = 0$ is called the slip velocity. The imaginary distance below the surface at which the extrapolated relative velocity of the fluid is zero, denoted by b, is called the slip length.

It has been found that slip at the wall arises from partially filled boxes due to the random shift, given that the shifted grid overlaps with solid surfaces and the collision boxes at boundaries will contain less particles on average than boxes in the bulk region.

A method to remove, or at least reduce, such spurious slip at the liquid-solid interfaces has been introduced by Lamura *et al.* [59]. The idea is to couple the solvent particles close to the wall to a bath of virtual particles that compensate for the lower number of fluid particles in the boundary boxes. These virtual particles have velocities generated from a Maxwell-Boltzmann distribution with zero average velocity and variance determined by the bulk temperature. The number of virtual particles in each collision box necessary to match the bulk density ρ is $(n-\rho)$, where n is the number of particles in the respective cell. Since the sum of normal distributed numbers (i.e. Maxwell-Boltzmann distributed) are again normal distributed numbers with a variance corresponding to the sum of the individual variances, it is enough if one effective virtual particle is considered in each collision box. The coupling with the virtual particles is done in the collision step in Eq. (2.11). The velocity of the center of mass in the partially filled collision boxes is then

$$\boldsymbol{v}_{cm} = \frac{\sum_{i=1}^{n} \boldsymbol{v}_i + \boldsymbol{a}}{\rho}, \tag{2.19}$$

where $\boldsymbol{a}$ is a vector whose components are chosen from a Maxwell-Boltzmann

distribution with zero average and variance $\langle a^2 \rangle = (n - \rho) k_B T$.

2.4 Hydrodynamic numbers

The effect of different MPC parameters for the macroscopic behavior of the fluid in concrete applications can be evaluated by hydrodynamic numbers. A detailed description of hydrodynamic numbers for colloidal suspensions and comparisons between real systems and MPC simulations is given in the work of Padding and Louis [82]. Following we discuss three of them.

Schmidt number

The Schmidt number characterizes the ratio of momentum and mass transport, namely the kinematic viscosity ν and self-diffusion coefficient D_{fluid}, and it is defined as $Sc = \nu / D_{fluid}$. The Schmidt number of liquids like water is usually in the range of 10^2 to 10^3. As discussed by Ripoll et al. in [100], Sc measures if the solvent is in the "particle regime" with a gas-like behavior corresponding to $Sc \simeq 1$, or in "collective regime" with a liquid-like behavior with values of Sc two or three orders of magnitude larger.

In the case of the MPC fluid, both quantities, ν and D_{fluid}, can be analytically calculated, and are given in Eqs. (2.15)-(2.18). Fig. 2.2 displays the theoretical values of Sc as a function the collision time for different parameters. In contrast with other mesoscopic models as LB or DPD where $Sc \simeq 1$, for MPC Sc becomes considerably larger than 1 for large values of the collision angle and small values of the collision time. Since hydrodynamic interactions are present in fluid-like solvent a typical choice of the MPC parameters will be $\alpha = 130^0$ for the rotation angle and $h = 0.1$ for the collision time.

Reynolds number

If a flow of the fluid with a velocity u encounters a geometric restriction with a characteristic length scale b or an objected of the length scale is moving with the velocity u against the fluid, this is characterized by the Reynolds number Re. The Reynolds number measures the importance of inertial forces over viscous forces and is given by $Re = ub/\nu$. For example the Reynolds number of a colloidal with a diameter of 1 μm particle moving with a velocity of 1= μm/s in water at room temperature (with a viscosity of $\nu = 10^6 \mu m^2/s$) is $Re = 10^{-6}$.

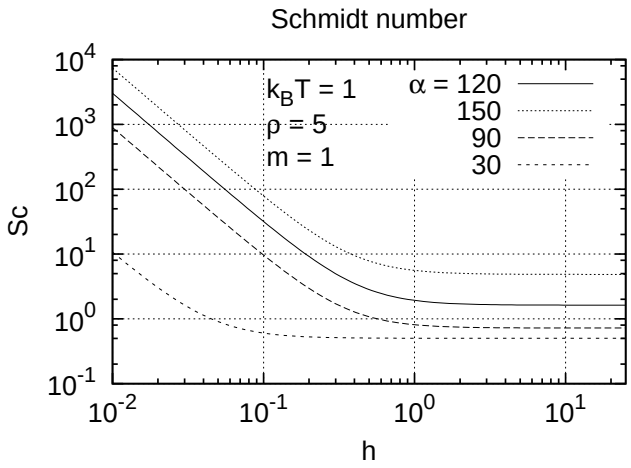

Figure 2.2: Schmidt number in the MPC solvent as a function of the collision time h for different parameter sets. Lines are analytically obtained from Eqs. (2.15)-(2.18).

Peclet number

The Peclet number Pe can be used to determine if convective or diffusive transport is dominant and is given by $Pe = ub/D$, where D is the diffusion constant of a macroscopic object of size b and velocity u. In our case this is $D_{colloid}$ given by Eq. (1.22) with the friction term given by Eq. (1.23) (in the case of slip boundary conditions). The diffusive transport is determined by the thermal fluctuations of the macroscopic object and the convective transport by its mobility in response to an external force which results in advection with a characteristic velocity u. For example in thermodiffusion experiments with polystyrene particles of $0.2\mu m$ diameter it was found by Duhr and Braun [22] that the particles have a thermophoretic mobility $D_T = 1.4\mu m^2/(sK)$. They had applied a temperature gradient in the order of $\nabla T \approx 0.08K/\mu m$ which leads to a thermophoretic velocity of $u = D_T \nabla T \approx 0.1\mu m/s$. They also measured the diffusion constant of the beads as $D = 2.1\mu m^2/s$. Hence the corresponding Peclet number is 10^{-2}, which indicates that diffusion is the dominant transport mechanism.

3 Solvent with inhomogeneous temperature

Existing computational studies on thermodiffusion have been performed so far with the atomistic approach of Molecular Dynamics [37, 96, 35]. The mesoscopic method MPC is used here essentially for the first time for an inhomogeneous temperature distribution. The validation and characterization of the method in the presence of a temperature gradient is therefore performed in detail. Some general aspects about the implementation of a temperature gradient are first discussed, like the resulting position dependent density profile and the particle velocity distribution along the temperature gradient. Then we discuss three different methods to impose the temperature gradient. Two methods include the interaction of the system with confining walls. The third method considers open boundary conditions by imposing energy fluxes. The three methods are compared and characterized in the parameter space. At last, we investigate the transport of energy characterizing the thermal diffusivity. The dependence of this transport coefficient on the method parameters and the validity of existing analytical theories is discussed.

3.1 General considerations

3.1.1 Temperature profile establishment

The idea is to impose a temperature difference to the system at the boundaries such that the in-between solvent can have the freedom to adapt to the imposed conditions. Effects induced by the solvent, like hydrodynamic interactions, or non-linear temperature profiles, will then be minimally disturbed.

We use a three dimensional simulation system with boundaries fixed at two different temperatures. The cold bath is held at a temperature T_c, and the hot bath at T_h (with $T_c < T_h$). The temperature gradient direction is referred as

z. In the perpendicular x, and y directions, we use standard periodic boundary conditions [2]. Initially the system is at uniform temperature, T_0. For convenience, the initial temperature is generally chosen to be $T_0 = (T_h + T_c)/2$. In the case of a linear temperature profile, the average system temperature $\overline{T}$ will then be very close to the initial temperature. When the system gets in contact with the boundaries, the temperature becomes position dependent. This spatial dependence is, after some equilibration time, invariant with time.

In order to measure the temperature profile, the temperature is computed in each slab of the system. The slab thickness is in principle arbitrary, but we normally chose the length of one collision cell a. Since there is no superimposed velocity field, the temperature T_j can be calculated from the kinetic energy of the N_j particles in the j slab,

$$\frac{3}{2}N_j k_B T_j = \sum_{i \in \text{ slab } j} \frac{1}{2} m \boldsymbol{v}_i^2, \tag{3.1}$$

with $j = 1, ..., L_z$.

For the simple solvent, with small temperature differences, and in the absence of any other external field, the temperature profile will be linear,

$$T(z) = T_c + \frac{T_h - T_c}{L_z} z, \tag{3.2}$$

with L_z the distance between the two baths. An example of the simulated temperature profile can be seen in Fig. 3.1. Standard values chosen for the boundary temperatures are $T_c = 0.9$ and $T_h = 1.1$. These values result in a relative temperature difference $(T_h - T_c)/\overline{T} = 0.2$. Considering as a reference value the room temperature $\overline{T} = 300K$, this relative difference would correspond to a temperature difference of $60°C$.

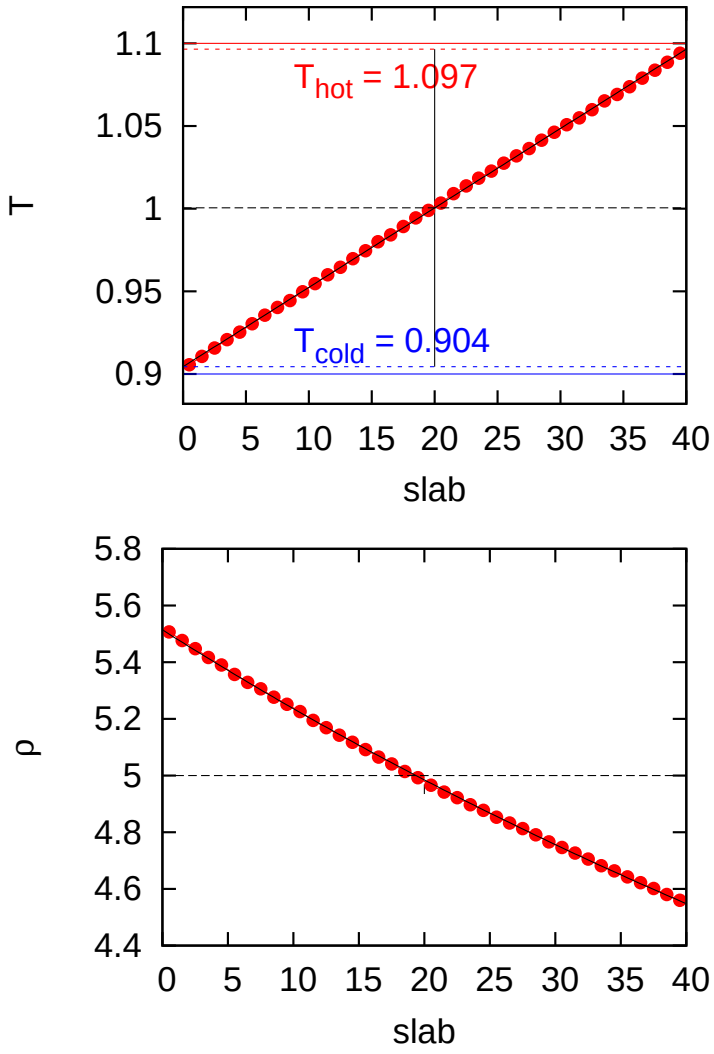

Figure 3.1: Example of a temperature profile (left) and the corresponding particle number density profile (right). The symbols report the simulated values and the lines correspond to Eq. (3.2) and Eq. (3.4) respectively.

3.1.2 Density profile

After the equilibration time not only the temperature, but also the density profile is stationary. This is the result of a constant pressure throughout the system and gives control over both, temperature and pressure. The fluctuations of the pressure are constant after this time and can be used as a convergence criterion. The fluctuations of the pressure can be obtained from the mean square deviations of the pressure profile

$$\langle \overline{\Delta p} \rangle = \left\langle \sqrt{\frac{1}{l_z} \sum_{j=1}^{L_z} (p_j - p_{av})^2} \right\rangle, \tag{3.3}$$

where p_j is the pressure in each slab, the bar refers to the spatial mean deviation, and the brackets to an average over the number of simulation steps.

The solvent density profile can be determined by the equation of state. The pressure p of the MPC fluid is known to behave with ideal gas equation of state, $pV = Nk_BT$, where V is the volume, N the number of particles, T the temperature, and k_B the Boltzmann constant. The particle number density $\rho(z) = N(z)/V$ is then,

$$\rho(z) = \frac{p}{k_B T(z)}. \tag{3.4}$$

If the temperature profile in Eq. (3.2) is considered, the pressure can be calculated taking into account that the total number of particles in the simulation box is constant *i.e.* $\int_0^{L_x} \int_0^{L_y} \int_0^{L_z} d^3r \rho(z) = N$. Solving the integral yields to

$$p = \rho \frac{k_B(T_h - T_c)}{\ln(T_h/T_c)}. \tag{3.5}$$

Using a Taylor expansion for the logarithm in the case $T_h/T_c \approx 1$, this expression simplifies to $p = \rho\ k_B T_0$, where ρ is the average density. The resulting density profiles for a given temperature profile can be seen in Fig. 3.1. Note that, although strictly speaking Eq. (3.4) corresponds to a inversely linear dependence with the position, in the limit of small temperature differences, the approximation of a linear density profile can be considered, as can be seen in Fig. 3.1.

3.1.3 Velocity distribution

The velocity vector distribution of the MPC solvent particles in equilibrium conditions has been demonstrated to have correct thermodynamic behavior by

following Maxwell-Boltzmann distribution function [69],

$$P(\mathbf{v}) = \left(\frac{m}{2\pi k_B T}\right)^{\frac{d}{2}} \exp\left(-\frac{m\mathbf{v}^2}{2k_B T}\right), \tag{3.6}$$

where d is the considered dimension number.

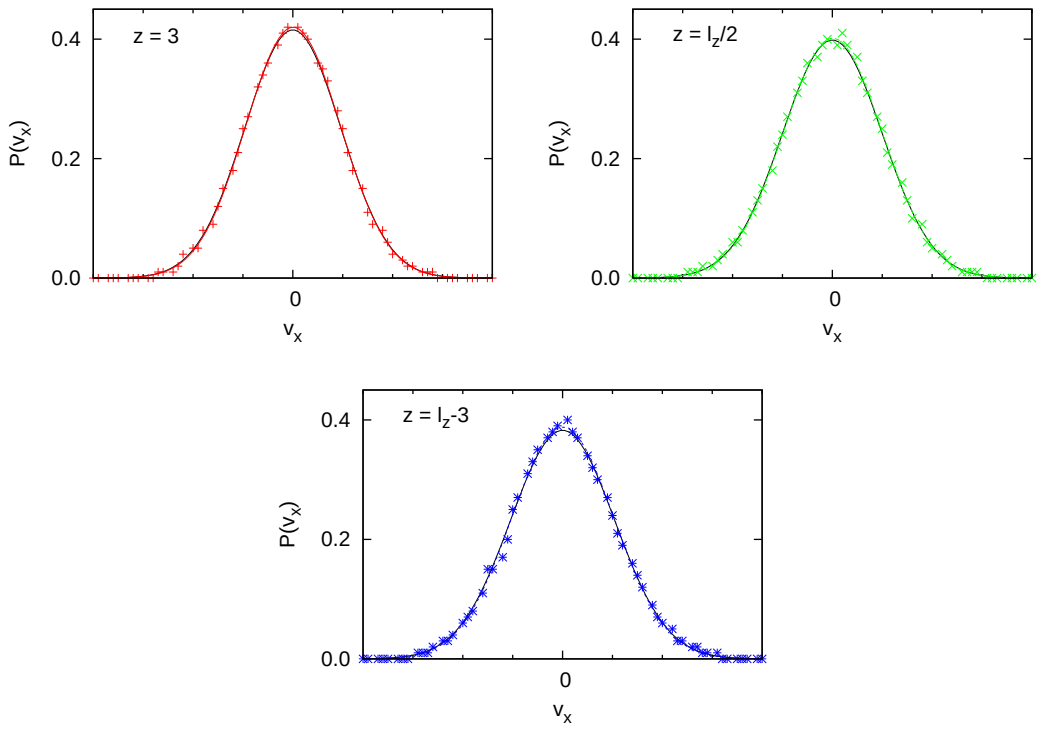

Figure 3.2: Velocity distribution in a direction perpendicular to the temperature gradient at three different positions: close to the cold boundary ($z = 3$), in the center of the simulation box ($z = L_z/2$), and close to the hot boundary ($z = L_z - 3$), in a system with $L_z = 40$. Symbols correspond to simulation results and lines to the Maxwell-Boltzmann distribution in Eq. (3.6) at the corresponding temperatures and densities.

In the presence of a temperature gradient, the velocity distribution will in general deviate from the equilibrium distribution. Nevertheless, when the temperature gradient is small enough, local thermal equilibrium is generally assumed. Here we analyze the velocity distribution as a function of the position. In Fig. 3.2, the velocity distribution in one of the directions perpendicular to the temperature gradient is displayed for slabs at three different positions together

with the Maxwell-Boltzmann distribution in Eq. (3.6), where the different temperatures have been taken into account. The simulation results are calculated considering the particles in just one configuration. The deviations between the data and the equilibrium distribution are minimal, what confirms that local thermal equilibrium is a very reasonable approximation.

3.2 Boundary conditions

3.2.1 Walls with virtual particles

The implementation of walls within the MPC solvent has been studied in homogeneous temperature conditions [59, 58], and already introduced in Sect. 2.3.1. In order to obtain stick boundary conditions, (particles close to the walls should have the wall velocity, zero in our case), two variations are included in the algorithm. In the streaming step, particles reaching the wall revert their velocities with bounce-back. In the collision step, collision boxes partially filled due to the presence of the walls, include the effect of virtual particles with an averaged fixed temperature that match the density in this boxes to the bulk density. If there are n_w particles in the partially full box at the wall with $n_w < \rho$, $\rho - n_w$ virtual particle will be considered. These particles are chosen with momenta drawn from a Maxwell-Boltzmann distribution with zero mean velocity and variance $(\rho - n)\sqrt{k_B T/m}$. Note that although the MPC algorithm conserves energy, the interaction with the virtual particles at the walls does not, such that the total energy fluctuates now around an average value determined by the system averaged temperature $\overline{T}$.

The idea that allows to implement a temperature gradient consist in considering the temperature and reference density of such virtual particles with different values in both walls, such that they behave as thermal cold and hot bath respectively. Virtual particles at the cold wall will have temperature T_c and at the hot wall T_h with densities ρ_c and ρ_h respectively, given by Eq. (3.4). Therefore, the interaction with the virtual particles in the hot wall will provide energy to the system, while the interaction with the virtual particles in the cold wall will absorb an equivalent energy.

As described in Sect. 3.1.1, we put the solvent in contact with the walls, equilibrate the system, and compute the resulting temperature profiles. Fig. 3.3 shows simulation results with different solvent parameters. It can be observed

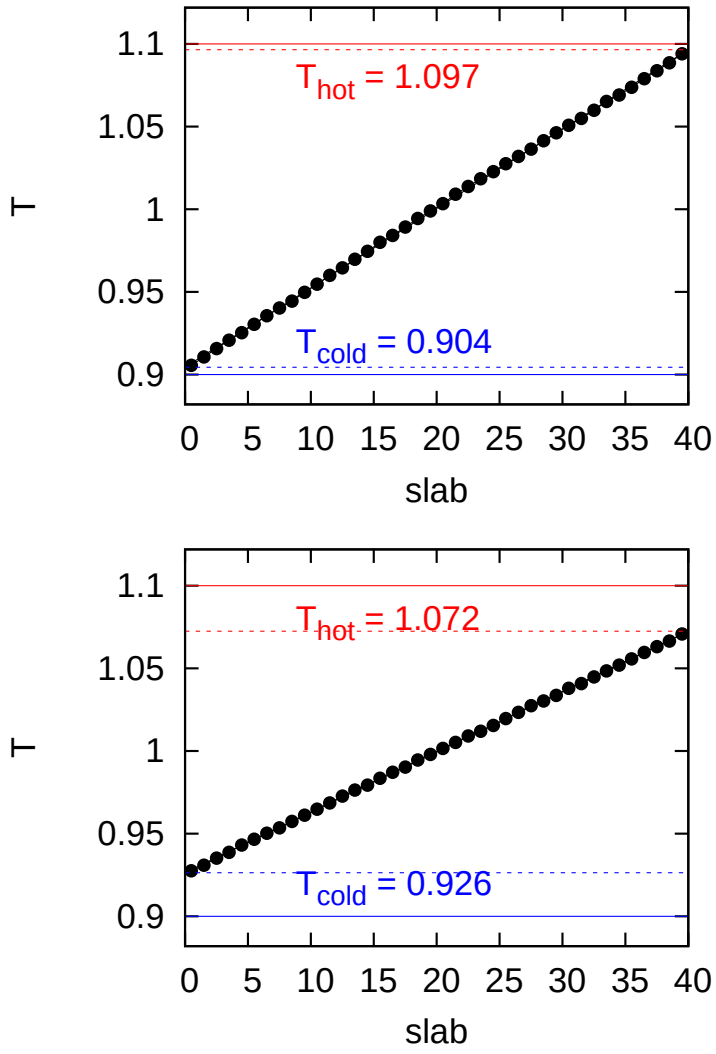

Figure 3.3: Temperature profiles of the MPC in contact with walls with virtual particles. The black dots are simulation results. The solid horizontal lines are the temperatures of the virtual particles, T_c and T_h, and the dashed lines correspond to the solvent temperatures at the walls, $T(z = 0)$ and $T(z = L_z)$ respectively. Simulations are performed with $\rho = 5$ and $\alpha = 120°$. Left figure corresponds to $h = 0.1$ and right to $h = 0.5$.

that linear temperature profiles are nicely reached. Nevertheless, the solvent in contact with the walls shows to have different temperatures than the walls. This effect reminds the slip velocity of particles close to a wall in the presence of solvent flow. The solvent temperatures at the walls, $T(0)$ and $T(L_z)$, are characterized from a linear fit, as can be seen in Fig. 3.3. The temperature mismatch varies with the solvent parameters and is characterized in Fig. 3.4.

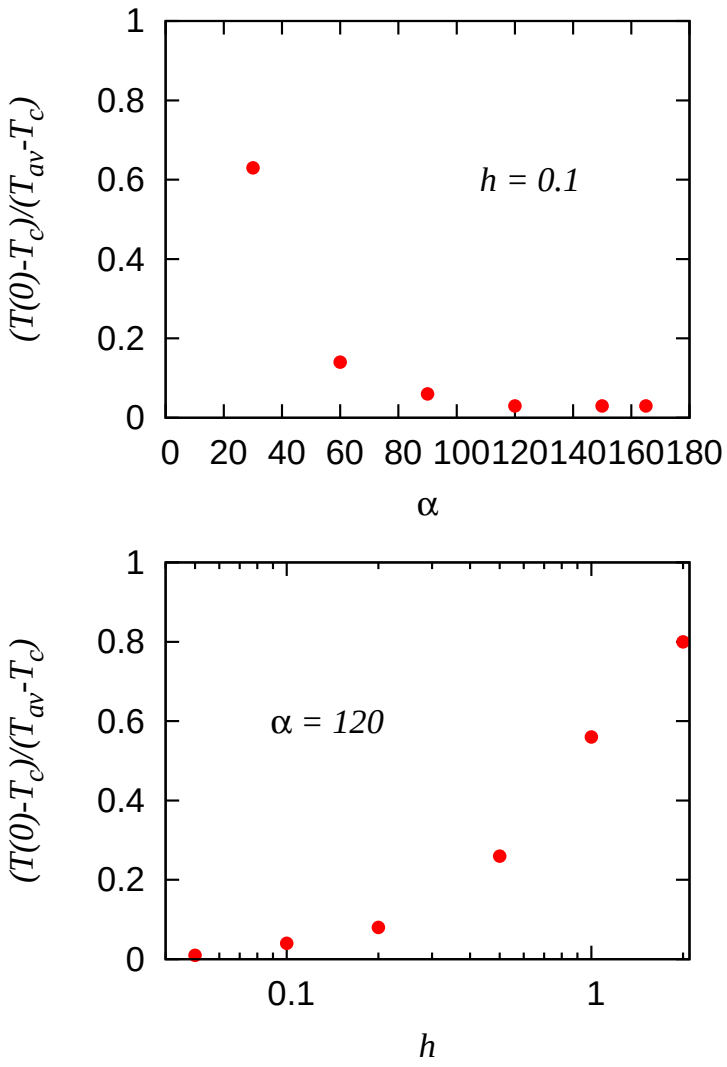

Figure 3.4: Deviation of the temperature at the walls as a function of the solvent parameters α and h. The employed average number of particles per box is $\rho = 5$.

In order to characterize this mismatch, we define the dimensionless quantity

T_s,

$$T_s = (T(0) - T_c)/(\overline{T} - T_c). \tag{3.7}$$

T_s quantifies the temperature deviation at the cold wall. In case of perfect match $T(0) = T_c$, T_s vanishes by construction. Meanwhile, in the limiting case of maximum mismatch, there would be no temperature variation upon contact with the heat bath, this is is $T(0) = \overline{T}$, and $T_s = 1$. Note that by symmetry, a similar definition could have been done with the deviation at the hot wall, without any variation of the results.

Fig. 3.4 shows T_s as a function of the solvent parameters. It can be seen, that for weaker collisional momentum exchange and large mean free paths, *i.e.* low α and large h, the temperature deviation becomes stronger. This seems to indicate that only a certain amount of heat can be transmitted by the virtual particles. Nonetheless, starting the simulation with initial linear temperature and density profiles with the wall temperatures does not change the final stationary state. In an attempt to reduce the values of T_s, we have performed some trial simulations in which the transfer of energy is increased by using much larger densities for the virtual particles than the bulk density, assigning higher masses to them, or increasing the number of layers in which they are present. These routes slightly change the solvent temperature at the walls, but the trend remains essentially the same.

3.2.2 Walls with thermostats

To investigate other routes that more accurately accommodate the temperature of the solvent particles close to the walls, we disregard the virtual particles at the walls, and implement thermostats in the boundary slabs next to the walls. The limiting temperatures T_c and T_h are now enforced by rescaling the kinetic energies of such solvent particles in each simulation step. From Eq. (3.1) the rescaling relations can be obtained,

$$\boldsymbol{v}_i' = \frac{3N_{c,h}k_B T_{c,h}}{2E}\boldsymbol{v}_i. \tag{3.8}$$

Here, N_c and N_h are the number of particles in the cold and hot slabs.

If external flow fields are applied one must rescale the velocities with respect to the center of mass velocity in order to locally conserve momentum, which is necessary to obtain a correct hydrodynamic behavior. The thermal energy of the particles is

$$E = \sum_{i=1}^{N} \frac{1}{2} m(\boldsymbol{v}_i' - \boldsymbol{v}_{cm})^2,$$

where $\boldsymbol{v}_{cm}$ is the center of mass velocity in the respective slab. This energy is rescaled to the new thermal energy $E' = \frac{3}{2}(N_{c,h} - 1)k_B T_{c,h}$ with the desired temperature. The rescaling relation becomes

$$\boldsymbol{v}_i' = \boldsymbol{v}_{cm} + (\boldsymbol{v}_i - \boldsymbol{v}_{cm})\sqrt{E'/E}.$$

Since we are using a solvent without any external fields or embedded particles that could result in a flow field, we have used the rescaling relation in Eq. (3.8).

The averaged temperature of the solvent in contact with the boundaries and in the stationary state is presented in Fig. 3.5. Linear sufficiently far away from the walls, the temperature profile attains a shoulder-like behavior at the boundaries. This is reflects that the particles can not adapt efficiently enough to the thermostat temperatures in the adjacent slabs. To account for this behavior, we fit the temperature profile by excluding the first three slabs at the boundaries. In this way the effective solvent temperature at the boundary layers is quantified, showing a mismatch with the wall thermostat temperatures T_c and T_h. We characterize this mismatch with T_s in Eq. (3.7). T_s is, similarly to the heat bath implemented with virtual particles, dependent on the method parameters, and it is shown in Fig. 3.6. It also becomes more significant for large mean free paths $\lambda = ah\sqrt{\frac{k_B T}{m}}$ or smaller α, i.e. less collisional momentum exchange. The

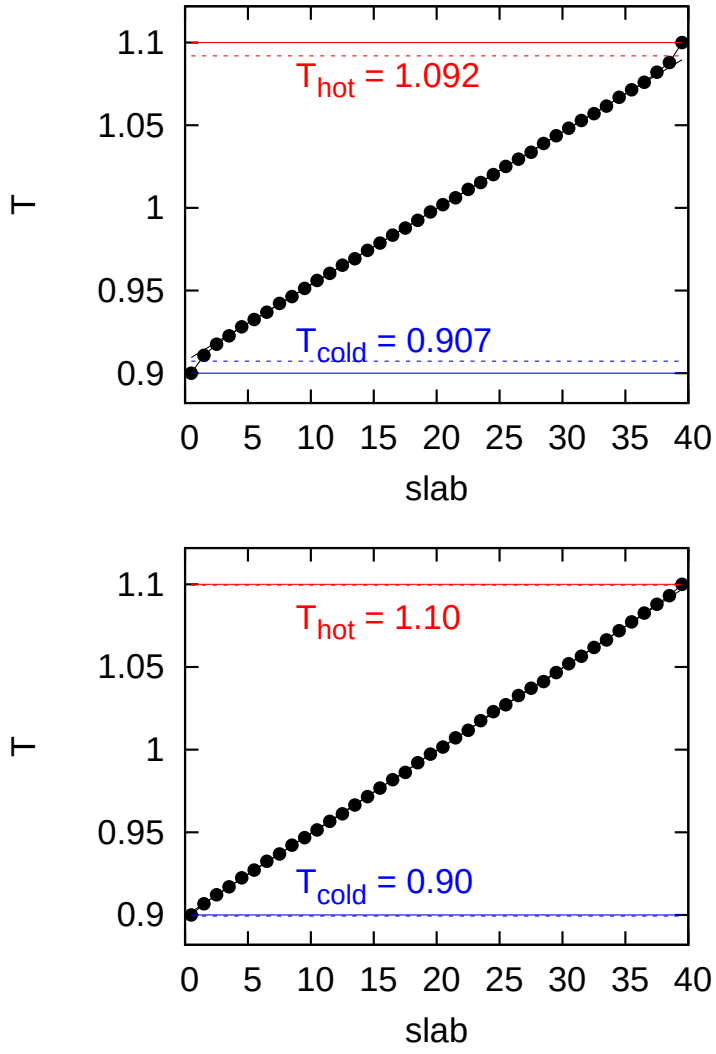

Figure 3.5: Temperature profile with a temperature gradient maintained by thermostats in front of two planar walls at the boundaries. Left side uses $\alpha = 30°$ and right side $\alpha = 120°$. The collision time is $h = 0.1$ in both cases.

deviation of the wall temperature is though much less pronounced than for the virtual particles (Fig. 3.4), but it is still significant for large mean free paths and small rotation angles α.

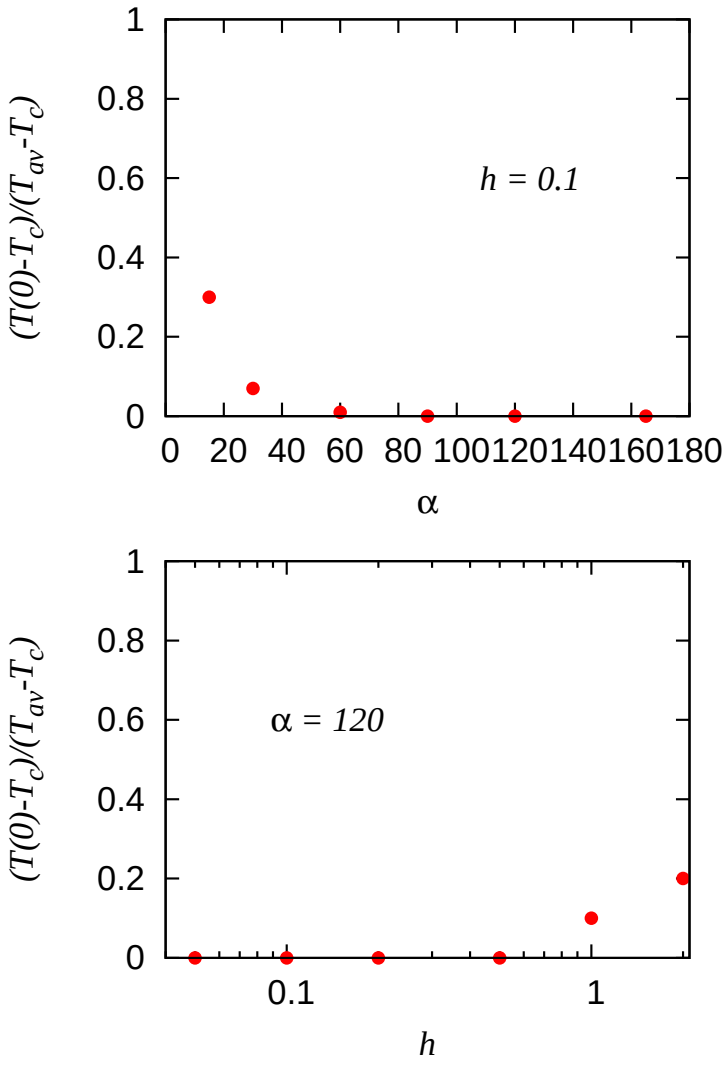

Figure 3.6: Deviation of the boundary slab temperature $T(0)$ from the imposed temperature T_c for different MPC parameters α and h. The average number of particles per box is $\rho = 5$ in both cases.

We can conclude that, in spite of the temperature mismatch at the boundaries, both these methods produce satisfactory linear profiles away from the walls. Therefore they can be employed to study the effects of temperature gradients

in the presence of confining walls. Furthermore, the parameters for which the temperature mismatch are smallest, namely small collision times h, and large α values, are the parameters for which the MPC algorithm has been mostly employed [99, 100, 73], since they are also the values for which the Schmidt number is larger (see Chapt. 2).

Previous simulations with MPC and a temperature gradient have been very briefly reported by Pooley and Yeomans [89]. They employ periodic boundary conditions in which they thermostat two broad layers as the cold and hot baths. They employ a system size with $L_z = 100$, and thermostats the layer between $z = 0$ and $z = 20$ as the cold bath, and between $z = 50$ and $z = 70$ as the hot bath. They do not report any temperature mismatch at the boundaries although with the employed parameters we would expect them to be present.

In order to compare the two methods for implementing walls at different temperatures, several issues have to be considered. First, we have characterized that the temperature mismatch is considerably more pronounced for the walls with virtual particles than for the thermostat ones. In practice, the effective temperature gradient will be calculated with the actual boundary temperatures, and given that in both cases the profiles are nicely linear, not further consequences are expected. From the computational point of view, it should be noted that virtual particles at the walls constitute an additional, but not really significant, effort since just three stochastic velocities per collision box are required. This computational cost is approximately the same as the thermalisation of the layers in the proximity of the wall. With both techniques the boundary layers have to be disregarded. In the case of the virtual particles one layer will be sufficient, while for the thermostated walls it will be necessary to not account for at least two layers. Consequently, the walls with virtual particles will be in general better suited to study temperature gradients in the presence of confining walls, although a more precise consideration should be performed in a particular application of the methods.

3.2.3 Velocity exchange algorithm

This method for imposing the temperature gradient considers periodic boundary conditions by imposing an energy flux. In contrast to the previous methods, where temperatures at the boundaries were imposed, here the temperature difference will be a consequence of the energy flux. In principle the idea could be

combined with the presence of hard walls, but since we are also interested in studying the effect of temperature gradients in the absence of confinement, here we restrict ourselves to the case with periodic boundary conditions.

The original method was introduced by Hafskjold *et. al* [37] and employed in the first simulations with Molecular Dynamics and temperature gradients [56, 40, 39]. They proposed to transfer fixed amounts of energy between a "cold" layer, placed at the system boundary, and a "hot" layer, placed at the center of the system. This unphysical energy transfer plays the role of the interaction with two thermal baths in the cold and hot slabs, and allows to establish the temperature gradient. As can be seen in Fig. 3.7, the simulation box is now divided in two half simulation boxes with increasing temperatures towards the center.

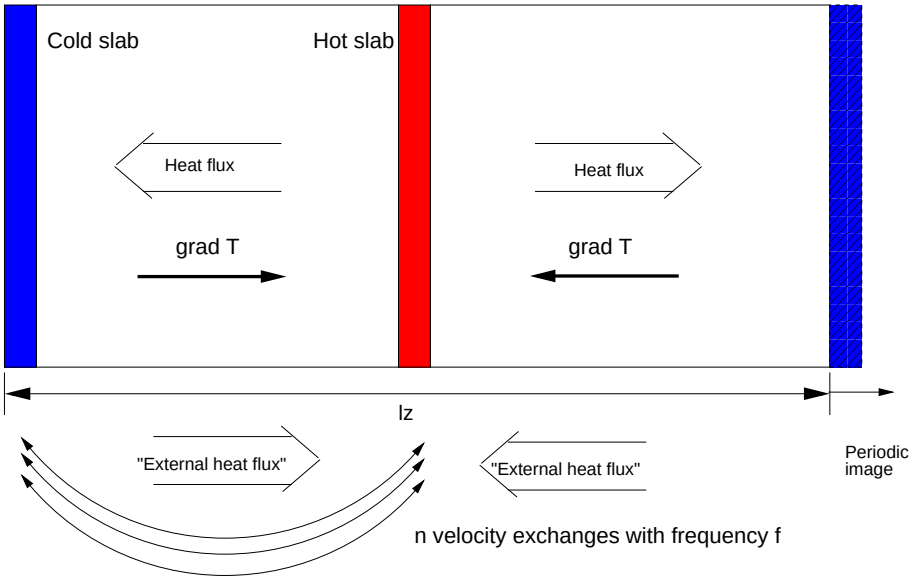

Figure 3.7: Illustration of the periodic simulation box for velocity exchange algorithm.

Here we employ the modification of this algorithm proposed by Müller-Plathe [72] and since then mostly employed with Molecular Dynamics. It consists in determining the hottest particles in the cold slab and the coldest particles in the hot slab, and then exchange their velocities (see Fig. 3.7). This method has the advantage that the total energy E and momentum $\boldsymbol{P}$ of the system are exactly conserved.

The distribution of particle velocity modulus $f(v)$ is derived from the distribution of vector velocities in Eq. (3.6) as $f(v)dv = \int_\Omega v^2 P(\mathbf{v})d\mathbf{v}$, where Ω denotes

the integration over the polar and azimuthal angles. It reads,

$$f(v) = 4\pi \left(\frac{m}{2\pi k_B T} \right)^{\frac{3}{2}} v^2 \exp\left(-\frac{mv^2}{2k_B T} \right). \tag{3.9}$$

In Fig. 3.8, $f(v)$ is displayed for the two temperatures typically used as cold and hot baths. It can be observed that the difference between the two distributions is not so large, such that the exchange of velocity is easily absorbed by the new distribution. Additionally, the number of particles in each layer is large enough, such that the Maxwell-Boltzmann velocity distribution is not significantly perturbed. Although the energy flux is locally applied in each exchange, on average the exchange is distributed over the whole slab.

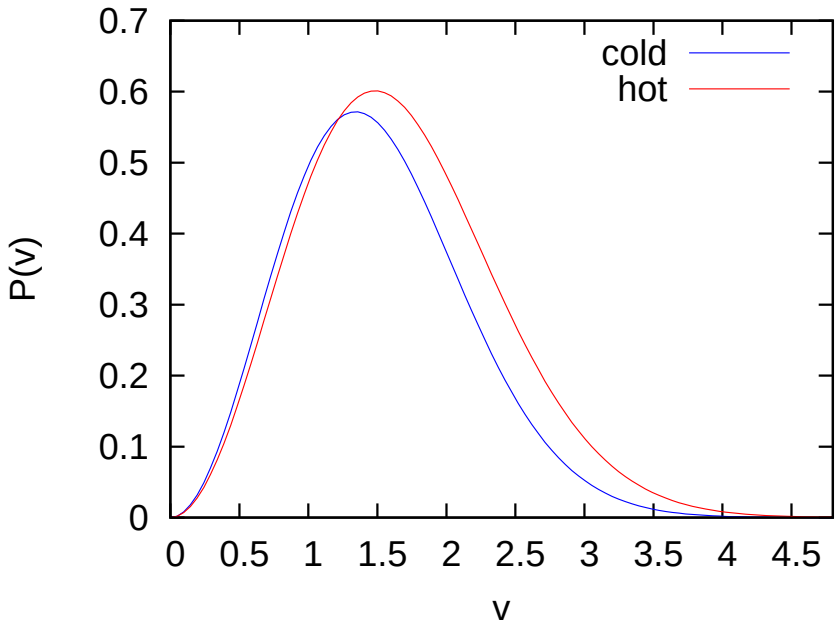

Figure 3.8: Velocity modulus distribution in Eq. (3.9) for the temperatures $T_c = 0.9$ and $T_h = 1.1$, typically used for the cold and hot baths.

The magnitude of the temperature gradient is controlled by tuning the frequency f_{ex} and the number of particles n_{ex} of the velocity exchanges. The frequency f_{ex} determines the number of simulation steps after which the exchange operation is performed. The more steps in between the exchanges, the lower is the resulting heat flux and temperature gradient. The determination of the temperatures in the cold and hot slabs given certain values for f_{ex} and n_{ex} will also depend on the systems density ρ and on the system size. We want

now to obtain a rough estimation of the temperature gradient in terms of the simulation parameters.

The temperature gradient ∇T is proportional to the heat flux $\mathbf{j}_q$,

$$\mathbf{j}_q = \kappa_T \nabla T, \tag{3.10}$$

with κ_T the thermal conductivity, whose analytical expression is known and will be discussed in the following section. By definition the heat flux can be calculated as

$$\mathbf{j}_q = \frac{\Delta E}{A \Delta t}. \tag{3.11}$$

Here, the area $A = L_x L_y$ is given by the simulation box, the time interval Δt is here the time between exchanges $\tau_{ex} = 1/f_{ex}$, inversely proportional to the frequency of exchanges, and the energy increment $\Delta E = \frac{1}{2} n_{ex} \Delta E_{ex}$ is given by the energy increment in each velocity exchange ΔE_{ex}, times the number of exchanges n_{ex}, and divided by 2 since the energy flux is distributed in the two half boxes. The energy increment in each velocity exchange is

$$\Delta E_{ex} = \frac{1}{2} m \left(v_{max}^2 - v_{min}^2 \right), \tag{3.12}$$

v_{min} corresponds to the coldest particle in the hot slab. In general we can approximate $v_{min} \simeq 0$, as can be seen in Fig. 3.8. v_{max} corresponds to the hottest particle in the cold slab. In order to get a rough estimation of such velocity in terms of the input parameters, we first approximate the temperature $T_C \simeq \overline{T}$ in Eq. (3.9). Second, since we are in the tail of the distribution, we neglect the correction given by the factor v_{max}^2 in Eq. (3.9), such that

$$f(v_{max}) \simeq c \exp\left(-\frac{m v_{max}^2}{2 k_B \overline{T}} \right), \tag{3.13}$$

with the numerical constant $c = 4\pi (m/2\pi k_B \overline{T})^{\frac{3}{2}}$. And third we assume that in such cold layer the density is the same as the average density $\rho_c \simeq \rho$, and that there will always be one, and only one, particle with the temperature at the tail of the distribution,

$$f(v_{max}) \simeq \frac{1}{A\rho}. \tag{3.14}$$

From Eq. (3.13) and Eq. (3.14), we obtain our rough estimation of v_{max},

$$v_{max} \simeq \sqrt{\frac{2 k_B T}{m} \ln(c \rho A)}. \tag{3.15}$$

Therefore, comparing the heat flux $\mathbf{j}_q$ in Eq. (3.10) and Eq. (3.11), and substituting Eq. (3.15) in Eq. (3.12), we get,

$$\nabla T = \frac{1}{2}\frac{n_{ex} f_{ex}}{\kappa_T h} k_B T \frac{\ln(c\rho A)}{A} \tag{3.16}$$

The temperature profile obtained with the velocity exchange algorithm in Fig. 3.9 shows to display a nice linear profile between the cold and hot slabs. Furthermore, it can be seen that Eq. (3.16) gives a reasonable estimation of the temperature gradient. This has been found true generally in other simulations. The various approximations, including the employed analytical value of the heat conductivity, are the origin of the deviations.

In practice, when a simulation is designed with certain values for the temperature gradient, mean temperature, system size, and solvent parameters, the exchange value τ_{ex}/n_{ex} is calculated. This value needs to be an integer, and τ_{ex} will be chosen as small a possible. The temperature gradient relaxes in between the velocity exchanges and the stationary temperature profile has to be kept. This means that it would not be reasonable to perform 100 exchanges every

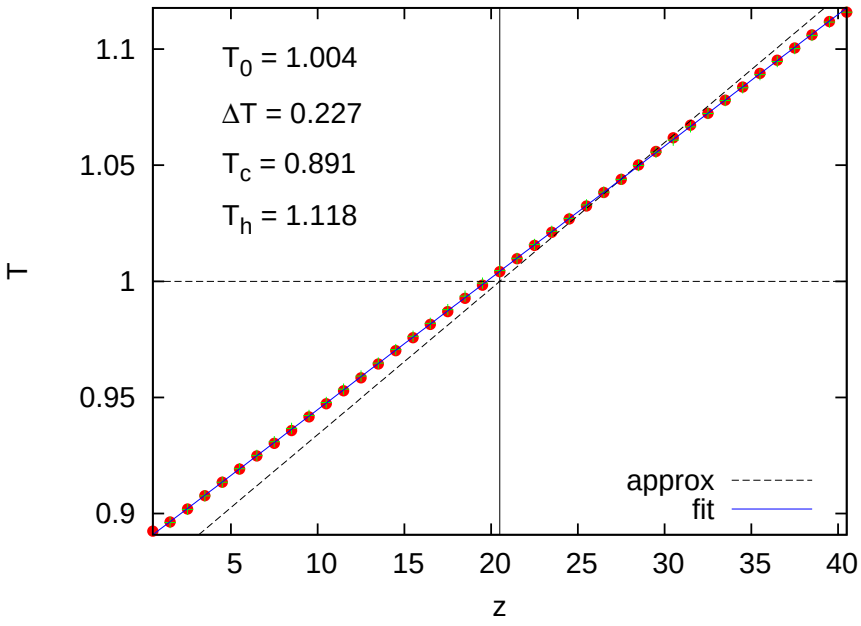

Figure 3.9: Temperature profile obtained from the velocity exchange algorithm. Symbols correspond to the measured temperatures. Solid line is a fit to the data, dashed-line is the estimated temperature profile from Eq. (3.16).

100 steps instead of one exchange in every step, even given the computational advantages.

To conclude, we can say that the application of the velocity exchange algorithm employed until now in Molecular Dynamics, provides a useful tool to study the effect of temperature gradients with open boundary conditions in combination with the MPC solvent. It should be noted, that given the artificial exchange of energy between the hot and cold slabs, these are usually disregarded from the analysis, similarly as it is done with the two previous boundary conditions. The velocity exchange is also responsible of perturbing the propagation of hydrodynamic interactions between the two half boxes and subsequent periodic images. The disruption is though not complete. In each velocity exchange, only a very small percentage of particles are affected, such that a big part of the hydrodynamic interaction will normally propagate. It will therefore be of interest to discuss the effect of the boundary layers in each particular application of the method.

3.3 Thermal diffusivity

In a series of papers Ihle, Tüzel, and Kroll have studied in great detail the transport properties of the MPC solvent [45, 46, 47, 48, 49, 112, 111]. By using a discrete-time projector operator technique, they calculate Green-Kubo relations to characterize the MPC transport coefficients. The shear viscosity has been measured by them and several other groups [47, 48, 54, 99, 120] showing in all cases very good agreement between analytical theory and simulation results for the whole range of MPC parameters. On the other hand, the simulation measurements of the self-diffusion coefficient shows a noticeable discrepancy for the MPC parameter region where the Schmidt number is larger (small collision times h, and large rotation angle α) [99, 100]. This was attributed to the breakdown of the validity of the molecular chaos approximation employed in the theory. Molecular chaos assumes the absence of particle correlations, which are the origin of the building up of the hydrodynamic interactions.

Thermal diffusivity k_T has been measured in equilibrium simulations by two types of measurements [47, 48, 49, 111]. One is performed by characterizing the dynamic structure factor, where information about thermal diffusivity and the

sound attenuation is obtained. Independent measurements of k_T are obtained by the quantification of the correlation of the entropy density. Most of the measurements have calculated the collisional contribution, k_T^{coll}, where very good agreement has been obtained. Simulations in the presence of a temperature gradient have been reported by Pooley and Yeomans [89] in which measurements of k_T agree well with the analytical for large values of the rotation angle α, although only the kinetic contribution is taken into account.

The analytical expression for the thermal diffusivity has two contributions, $k_T = k_T^{kin} + k_T^{col}$ that read,

$$k_T^{kin} = \frac{k_B T h}{2m}\left[\frac{d}{1-cos(\alpha)} - 1 + \frac{2d}{\rho}\left(\frac{7-d}{5} - \frac{1}{4}\csc^2(\alpha/2)\right)\right] \tag{3.17}$$

$$k_T^{col} = \frac{A_0^2}{h}\left[\frac{1}{3(d+2)\rho}\left(1-\frac{1}{\rho}\right)[1-cos(\alpha)]\right] \tag{3.18}$$

where k_T^{kin} and k_T^{kin} are respectively the kinetic and the collisional contributions. The expressions are valid for $d = 2$ or $d = 3$ dimensions.

We report simulation results in the whole range of parameters, which are performed with temperature gradients induced with the three types of boundary conditions discussed in the previous section. We verify the validity of the analytical expressions where both contributions are taken into account, and compare the performance of the different boundary conditions employed in this work.

In the simulations, we impose a temperature gradient and the flux of energy $\mathbf{j}_q$ is calculated with Eq. (3.11) similar to the previous section. The thermal conductivity κ_T is obtained with with Eq. (3.10) and related to thermal diffusivity k_T as

$$\kappa_T = \rho c_p k_T, \tag{3.19}$$

where $c_p = (d+2)k_B/2$ is the specific heat per particle at constant pressure. The energy exchanges ΔE in Eq. (3.11) are now exactly calculated as the kinetic energies of the solvent before and after the contact with each heat bath. The exchange in the hot and the cold bath are exactly the same by construction in the case of the velocity exchange periodic boundary conditions. When the temperature gradient is simulated in combination with the walls, both quantities are not exactly the same, but very similar on average.

Simulations with the different types of temperature gradient implementations described in the previous sections have been performed. The agreement among the different implementations is in general quite good. The simulations have

been run with 10^5 steps for equilibration and 10^5 steps to collect the data for ΔE. The system size is $L_x = L_y = L_z = 40$ for the simulations using virtual particles and thermostat. In simulations with the velocity exchange algorithm we have used $L_z = 80$.

Fig. 3.10 displays the dependence of the thermal diffusivity k_T as a function of the rotation angle α. k_T shows to be almost constant for high values of α and the agreement with the theoretical approach seems reasonable. Fig. 3.11 shows the dependence of k_T on the collision time h, which is related to the mean free path $\lambda/a = h\sqrt{k_B\overline{T}/m}$. The zoom-in for small h values indicates a certain trend in the data deviation.

In order to precisely quantify the quality of the agreement, we present in Fig. 3.12 the relative deviation of the simulated thermal diffusivity $k_{T,sim}$ with respect to the analytical approach k_T in Eq. (3.18). The analytical approach shows to underestimate the simulated values in about 10%, but up to 20% in some cases. Interestingly, the deviation shows to significantly decrease with

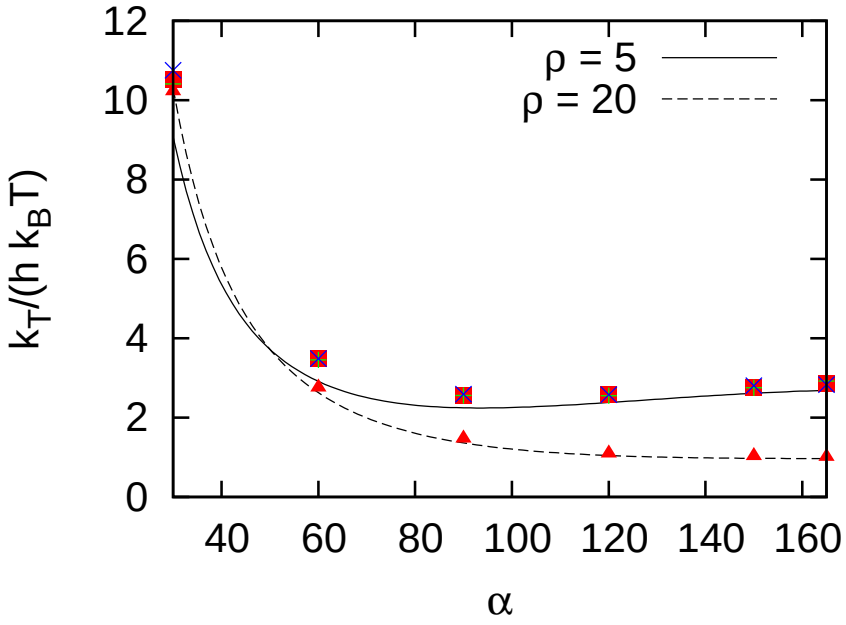

Figure 3.10: Dimensionless thermal diffusivity as a function of α, with $h = 0.1$. Lines correspond to the analytical approach in Eq. (3.18) and symbols to simulation results. Red symbols relate simulation with velocity exchange algorithm, green symbols to walls with virtual particles, and blue symbols to walls with thermostats.

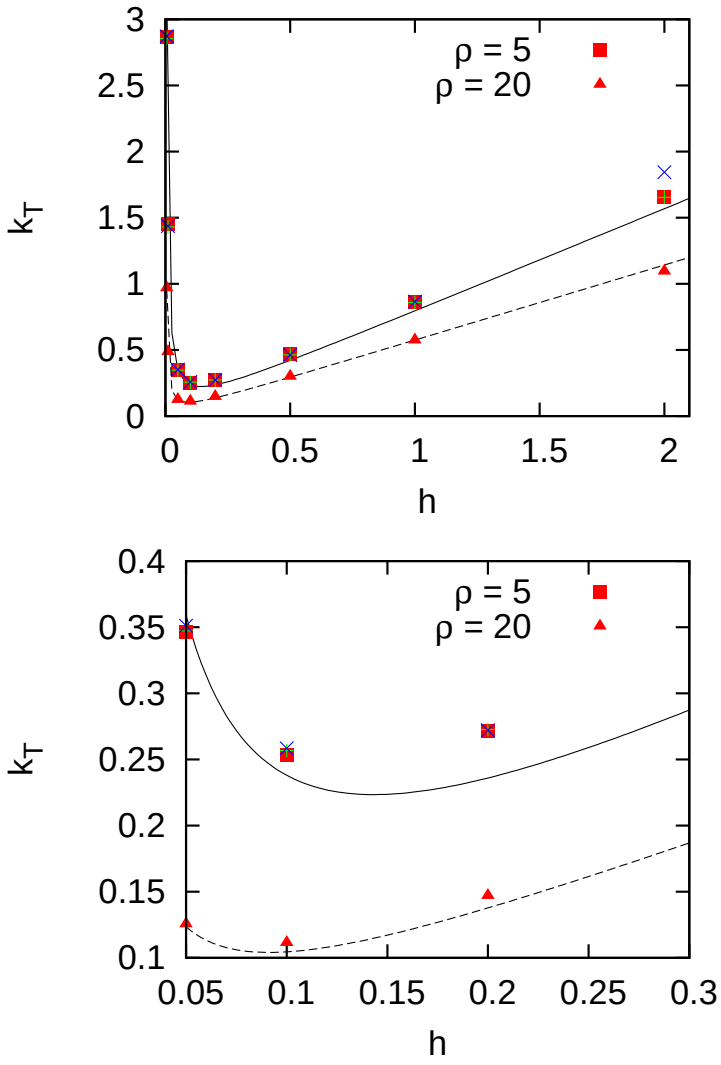

Figure 3.11: Dimensionless thermal diffusivity as a function of h, with $\alpha = 120°$. Symbols and lines similar to Fig. 3.10. The second plot is a zoom-in for small h values.

increasing density. Furthermore, the deviation shows to have a maximum for rotation angles between 60° and 120°, and for collision times between $h = 0.1$ and $h = 0.2$.

The expressions for the heat diffusivity in Eq. (3.18) are of $\mathcal{O}(1/\rho)$ for large values of ρ as reported by Ihle *et al.* in Ref.[49]. This is in contrast to the calculations for viscosity. Higher order terms can be calculated for k_T [49]. This are,

$$k_T^{col} = \frac{A_0^2}{h}\left[\frac{1}{3(d+2)\rho}\left(1 + e^{-\rho}(\ln\rho - 1) - \frac{1}{\rho} - \frac{1}{\rho^2} + O\left(\frac{1}{\rho^3}\right)\right)[1 - cos(\alpha)]\right]. \tag{3.20}$$

In Fig. 3.13, the relative deviation between simulated thermal diffusivity and the expression in Eq. (3.20) is displayed. The additional terms do not really improve the agreement and the differences with the comparison with Eq. (3.20) are quite minimal.

Similarly to the transport of mass characterized by the self-diffusion, it seems that the molecular chaos approximations performed to characterize the transport of energy produce significant errors in the estimation of the heat diffusivity in the region of small α, ρ, and h values. In spite of the deviations, the analytical values are reasonable, and the energy transport can be easily characterized within the MPC solvent. This puts the method forward as an attractive tool to study mass and energy transport of soft matter systems in the presence of a temperature gradient.

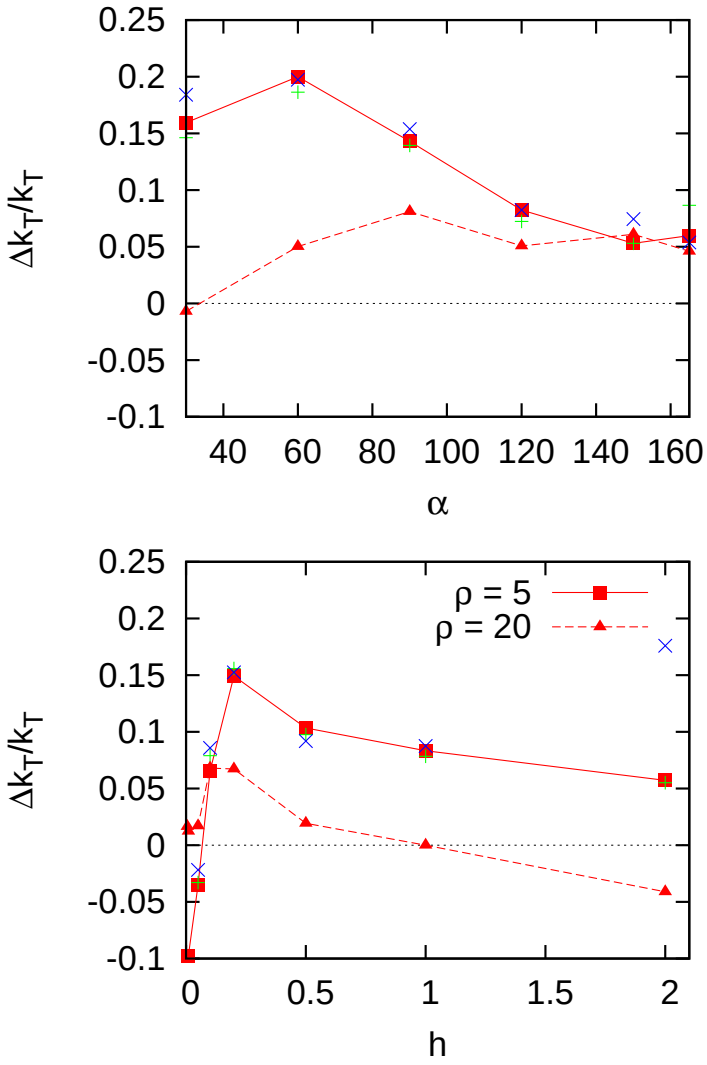

Figure 3.12: Relative deviation $\Delta k_T = (k_{T,sim} - k_T)/k_T$ of the simulated thermal diffusivity $k_{T,sim}$ with respect to the analytical approach k_T in Eq. (3.18). Symbols and parameters are similar to Fig. 3.10 and Fig. 3.11. Red lines are guides to the eye and the zero line corresponds to a perfect agreement.

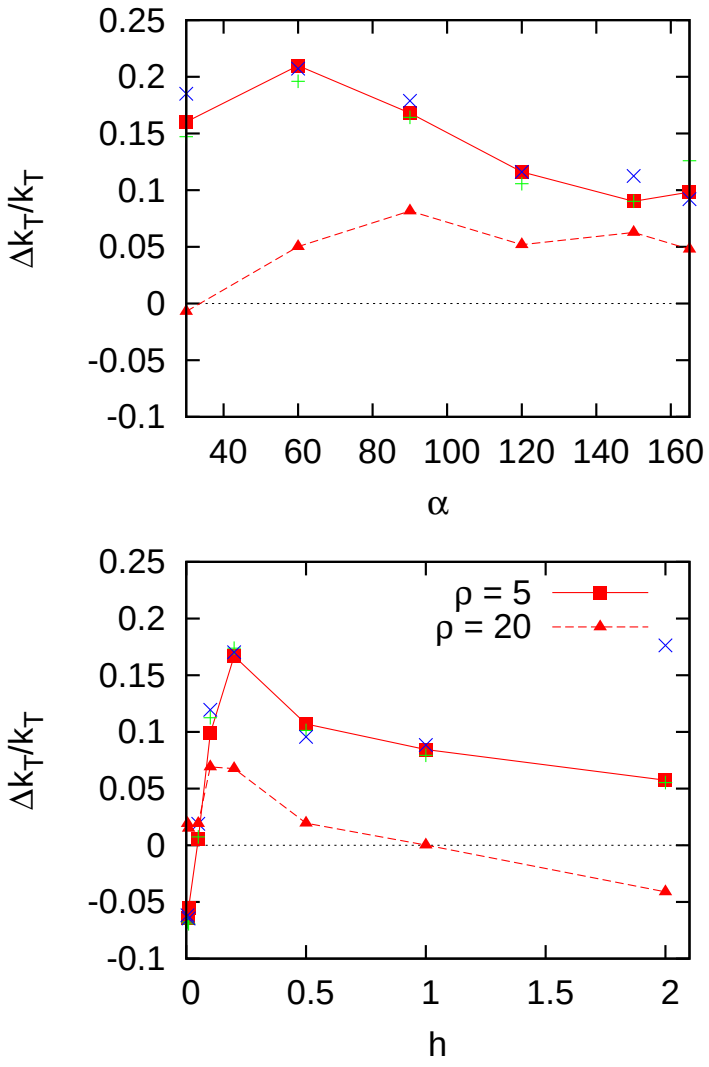

Figure 3.13: Relative deviation with respect to the higher order analytical approach of k_T in Eq. (3.20). Symbols and lines similar to those in Fig. 3.12.

4 Concentrated colloidal suspensions

4.1 Introduction

Most of the existing work on thermodiffusion is performed in the regime of very dilute systems, where the interactions between macromolecules are not important. Only a small number of theoretical and experimental investigations focus on strongly interacting systems and these studies conclude that there is a pronounced concentration dependence of the thermodiffusive behavior. Three of these studies are following mentioned. Experiments with micellar systems [86] display a linear dependence of the Soret coefficient on concentration, this dependence is reversed with the addition of surfactant. Measurements on polystyrene solutions [94] show a strong dependence of the thermodiffusive properties. The approach of this system to the glass transition leads to sharp decay of both D_c and D_T, while the Soret coefficient decreases slowly with the concentration, insensitive to the glass transition. More recently, the contribution of inter-colloidal interactions to the thermal diffusion coefficient has been studied theoretically [19, 20] using a microscopic approach. The temperature dependence of the potential of the mean-force was shown to give rise to sign changes of the Soret coefficient on changing temperature and/or concentration under appropriate conditions. Experiments with colloidal suspensions of varying interactions [77] have shown a reasonable agreement with the theory at low concentrations. Nevertheless, the contribution of the inter-colloidal interactions or *collective contribution* is found to be much less important than the contribution of the colloid-solvent interaction or *single particle contribution*. Furthermore, the theory is developed for a regime of low volume fractions. A detailed study of the collective contribution to the thermodiffusion of colloidal systems by means of computer simulations is therefore essential to understand these systems.

In this work, simulations of concentrated systems are performed with different

inter-particle interaction potentials. The employed model disregards single particle effects becoming an ideal candidate to study the importance of collective interactions in the thermodiffusion phenomena. In this chapter we first carefully discuss and reanalyze the experimental data that we can compare with. Second, the simulation model and the procedure to perform the measurements is introduced, and third the simulation results are presented. The effects of the different characteristics of the interaction potentials are separately analyzed, like the effect of the hardness of the repulsion potential, the range or the strength of the attractive interaction.

4.2 Experiments on colloidal suspensions with different volume fractions

In the experimental investigation of Ning *et al.* [77], the thermal diffusion behavior of coated colloids in toluene (a solvent commonly used to dissolve paints) as a function of the volume fraction has been analyzed at different temperatures. The coating consists of octadecyl chains with a length of 18 carbon groups, what can be thought of as a brush covering the colloid. The length of the brush hairs corresponds to roughly 1 % of the colloid size. The coating has a temperature dependent behavior and can change the properties of the colloids. At low temperatures, the attached brushes are in a collapsed state and the colloid core determines the interactions among the colloidal particles. At high temperatures, the brushes tend to be extended and screen interactions which arise from the core. The core interactions are essentially attractive and the coating of the colloids is typically employed to stabilize the suspension. Therefore, at high temperature the colloid-colloid interactions are close to a hard sphere like behavior, whereas at low temperatures they are attractive at short distances. Then the range of the attractive potential, is in the order of the thickness of the brush, 0.3 nm, while the range of the repulsion corresponds to the particle radius, 27 nm.

The theory of Dhont [19, 20] predicts that colloids with hard sphere interparticle interactions, at low concentrations, display an approximately linear decay of the Soret coefficient with the volume fraction ϕ that can be described by

the expression,

$$S_T^{low} = \frac{1}{T}\frac{1-0.35\phi}{(1-\phi)(1+1.45\phi)} + \frac{D_{T,sing}}{D_0(1+1.45\phi)} \quad (4.1)$$

$$\simeq \frac{1}{T}(1-0.80\phi) + S_{T,sing}(1-1.45\phi), \quad (4.2)$$

where D_0 is the translational diffusion coefficient in the limit infinite dilution. Here $D_{T,sing}$ and $S_{T,sing}$ refer to the single particle contribution of the thermal diffusion and the Soret coefficients respectively. These are the coefficients that one would measure at infinite dilution where the colloid-colloid interactions are absent. The single particle contribution relates to specific interaction of the colloidal interface and the solvent, which are in general temperature dependent.

Experiments at different temperatures and volume fractions of colloids are performed by Ning *et al.* [77]. The experimental results of the Soret coefficient are summarized in Fig. 4.1 a. The range of concentrations goes from the very dilute solutions with about 1 % volume fraction of colloids up to 30 % volume fraction. In the range below 10 % the *magnitude* of the Soret coefficient decreases slightly in all cases. In this regime the experimental data is compared to the theoretical results in Eq. (4.1) shown as solid lines. This comparison allows to determine the values of the single particle contribution $S_{T,sing}$ in Eq. (4.2), and extrapolation of zero concentration $S_T(\phi = 0)$ can also be straightforward obtained from Eq. (4.2). Both values are presented in Fig. 4.1 b, where the strong temperature dependence can be observed. Similar behavior is experimentally observed in colloids in aqueous solutions [7] in the limit of very low concentrations. The difference between $S_{T,sing}$ and $S_T(\phi = 0)$ corresponds to the ideal gas contribution [8].

For larger volume fractions, the theory of Dhont to describe the Soret coefficient does not apply. In Fig. 4.1 a, it can be seen that for volume fractions larger than 10 % S_T becomes a decreasing function in all cases, eventually even displaying a sign change. Furthermore, the functional form of all these decays can be universally described by a logarithmic decay

$$S_T^{high} = -0.01 \ln \phi + S_{T,0}^{high}. \quad (4.3)$$

The extrapolated value at zero concentration $S_{T,0}^{high}$ includes all the temperature dependence of S_T^{high} and is displayed in Fig. 4.1 c.

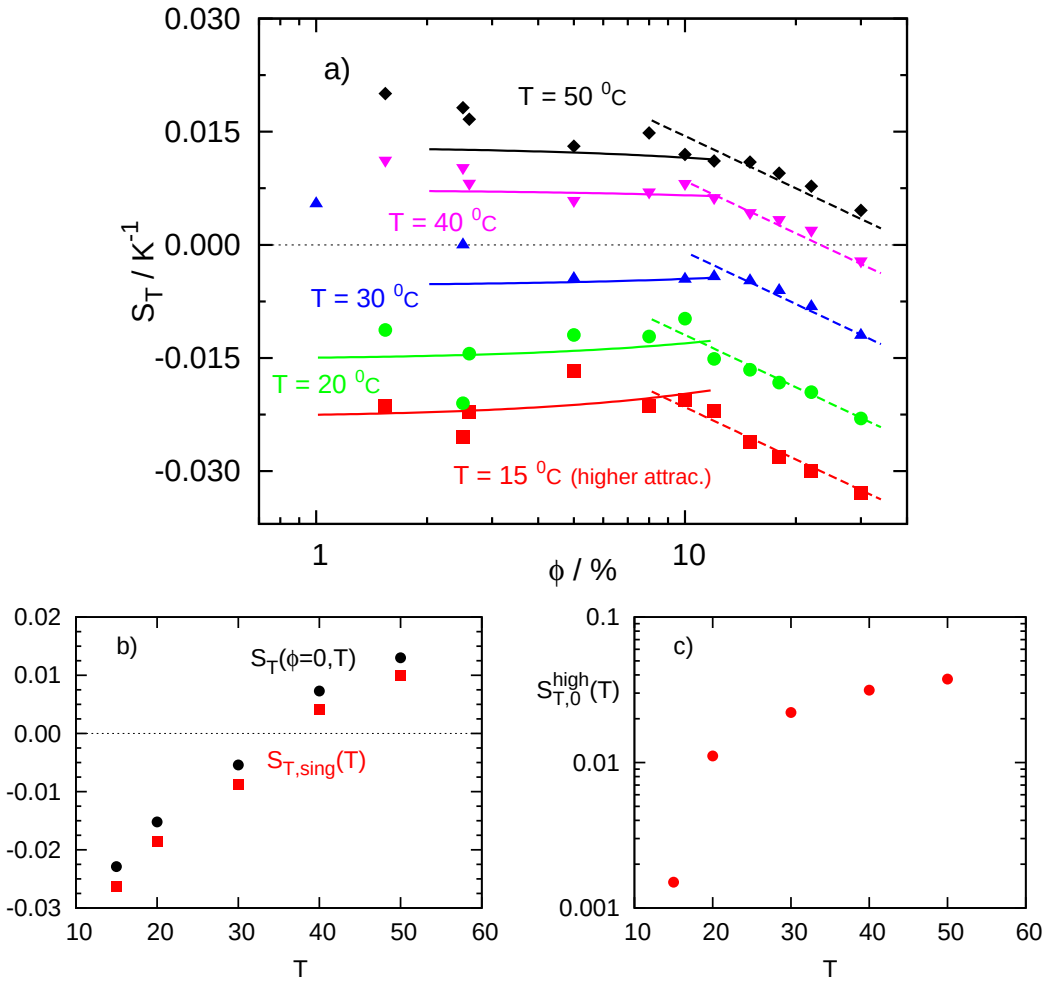

Figure 4.1: a) Soret coefficient for octadecyl coated silica particles in tolune as a function of the volume fraction ϕ for different values of the average temperature. Solid lines are a fit to Eq. (4.1) for low ϕ, and dashed lines a fit to Eq. (4.3) for high ϕ. b) Values of the Soret coefficient at the limit of zero volume fraction, and the single particle contribution as a function of the temperature, obtained from the fit of the data to Eq. (4.1). c) Temperature dependence contribution of S_T at high ϕ values are obtained from a fit of the data to Eq. (4.3). (Data by courtesy of S. Wiegand).

As shown in Fig. 4.1, single particle effects have a very strong contribution to the Soret coefficient in all the range of volume fractions. It is though interesting to find a representation in which these effects are disregarded such that the behavior of the purely collective effects can be investigated. With this purpose, Fig. 4.2 compares the different sets of data displacing them all to the same vanishing value at limiting zero concentration.

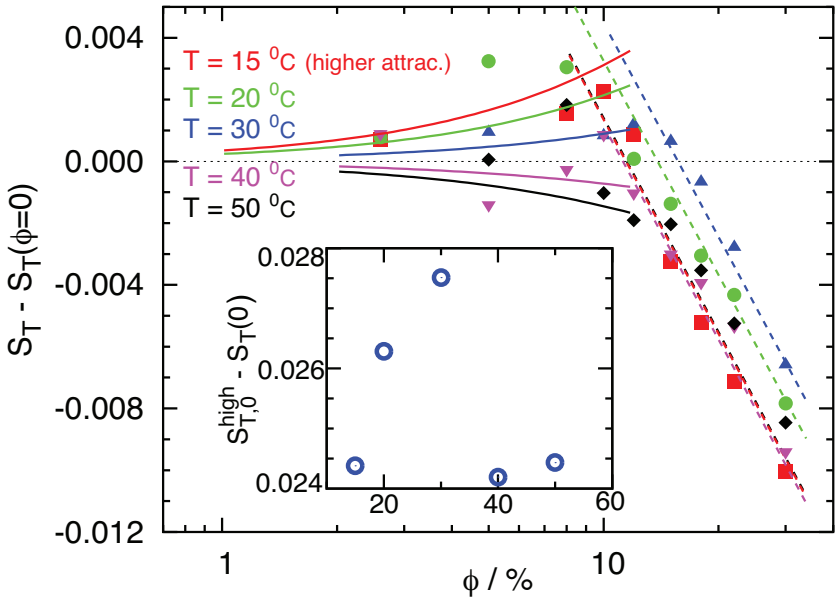

Figure 4.2: Soret coefficients in Fig. 4.1 as a function of the volume fraction ϕ displaced to the vanishing value at limiting zero concentration. Lines correspond to those in Fig. 4.1. Inset: differences of the Soret coefficients extrapolated to zero concentration for low concentrations in Eq. (4.2) and high concentrations in Eq. (4.3). (Data by courtesy of S. Wiegand)

At low volume fractions, the collective contribution to the Soret coefficient in Fig. 4.2 shows to increase in magnitude with increasing temperature, which is only due to the displacement and consequent sign change. This trend is observed from the analytical curves from Eq. (4.1) in Fig. 4.2 since the relative error of experimental data in this representation is magnified in the low concentration regime. Apart from the differences directly inferred by the different average temperatures, the employed octadecyl coated silica particles are characterized by having temperature dependent inter-colloidal interactions. Ning *et al.* have characterized in Ref.[77] that suspensions at low temperatures (15 ^{0}C) have high

attractive interactions, while suspensions at higher temperatures (50 ^{0}C) display a typical hard sphere behavior. With this consideration two main conclusions can be drawn from the data at low concentrations in Fig. 4.2. The first one is that increasing the strength of the attraction increases the value of the Soret coefficient, or equivalently, with increasing attraction the colloids accumulate more effectively in the cold areas. The second conclusion is consequence of the first one, and it is that the collective contribution to the Soret coefficient is typically negative for purely repulsive colloids and positive for colloids with a short range attraction.

More puzzling is the observed behavior of the collective contribution to the Soret coefficient in the regime of large colloidal volume fractions. The logarithm decay described in Eq. (4.3) does trivially remain, but the dependence is non-monotonous with changing temperature. This non-monotonous dependence can be observed directly in the data in Fig. 4.2, and in the differences of the Soret coefficients extrapolated to zero concentration for low concentrations in Eq. (4.2) and high concentrations in Eq. (4.3), as displayed in the inset of Fig. 4.2. The origin of this non-monotonicity is not known, but seems to be more an artifact than a real physical effect. A possible explanation is the poor experimental precision in determining the contribution to the Soret coefficient in the limit of zero concentration, which was in the not the main goal of these experiments. More precise experimental data, and/or simulation results, can contribute to clarify whether the behavior at high concentrations depends on the interaction, and in that case if it has the same, or opposite trend as in the low concentration regime. Namely, that increasing attractive interaction helps the colloids to accumulate more effectively in the cold areas. Another possible explanation is that the performed separation of the single particle contribution to the Soret coefficient is not completely accurate. For example, this contribution is determined at the limit of vanishing concentration and is assumed not to change with increasing concentration. The well known strong dependence with temperature invites to consider that the interactions between the colloidal interface and the surrounding solvent may change with concentration, although we do not have any related information.

4.3 Simulation model

Concentrated colloidal suspensions are simulated by a hybrid model that considers interactions between colloids by explicit potentials, and the interactions among solvent particles and between solvent and colloids by means of the mesoscopic technique of MPC.

4.3.1 Colloid-solvent interactions

The MPC interaction of the colloids with the surrounding solvent is performed together with the MPC solvent-solvent interactions. The interchange of energy and momentum occurs in the collision step (see chapter 2), in which the colloids are considered as point particles of different mass than the fluid particles. Hence the calculation of the center of mass velocity by means of Eq. (2.9) has to be replaced by

$$\boldsymbol{v}_{cm} = \frac{\sum\limits_{i|\boldsymbol{r}_i \in Cell} m_i \boldsymbol{v}_i(t)}{\sum\limits_{i|\boldsymbol{r}_i \in Cell} m_i}. \tag{4.4}$$

The fact that colloid-solvent interactions do not have any exclude volume potential implies that the solvent particles can penetrate the colloids since they perceive them only as heavy point particles. A consequence is that local effects are not taken into account. One example of such local effects are lubrication forces, which arise from the confinement of a fluid between solid surfaces. Another example are the specific interactions of the colloidal interface and the surrounding solvent, that determine the single particle contribution to the Soret coefficient.

In spite of its clear drawbacks, this coupling has shown to capture the dynamics of solute particles [100] and has been used in similar fashion to correctly describe some aspects of concentrated colloidal solutions [100, 122]. One of the most successful characteristics of the method and this coupling is that hydrodynamic interactions are properly taken into account. This has been verified in dilute polymer solutions [99, 73] simulated with this coupling, and it has been frequently employed in systems like rod-colloids [121, 98, 103, 63], star polymers [101, 102], or self-propelled structures [127, 26, 27], among others.

The main advantage of this coupling between colloid and solvent is that is computationally very efficient, since solvent-colloid explicit forces are not present. For each colloid there are normally many solvent particles and the calculation

of interaction forces can be, in CPU terms, the most demanding part of the simulation.

On the other hand, we have to consider that in this chapter we study the effects of the temperature gradients in concentrated colloid solutions. This coupling can be understood as a way of decoupling the collective effects in thermodiffusion, from the purely single particle effects, providing useful information.

4.3.2 Colloid-colloid interactions

The colloids interact among themselves with an explicit potential and their mutual forces are calculated with MD which is incorporated into the MPC algorithm as explained in chapter 2. The colloid-colloid interactions are given by a pair potential $U_{cc}(\boldsymbol{r}_i, \boldsymbol{r}_j)$ which is varied to analyze the influence of the differences between potential, like the softness or the strength of the attraction. In this way, we have used both purely repulsive potentials, and repulsive in combination with attractive potentials. We employ basically two types of functional forms for the potentials. One is the Lennard-Jones type potentials given in chapter 2 in Eq. (2.4) and the other in Eq. (2.5).

In order to more accurately match the experimental interactions in Ref. [77], we have used another type of potential which can eventually become very short ranged. To this potential we refer as *sticky* potential, $U^{sticky}(r_{ij})$, in correspondence to the *sticky spheres* in experiments. The hydrodynamic radius of the colloids in the experiments is 27 nm and the range of the attractive interactions is estimated to be around 0.3 nm, which corresponds to a ratio of approximately 1% of the particle radius.

Similarly to the Lennard-Jones potential, the sticky potential is composed by two terms, a repulsive core and an attractive tail. The repulsive core is given by

$$U_r^{sticky}(r_{ij}) = \lambda_r \left(\frac{\sigma}{r_{ij}}\right)^{48} \tag{4.5}$$

and the attractive part that is chosen to reproduce the functional form of depletion interactions [70],

$$U_a^{sticky}(r_{ij}) = -\lambda_a \left[1 - \frac{3}{4}\left(\frac{r_{ij}}{a}\right) + \frac{1}{2}\left(\frac{r_{ij}}{2a}\right)^3\right]. \tag{4.6}$$

The coefficients λ_r and λ_a determine the relative strength of the two contributions. The colloid diameter is estimated by σ, and the range of the attractive

part of the potential is determined by a. The attraction range will be varied in the simulations from values comparable to the experimental conditions, to values similar to the simulation standard Lennard-Jones. The total potential is given by

$$U_{cc}^{sticky}(r_{ij}) = \epsilon \left[U_r^{sticky}(r_{ij}) + U_a^{sticky}(r_{ij}) - U_r^{sticky}(r_c) \right], \tag{4.7}$$

where ϵ is the strength of the potential and r_c the cutoff radius.

We have used the parameters in Table 4.1 for the simulations in Sect. 4.4.

r_c/σ	λ_r	λ_a	a/σ
1.0365	4.	1940.	0.522
1.1	1.3	185.	0.55
1.2	1.0	43.	0.6

Table 4.1: Parameters to construct sticky potentials.

4.3.3 Simulation setup

Simulations are started by arranging the colloidal particles on a grid in order to make sure there is no potential overlap. Thus the initial total energy of the system is only kinetic and corresponds to a temperature T_0. The maximum volume fraction which can be achieved in this way is the one of simple cubic packing of 52%, which is not a constraint for our purposes. Similar to the experimental values we have varied the volume fraction of colloids from $\phi_c = 0.1\%$ to $\phi_c = 30\%$.

In order to implement the temperature gradient, the velocity exchange algorithm has been used along the z-direction. This method is described in chapter 3, and has shown to be the most appropriate for our purposes. The employed temperature differences are small enough to ensure that the temperature and density profiles of the individual components are linear. In this setup, the simulation box is divided in two halves as illustrated for a colloidal suspension in Fig. 4.3.

The MPC parameters for the solvent are: time step $h = 0.1$, number of fluid particles per cell $\rho = 5$ and the collision angle is $\alpha = 120°$. The initial temperature is $T_0 = 2$ in all simulations unless stated different. The initial and average temperature are not the same but almost.

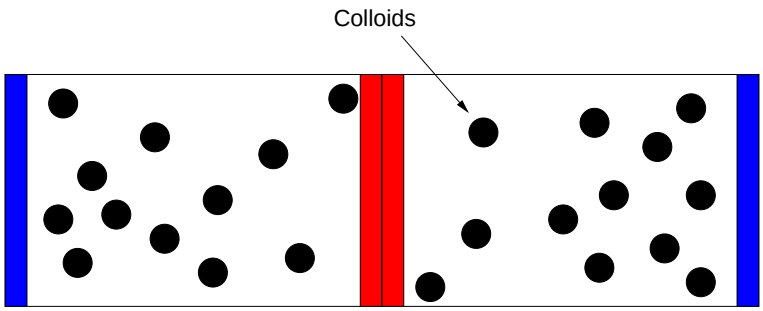

Figure 4.3: Simulation box for concentrated colloidal suspension. Example distribution of colloids with an excess on the cold side.

The simulation box size is $L_x = 30$, $L_y = 30$ and $L_z = 40$ for the purely repulsive potentials and $L_x = 10$, $L_y = 10$, $L_z = 40$ for the attractive potentials. The system size for the attractive potentials have been chosen smaller because the computational effort for the colloid-colloid forces is greater due to the larger cut off radii. The employed diameter of the colloids is $\sigma_{cc} = 1.0\ a$ and the mass is $m_c = 5.0$; this is the value that matches the mass of the fluid in one collision box and has been shown to be an appropriate value to enhance the effect of hydrodynamic interactions [100].

4.3.4 Determination of the Soret coefficient

In order to determine the Soret coefficient we measure the temperature profile and the mass distribution of colloids and solvent within the simulation box. The procedure is very similar to the one described in chapter 3. The simulation box is subdivided in slabs, that for convenience are chosen to have thickness a, this is the length of MPC collision box. In each slab, we calculate the number of colloids $N_c(z)$ and of fluid particles $N_f(z)$. The densities are then given by the number of particles per cell of each component k, *i.e.* $\rho_k(z) = N_k(z)/L_x l_y$, where $L_x l_y$ is the is the volume of the slab, determined by the two directions perpendicular to the temperature gradient. The temperature profile is determined from the kinetic energy of the fluid particles. The profiles are averaged over simulation steps such that local fluctuations in temperature and density are averaged out. For further analysis, the first two boundary slabs in all cases, where the velocity exchange is performed, are disregarded.

The average density ρ_k^0, is the density that the system would have in the absence of a temperature gradient. It is instructive to show in which percent-

age each component varies its density with respect to the average value. The normalized relative density is then defined as

$$\Delta\rho_k(z) = \frac{\rho_k(z) - \rho_k^0}{\rho_k^0}. \tag{4.8}$$

Fig. 4.4a shows a typical temperature profile. Fig. 4.4b and Fig. 4.4c are two examples of relative density profiles of the solvent and colloids. The profiles are only shown for the left side of the bi-periodic simulation box, although the averages consider both boxes. The density profile of the fluid is determined by the ideal gas equation of state, as already reported in chapter 3, which essentially does not change due to the presence of the colloids.

In order to characterize the strength of the response to the temperature gradient, we determine the Soret coefficient which is determined from the gradients of the mass fraction and temperature

$$S_T = -\frac{1}{w_c^0(1 - w_c^0)} \frac{\nabla_z w_c}{\nabla_z T}, \tag{4.9}$$

where w_c is the mass fraction of colloids, defined as,

$$w_c(z) = \frac{\rho_c(z) m_c}{\rho_c(z) m_c + \rho_f(z) m_f}. \tag{4.10}$$

The average colloid weight function is then $w_c^0 = \rho_c^0 m_c / [\rho_c^0 m_c + \rho_f^0 m_f]$. It is straightforward to prove that,

$$\Delta\rho_c(z) > \Delta\rho_s(z) \Leftrightarrow w_c(z) > w_c^0(z). \tag{4.11}$$

The resulting normalized relative mass fractions are shown in Fig. 4.4d and Fig. 4.4e. If the colloids have a relative density variation larger than the solvent in the cold part of the system, the weight fraction decreases with increasing temperature, or similarly that $S_T > 0$. This is the case displayed in Fig. 4.4b and Fig. 4.4d, while the reciprocal situation can be seen in Fig. 4.4c) and Fig. 4.4e).

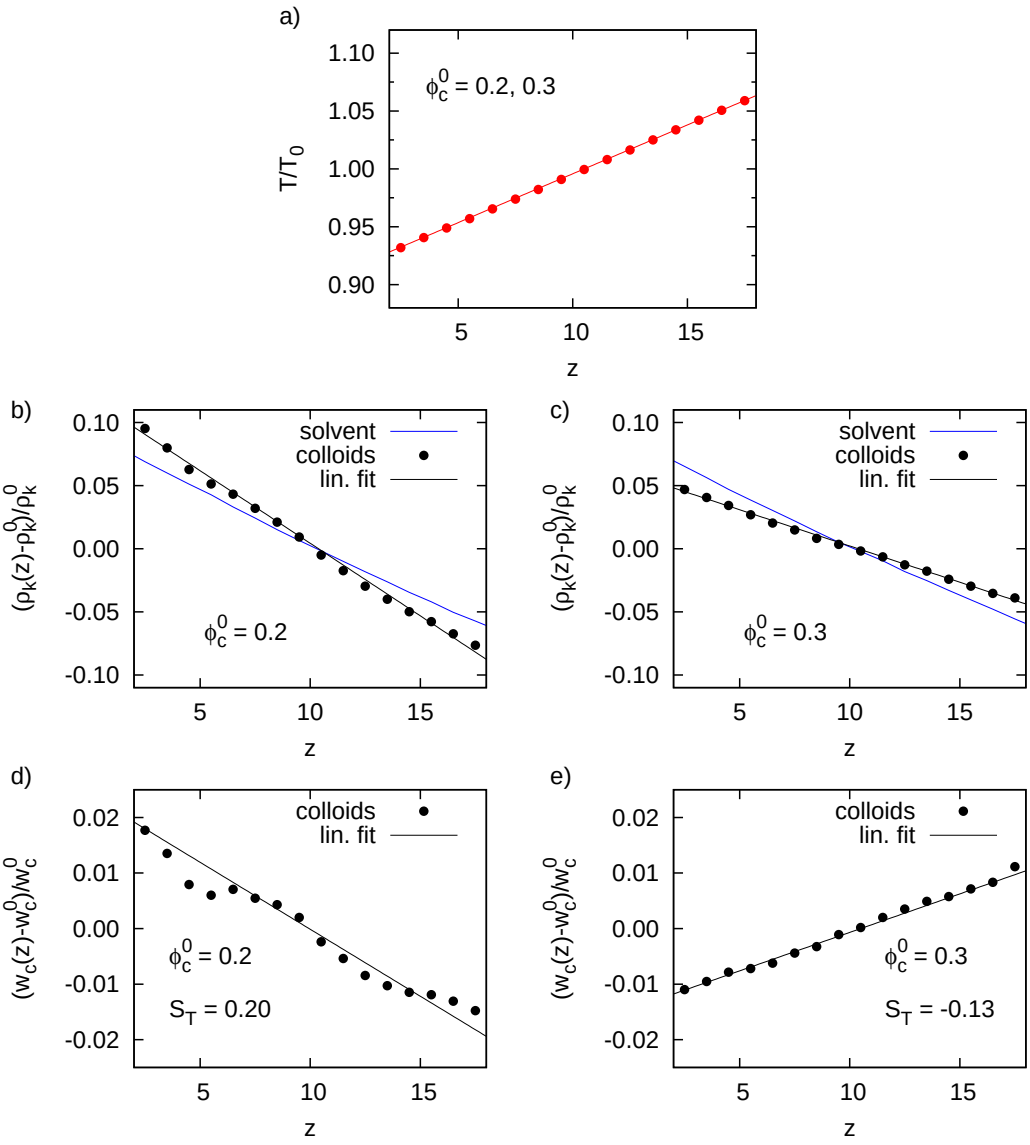

Figure 4.4: Profiles for concentrated colloids suspensions interacting with the LJ 12-6 potential. a) Temperature profile. b), c) Normalized relative density profiles of solvent and colloids. d), e) Corresponding normalized weight fraction profiles. b) and d) $\phi_c^0 = 0.2$, example for an excess of colloids on the warm side. c) and e) $\phi_c^0 = 0.3$, excess on the cold side.

4.3.5 Condensation effects

We report now an effect that can arise in simulations with attractive colloid interactions due to the non-homogeneous distribution of temperature. In simulations at lower temperatures and the same interaction strength ϵ a phase separating behavior was observed for large volume fractions. This is because the temperature and volume fraction can be below the critical point in the low temperature region of the system which leads to a condensation of the colloids. MD simulations of Vliegenthart *et al.* [115] of Lennard-Jones fluids have shown that the critical point of a LJ 12-6 fluid is at $T_c = 1.316$ and $\phi_c = 0.165$. In dimensionless units used in MD this corresponds to $T_c^* = T_c/\epsilon = 1.316$ and $\rho_c^* = \phi_c/\phi_{sc} = 0.361$, where $\phi_{sc} \approx 0.52$ is the simple cubic packing fraction. Below the critical point the system is in the liquid-gas coexistence regime and a phase separation due to the temperature gradient is observed as can be seen in Fig. 4.5. In this example where the average temperature is below the critical temperature the volume fraction profile of the colloids is not linearly changing, but drops abruptly indicating a liquid phase of colloids on the cold side and a gas phase on the warm side.

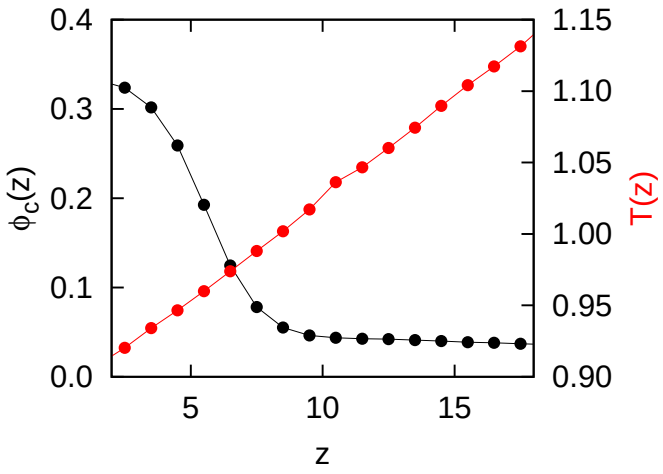

Figure 4.5: Phase separation of colloids in liquid-gas coexistence regime below critical point with LJ 12-6, $\epsilon = 1.0$, $\phi_c = 0.1$ and $T_0 = 1.0$. The volume fraction on the cold side of the system is $\phi_c \approx 37\%$ corresponding to a reduced density of $\rho^* \approx 0.75$, which indicates a liquid state. On the hot side we have $\phi_c \approx 3\%$ corresponding to a density of $\rho^* \approx 0.06$ indicating a gas phase.

In principle it is also possible that the colloids form clusters or droplets, a fact which might not be easily observed in density profiles. For critical simulation parameters (i.e. high attraction strengths and low temperatures) we have checked that there are no unusual accumulations of colloids in 3D plots of the final particle positions after the simulations. We assume that this check is sufficient although a more exhaustive analysis would require the study of pair correlation functions.

4.4 Simulation results

To study collective effects in the thermodiffusion of colloidal suspensions, we perform simulations in a large range of colloidal volume fractions for various colloid-colloid interactions. We following discuss the different characteristics of the interactions and their effects on the Soret coefficient. These characteristics are the purely repulsive or attractive nature of the interaction, the steepness of the repulsion, the range, and the strength of the attractive interaction.

4.4.1 Attractive vs. repulsive colloid-colloid interactions

The first feature that we discuss is the difference between a purely repulsive interaction and an accompanying a short-range attraction. For this purpose, we employ the different types of Lennard-Jones potentials given in chapter 2 in Eqs. (2.4) and (2.5).

Fig. 4.6 a displays the employed repulsive rLJ 12-6 and attractive LJ 12-6 potentials. The potential strength is fixed to $\epsilon = 1$. Fig. 4.6 b shows the measured Soret coefficient with these potentials. The most remarkable feature is that repulsive interactions always lead to a larger mass fraction of colloids on the hot side and therefore a negative Soret coefficient. This is with the exception of very low average volume fractions of colloids that will be discussed in the next section. Attractive interactions favour the colloids to accumulate more efficiently in the cold side leading to positive and significantly larger values of the Soret coefficient.

For repulsive interactions, the Soret coefficient decreases with increasing volume fraction. Since the values are always negative, this means that the magnitude increases, indicating a stronger separation of the colloids and solvent for larger colloid concentration. For the attractive interactions checked in this sec-

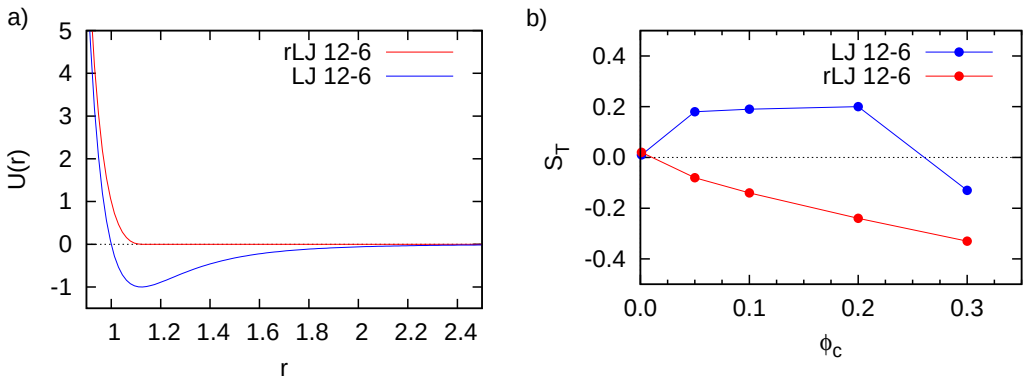

Figure 4.6: a) Repulsive and attractive Lennard-Jones potentials employed for the inter-colloidal interactions. b) Simulated Soret coefficients as a function of the colloidal volume fractions ϕ_c for colloids with the interactions in a).

tion, there is a regime of volume fractions, *i.e.* $5\% < \phi_c < 20\%$ in which S_T does not vary significantly. If this volume fraction is exceeded, the colloids are slowly driven away from their preferential region on the cold temperatures, and in this case the Soret coefficient changes its sign.

The main trend of the results agrees with the experimental findings as shown in Fig. 4.2, and can be explained by the following phenomenological argument. The *excluded volume* interactions do not facilitate an inhomogeneous distribution of the colloids with the temperature gradient. Colloids interacting with purely repulsive interactions have a density gradient smaller than the solvent, such that the Soret coefficient is negative. Increasing concentration translates in smaller density gradients which differentiate stronger from the solvent and therefore have more negative Soret coefficients. On the other hand, the *attractive interactions* favor that colloids eventually can get closer. The cold area in then more favorable since they can approach to each other decreasing their potential energy. This explains that the relative density of colloids in the cold area is higher than the solvent, what translates into a positive Soret coefficient. Increasing colloid concentration makes that the repulsive part of the potential becomes progressively more relevant, what produces a decrease of the Soret coefficient even to negative values.

4.4.2 Limiting cases

MPC binary mixture

As already discussed, the model employed in this chapter essentially disregards the single particle effects, apart for the remaining mass contribution. In order to gain some insight on this contribution, simulations without potential interaction among colloids are performed. In this case, the colloids are reduced to be *heavy particles*, this is MPC particles of larger mass than the solvent particles.

Simulation results of S_T for such MPC binary mixture, and various concentrations are shown in Fig. 4.7. The concentrations are expressed in terms of the heavy particle mass fraction. For comparison, the upper axis displays the volume fraction that the same number of particles would have had with a potential interaction with an excluded volume interaction at distances $\sigma = 1$. The concentration dependence show to be practically negligible, and more importantly, the absolute numbers are one order of magnitude smaller than the ones in which potential interaction between particles are included like those in Fig. 4.6 b. It is furthermore noticeable that the values of S_T are always positive. This agrees with the well described mass effect for Lennard-Jones mixtures [96, 35, 33], that describes that for a binary mixture of particles of different mass, the heavier particle will accumulate more effectively in the cold areas.

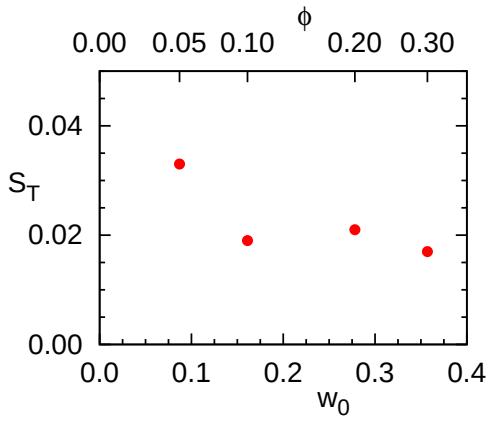

Figure 4.7: Soret coefficient for an MPC binary mixture, as a function of the mass weight of heavy MPC particles w_0. Values in the upper index indicate the corresponding volume fraction for colloids with diameter $\sigma = 1$.

We can conclude that in the simulations with potential interactions shown in the rest of this chapter, the mass effect is always present, although it is weak and does not dependent on the volume fraction, such that is not responsible of the main effects discussed in the chapter.

Low volume fraction limit

We come back now to discuss colloidal suspension with potential inter-particle interactions. In the limit of very low volume fractions, there are no interactions among colloids, such that the values of S_T should be independent of the interaction potential. This is the single particle limit in which S_T is determined by the colloid-solvent interactions. In general, these are interactions of fundamental importance in thermodiffusion, although in the model discussed in this chapter they are essentially disregarded allowing us to study the influence of collective effects.

In order to have a reference value for the low volume fraction limit, simulations with $\phi_c = 0.001$ have been performed with two potentials rLJ 12-6 and LJ 12-6. The obtained values are compared in Table 4.2 together with the result at lowest density of the MPC binary mixture presented in the previous subsection. Values in Table 4.2 show, as expected, to be very similar in spite of the very different interaction among colloids. The S_T values are positive and one order of magnitude smaller than those at higher volume fractions.

interaction	S_T
rLJ 12-6	0.037
LJ 12-6	0.036
MPC binary mixture	0.033

Table 4.2: Values of the Soret coefficient for various interactions at very low concentrations.

High volume fraction limit

In the limit of very high volume fraction of colloids the system will crystallize. In that case, the density of the colloids will be practically constant along the temperature gradient, and the separation will come only from how the solvent adapts to the temperature gradient. The experiments performed by Ning *et al.*

[77] stay far away from that limit. Experimental results of concentrated solutions of polymers [95, 93], present always positive values of the Soret coefficient, which shows a clear decrease close to the gelation density.

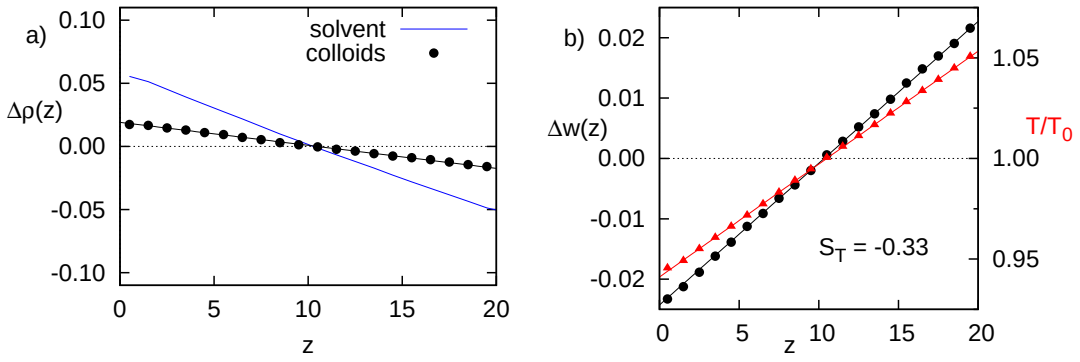

Figure 4.8: Distribution of normalized relative densities and weight fraction of colloids interacting with rLJ 12-6 at $\phi_c = 0.3$.

With the simulation model employed in this work, the separation between solvent and colloids will remain also in the case of colloid concentration at the close packing value. The corresponding value is $S^h_{T,cp} = -0.35$. In Fig. 4.8 it is displayed an example of colloids interacting with repulsive interactions, with the potential rLJ 12-6 at $\phi_c = 0.3$, the highest volume fraction that we have simulated. The resulting Soret coefficient is clearly negative, and the colloid density profile still accumulates in the cold area, although is already close to constant. In all the simulations performed with this model, the colloids accumulate in the cold area. Given the fact, that there is no mechanism that brings the colloids to accumulate in the warm area, we do not expect accumulation in the warm area and therefore any $S_T < S^h_{T,cp}$.

4.4.3 Effect of the repulsion softness

The repulsive interaction between colloids in experiments, and in their counterpart simulated models, can range from a completely hard to very soft interactions. In the hard limit interaction, there is an abrupt transition from no interaction to an infinite repulsion potential. Soft interactions consist in a very weak repulsion at large distances, that becomes progressively stronger, and only diverge when the overlap between colloids is complete.

We investigate the effect of the repulsion softness by repulsive Lennard-Jones

type potentials in Eq. (2.4). An increase of the exponent n is equivalent to an increase of the steepness of repulsion, or decrease of softness, as illustrated in Fig. 4.9 a.

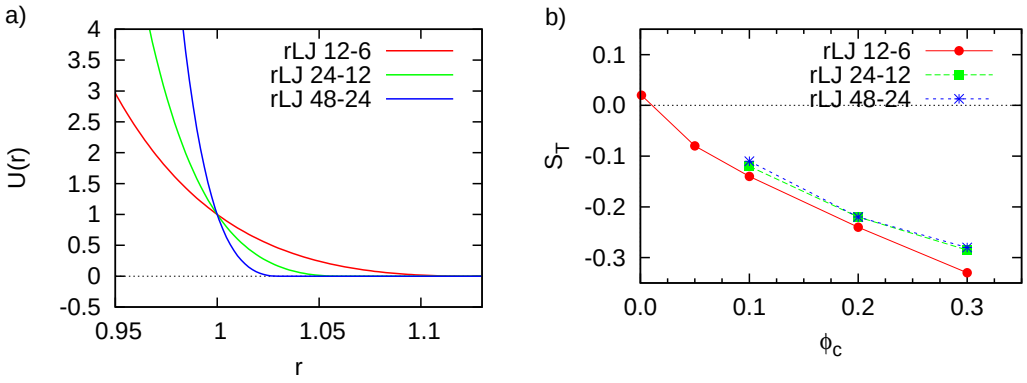

Figure 4.9: a) Repulsive Lennard-Jones potentials with different exponents n. b) Soret coefficient S_T for different mean volume fractions ϕ_c for colloids with rLJ 2n-n potentials with different steepness.

Measurements of the Soret coefficient for various repulsion potentials as a function of the volume fraction are displayed in Fig. 4.9 b. The main conclusion of these results is that the change from the already discussed soft repulsive colloid-colloid interaction potential rLJ 12-6, to increasingly steeper repulsion rLJ 24-12 and rLJ 48-24 hardly affects the Soret coefficient. Although, the softer rLJ 12-6 potential shows magnitudes of S_T slightly larger for all mean volume fractions than for the other two potentials, the differences are very small.

4.4.4 Effect of the attraction range

In order to investigate the effect of different attraction ranges in the thermodiffusion properties of concentrated colloidal suspension, two types of attractive potentials are used, Lennard-Jones and sticky. First we compare two different Lennard-Jones potentials LJ 12-6 and LJ 24-12. As displayed in Fig. 4.10 a, the difference between these two potentials is the steepness of the repulsion, and the range of the attractive interaction. These are then good candidates to test the attraction range effect since our results in the previous section indicate that the difference in steepness does not significantly affect the Soret effect.

The shape of the $S_T(\phi_c)$ dependence is similar in both cases, namely there is a volume fraction interval where S_T does not appreciably change, and decreases

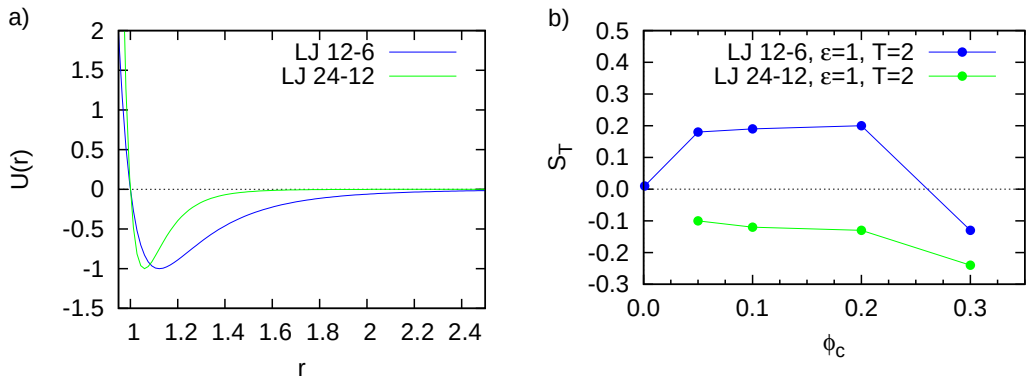

Figure 4.10: a) Lennard-Jones potentials LJ 2n-n. b) Soret coefficients S_T as a function of the volume fraction ϕ_c for the potentials in a).

for larger volume fractions. Nevertheless, whereas the long-ranged potential features positive Soret coefficients, S_T is always negative for the shorter ranged potential. This behavior is consistent with the picture that for shorter attractions the excluded volume interaction becomes more important, what contributes to decrease the S_T values.

We analyzed the attraction range importance also with a set of sticky potentials shown in Fig. 4.11 a. The functional dependence in the case of these potentials is, independently of the precise potential parameters, monotonously decaying with increasing colloidal volume fraction. In Fig. 4.11 b, results with three attraction ranges are presented for $\epsilon = 2$, which is a high interaction strength. These data show a clear agreement with the results obtained with the Lennard-Jones potential, this is that decreasing the interaction range translates into smaller Soret coefficients. Fig. 4.11 c and Fig. 4.11 d show similar results for smaller interaction strengths, $\epsilon = 1$ and $\epsilon = 0.5$. In this case, the Soret coefficient seems to be dominated by the repulsive interactions, not showing a significant distinction for varying interaction range.

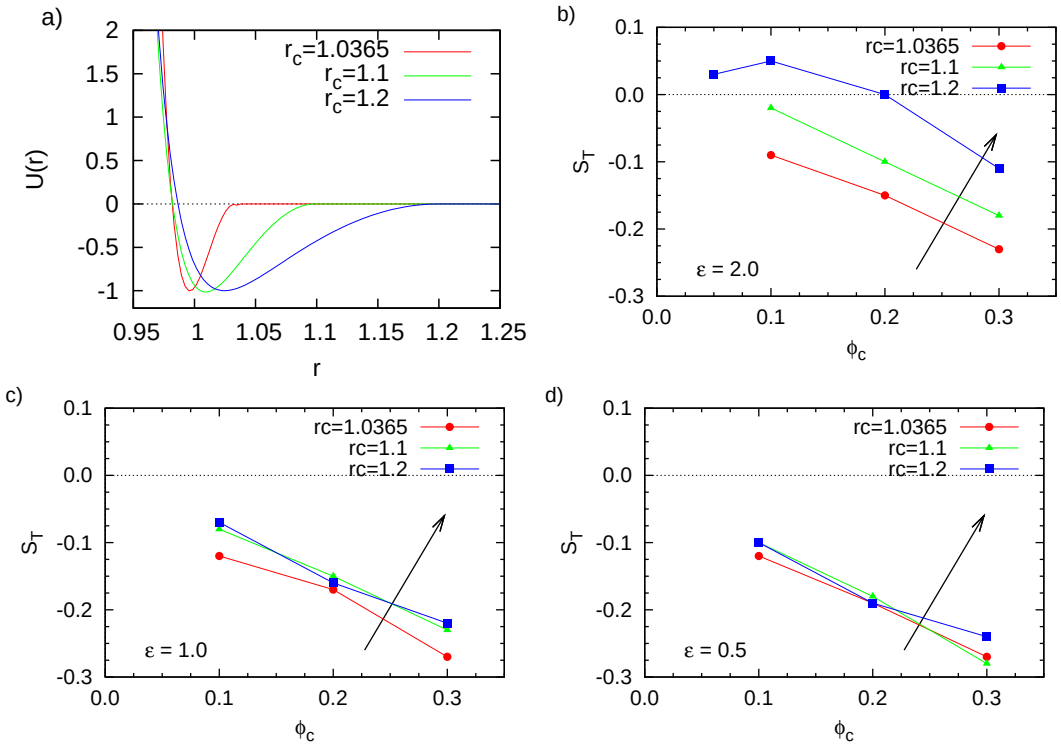

Figure 4.11: a) Sticky potential in Eq. (4.7) with fixed attraction strength ϵ and various attraction ranges r_c. b), c), d) Soret coefficients S_T as a function of the volume fraction ϕ_c for different interaction strengths ϵ/k_BT. Arrows indicate increasing attraction ranges.

4.4.5 Effect of the attraction strength

The relevance of the attraction strength is analyzed with a set of sticky potentials shown in Fig. 4.12 a. Results for various attraction ranges and strengths are shown in Figs. 4.12 b,c,d. The data are the same that those presented in Fig. 4.11, although sorted now in different plots for fixed attraction range. In all cases, it is observed that an increase of the interaction strength increases the Soret coefficient, or equivalently, the preference of the colloids to accumulate more effectively on the cold areas. Although the effect is more significant the larger the attraction range, it is present in all analyzed cases. This result is in consistency with the discussed argument. Attractive interactions favor the accumulation of colloids that tend more easily to accumulate in the cold with less kinetic energy. Note that due to condensation effects, the values of ϵ have a maximum threshold.

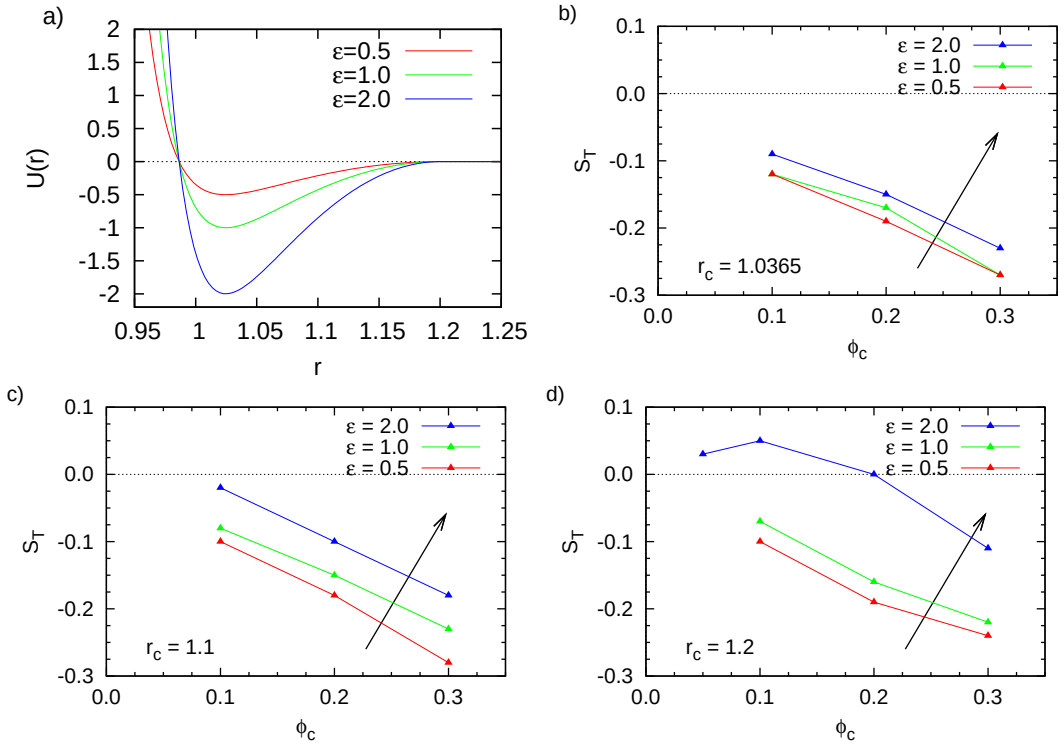

Figure 4.12: a) Sticky potential in Eq. (4.7) with fixed attraction range r_c and various attraction strengths ϵ. b), c), d) Soret coefficients S_T as a function of the volume fraction ϕ_c. Arrows indicate increasing attraction strengths.

From all the discussed effects, the attraction is the one that we can really compare with the experimental data of Ning *et. al* [78] since the employed octadecyl coated silica particles are characterized by having difference attractive inter-colloidal interactions as a function of the average temperature. The trend found in simulations agree with the experimental trend at low volume fractions, as explained in Sect. 4.2. The experimental trend at high volume fractions shows a non-monotonous behavior with varying the intensity of the interaction which origin is not understood, and which differs to the one we observe in the simulations.

4.4.6 Effect of the potential shape

Finally we comment on the influence of the shape of the potential on the volume fraction dependence of the Soret coefficient which can be seen in Fig. 4.13 a. It can be observed that the values for the Soret coefficient are quantitatively in the same order although the functional dependence of $S_T(\phi_c)$ is slightly different. We therefore infer that the exact shape of the potential is not very important when the strength and range of attraction are comparable.

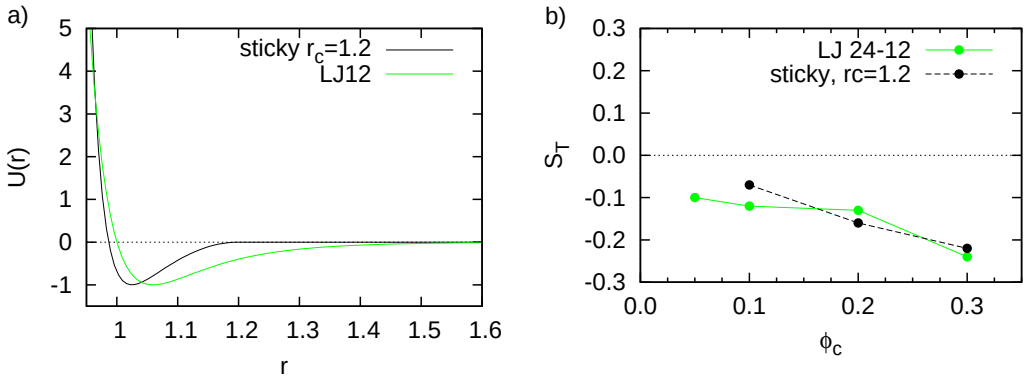

Figure 4.13: a) Interaction potential LJ 24-12 in Eq. (2.5) and a sticky potential with range $r_c = 1.2$ in Eq. (4.7), both with $\epsilon = 1$. b) S_T for the two interactions.

4.5 Analytical estimation of the collective contribution to the Soret coefficient

The definition of the Soret coefficient in stationary state in Eq. (1.20) can be formulated in terms the densities of each component as,

$$S_T = -\frac{1}{\nabla_z T}\left(\frac{\nabla_z \rho_c}{\rho_c} - \frac{\nabla_z \rho_s}{\rho_s}\right), \tag{4.12}$$

The density gradients of the colloids $\nabla_z \rho_c$ and of the fluid $\nabla_z \rho_s$ refer in this definition to their values in the presence of both components. In a first approximation though, the contribution due to the presence of the other component can be neglected, such that each density gradient can be approximated by their individual equation of state. The standard definition of the thermal expansion β_T can be rewritten as

$$\beta_T = \frac{1}{V}\frac{\partial V}{\partial T} = -\frac{1}{\rho}\frac{\partial \rho}{\partial T} = -\frac{1}{\rho}\frac{\nabla_z \rho}{\nabla_z T}. \tag{4.13}$$

The idea then is to approximate the Soret coefficient in Eq. (4.12) by

$$S_T \simeq \beta_{T,c} - \beta_{T,s} \tag{4.14}$$

Here $\beta_{T,s}$ is the thermal expansion coefficient of the fluid is $\beta_{T,s} = 1/T$. The thermal expansion coefficient of the colloids $\beta_{T,c}$, can be estimated by considering the Carnahan-Starling expression for hard spheres [11, 12, 119],

$$\beta_{T,c} = \frac{1}{k_B T}\left(\frac{1 - 2\phi^3 + \phi^4}{1 + 4\phi + 4\phi^2 - 4\phi^3 + \phi^4}\right), \tag{4.15}$$

where ϕ is the average volume fraction of the colloids. This approximation neglects the softness of the potentials employed in the simulations, what should not be a problem as discussed in Sect. 4.4.3. Furthermore, the change of the effective diameter is not taken into account. This should also not have a big effect on the result, since the estimation of the effective diameter with an expression like Barker-Henderson [5] has shown to increase the diameter only by 1 % with our choice of parameters [100]. The comparison of Eq. (4.14) and the simulation results in Fig. 4.14 show a very reasonably agreement. This shows that the approximation above is reasonable in the case of our model where the colloids to not "expell" the solvent. Besides the considered approximation, the mass effect discussed in Sect. 4.4.2 will constitute an additional contribution to the

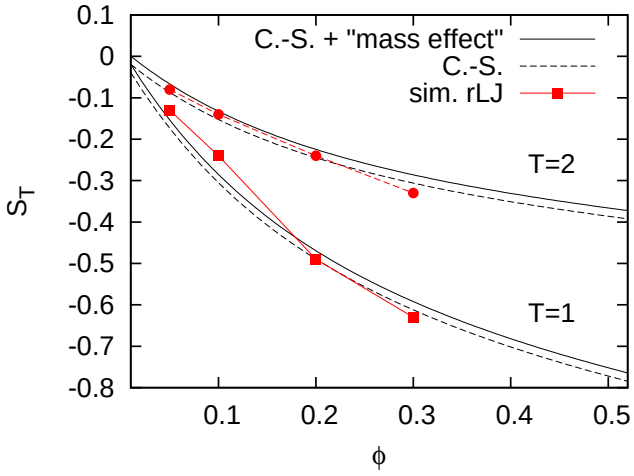

Figure 4.14: Soret coefficient S_T as a function of the volume fraction ϕ. Symbols are simulation results with repulsive LJ 12-6 colloid-colloid interactions with $\epsilon = 1.0$ at temperatures $T_0 = 1$ and $T_0 = 2$. Dashed lines correspond to Eq. (4.14) with $\beta_{T,c}$ in Eq. (4.15). Solid lines include the additional contribution $S_T^m = 0.02$.

two components in Eq. (4.14). The value estimated in Fig. 4.7 as $S_T^m \simeq 0.02$ shows not to change the agreement of the prediction shown in Fig. 4.14 for what more precise simulation data would be required.

This analysis and previous findings leads to the conclusion that the collective contribution to the Soret coefficient in our system is mainly determined by the equations of state of each of the components. In a further analysis, the argument needs to be validated for colloids with attractive interactions, and how this situation changes when single particle effects are included in a more precise manner.

4.6 Conclusions

In this chapter we have presented a simulation study of the thermodiffusion properties of concentrated colloidal suspensions. The employed model disregards the specific interactions of the colloids surface with the surrounding solvent. These interactions are responsible of the single particle effects which are the main contribution to the Soret coefficient. This simulation model therefore allows us to separately investigate the effect of the much less understood contribution of

collective interactions to the Soret coefficient.

We first discuss and reanalyze the experimental data of Ning *et al.* [77] by subtracting the single particle contribution. This enables us to perform comparison of our simulation data with experiments. Our simulation study considers different inter-particle interactions. These are purely repulsive, or repulsive combined with an attraction range. With the repulsive potentials we consider several softness at short distances, while with the attraction we study the effect of the range and strength of the attraction with two different potential shapes.

The main trends found in our study can be summarized as follows. *Excluded volume interactions* among colloids disfavor an inhomogeneous distribution of the colloids with the temperature gradient. In our simulation model this translates to negative values of the Soret coefficient of increasing magnitude with increasing concentration. In contrast, *attractive interactions* favor an inhomogeneous distribution of the colloids with the temperature gradient, what translates into a more effective accumulation of the colloids in the cold areas and therefore higher values of the Soret coefficient. In this way, increasing the concentration, always increases the importance of the repulsive interaction, such that the S_T values always decreases. On the other hand, increasing the range or strength of the attraction leads to larger values of S_T, while changing details in the interaction like potential shape or repulsion steepness has small consequences. These trends nicely explain all our simulation results qualitatively. Experimental results also follow this behavior but only in the low volume fraction regime, since conclusions are not very easy to draw from the data at high volume fractions.

A theoretical estimation of our simulation results with repulsive interactions is obtained by assuming that colloids and fluid distribute along the temperature gradient following their respective equations of state, this is disregarding the mutual interactions.

In order to better understand the interplay between the single and collective contributions to the Soret coefficient further research is required. Complementary simulations need to include also the single particle contribution to the Soret coefficient and the colloid-solvent interactions in a more realistic way, such that the overall behavior of the Soret coefficient can be determined.

5 Dilute colloidal suspensions

5.1 Introduction

In the previous section we have studied the collective contribution to the Soret coefficient in a model system with a simplified and computationally effective coupling of the colloids to the solvent. In the highly diluted regime this coupling results in a very small single particle contribution to the Soret coefficient, which is related to the mass effect in thermodiffusion. In this way, the Soret coefficient for concentrated systems was dominated by the collective contribution. However, experiments show that the Soret coefficient has a large single particle contribution that originates from colloid-solvent interactions, showing for example strong dependences on the particle size, temperature or specific interactions.

In this chapter, we use a more realistic coupling of solvent and colloids and focus on the single particle Soret coefficient.

5.1.1 Experiments on dilute colloidal suspensions

Temperature dependence

Experimental results show a strong dependence of the Soret coefficient on the average system temperature. This is true for concentrated and dilute suspensions. In the experiments by H. Ning *et al.* [77] of colloid suspensions in toluene with varying concentration it was found that there is a strong temperature dependence for all observed concentrations (see also chapter. 4). The strong temperature dependence of the Soret coefficient is already present at small volume fractions of colloids (see Fig. 4.1). This indicates that the Soret effect exists if the presence inter-colloidal interactions is negligible, i. e. that the average distance between the colloids is much larger than their size or range of interparticle interactions. For low temperatures the colloids have negative Soret coefficient and accumulate in the warm side of the system. By increasing the temperature

the situation reverses and the Soret coefficient is positive, except at very high concentrations.

In dilute suspensions, this behavior has been analyzed in more detail by Piazza *et al.* [44, 85] in aqueous colloid suspensions. Fig. 5.1 shows the temperature dependence of the Soret coefficient for dilute colloid suspension with different particle sizes.

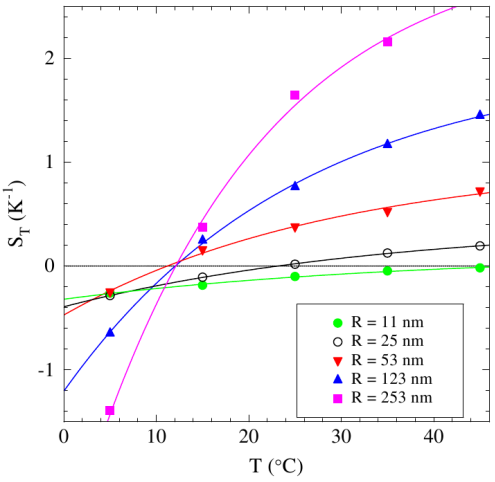

Figure 5.1: Experimental results for dilute colloidal suspensions for the dependence of the Soret coefficient on the temperature for different particle sizes. The results have been obtained with polystyrene particles in aqueous solutions. Figure from [7].

The temperature dependence can be described by the following empirical exponential relation which has been first proposed in [44], given by

$$S_T(T) = S_T^{\infty}\left[1 - \exp\left(\frac{T^* - T}{T_0}\right)\right]. \tag{5.1}$$

This expression assumes the frequent observation that the Soret coefficient is negative for small enough temperatures and that there is a temperature T^* for which the Soret coefficient changes its sign. The equation also reflects that S_T saturates at large temperatures given by S_T^{∞}. T_0 takes into account that for some substances the temperature dependence is stronger than in others.

Size dependence

Several experimental groups have analyzed the variation of the Soret coefficient with colloids of different sizes. Braibanti *et al.* [7] found that the magnitude of

the Soret coefficient increases linearly with the colloid size at all observed solution temperatures. A linear size dependence is also found in other experiments by Vigolo *et al* [113] and Putnam *et al.* [91]. Controversially, in experiments of Duhr and Braun [22] the size dependence of the Soret coefficient is found to be quadratic. A summary of all these results is shown in Fig. 5.2. So far there is is no clear explanation why these experiments lead to different results. Both experiments have been performed with polystyrene colloids in water and the different scaling of the Soret coefficient with size is still a matter of debate.

Nevertheless, it can be concluded that the Soret coefficient strongly varies with the size of the colloidal particles (in experiments with highly diluted solutions), which is another indication of the relevance of the single colloid properties.

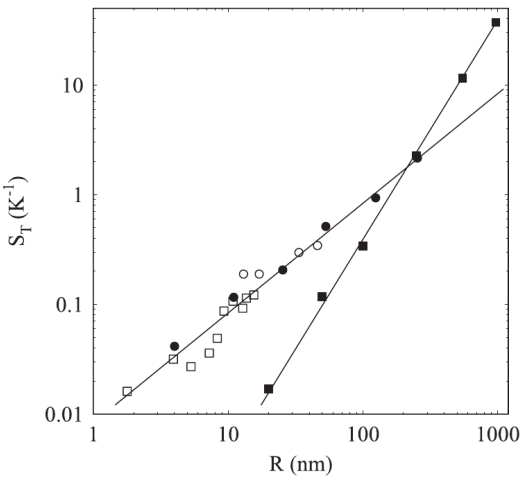

Figure 5.2: Particle size dependence of S_T, linear/quadratic power law. Contradictory experimental results for dilute colloidal suspensions. Figure origin: Piazza and Parola [84]. Data origin: full squares: Duhr and Braun [22], full circles: Braibanti *et al.* [7], open circles: Vigolo *et al.* [113] and open squares: *et al.* [91].

5.1.2 Thermophoretic force and drift velocity

The description of the dynamic behavior of colloids in a solvent should take into account that the relevant size and time scales of solvent and colloidal particles are separated by several orders of magnitude. Furthermore, in the presence of temperature gradients the non-homogeneous character of the system should be

considered. We therefore start from the extended Fokker-Planck equation proposed by van Kampen [52] to characterize the particle flow $\boldsymbol{j}$ in dilute systems,

$$\boldsymbol{j}(\boldsymbol{r}) = \rho_c(\boldsymbol{r})\mu(\boldsymbol{r})\boldsymbol{f} - \mu(\boldsymbol{r})\nabla[\rho_c(\boldsymbol{r})k_BT(\boldsymbol{r})]. \tag{5.2}$$

Here $\mu(\boldsymbol{r})$ is the colloid mobility that we assumed to be related to the self-diffusion coefficient by the Einstein relation $D_s(\boldsymbol{r}) = k_BT(\boldsymbol{r})\mu(\boldsymbol{r})$. The force $\boldsymbol{f}$ accounts for the external force fields acting on the particle, which in the presence of a temperature gradient will be the *thermophoretic force* $\boldsymbol{F}_T$ exerted on the colloid by the surrounding solvent. It should be emphasized that the external force $\boldsymbol{f}$ is different from the frictional forces that might be also present in the system. This equation can be rewritten by adding and subtracting the term $k_BT(\boldsymbol{r})\nabla\mu(\boldsymbol{r})$ as

$$\boldsymbol{j}(\boldsymbol{r}) = \rho_c(\boldsymbol{r})\boldsymbol{v}_d - \nabla\left[\rho_c(\boldsymbol{r})D_s(\boldsymbol{r})\right], \tag{5.3}$$

where the drift velocity $\boldsymbol{v}_d$ is not directly proportional to the driving force, but has an additional contribution due to the inhomogeneity of the mobility or equivalently of the self-diffusion coefficient,

$$\boldsymbol{v}_d = \mu(\boldsymbol{r})\boldsymbol{f} + k_BT(\boldsymbol{r})\nabla\mu(\boldsymbol{r}). \tag{5.4}$$

The validity of this framework in the presence of a temperature gradient has been proven by means of computer simulations by Yang and Ripoll [126]. In the case of dilute suspensions that we are concerned with, the comparison of Eq. (5.3) with the thermodiffusion phenomenological equation for the particle flux in Eq. (1.17) with $\rho_m = m_c\rho_c + m_f\rho$ leads to,

$$\boldsymbol{v}_d = -D_T\nabla T - D_s\beta_T\nabla T + \nabla D_s, \tag{5.5}$$

where β_T is the thermal expansion coefficient at constant pressure of the solvent. This expression was also previously proposed by Bringuier in Ref. [9]. It shows that, against the widely believed opinion [23, 125, 84],

$$\boldsymbol{v}_d \simeq -D_T\nabla T \tag{5.6}$$

is only an approximation. This approximation will be acceptable when $|dD_s/dT - D_s\beta| \ll |D_T|$, which is the case in most complex fluids. Nevertheless, for complex fluids with low D_T/D_s, or for molecular mixtures, the two first terms in Eq. (5.5) need to be considered. When dealing with colloidal systems, Eq. (5.6) can be considered, and with $\boldsymbol{v}_d = \mu\boldsymbol{F}_T$, such that

$$\boldsymbol{F}_T = -S_Tk_BT\nabla T. \tag{5.7}$$

In this chapter, we employ both the expression of the thermophoretic force and the drift velocity to measure the Soret coefficient. Moreover, we will check in one case the values of the three terms in Eq. (5.5) what will ensure the validity of the performed approximations.

5.2 Simulation model

In our simulations we address three of the relevant properties that influence the single particle Soret coefficient: the influence of the nature of the colloid-solvent interactions by using different potentials, the effect of the size of the colloids and the temperature dependence of the Soret coefficient.

5.2.1 Soft colloid-solvent interactions

In contrast to the model system in chapter 4 the colloid-solvent interactions are taken into account by a potential. The main difference is that the potential ensures that the solvent particles are excluded from the colloid volume. In this way the repulsive core determines the size of the colloid. We use soft repulsive and attractive colloid-solvent interactions. For repulsive colloid-solvent interactions we use the Lennard-Jones potential given by Eq. (2.4). We denote the parameters of the potentials that refer to colloid-solvent interactions by the index cs. Then the radius of the colloid is given by σ_{cs}. To include possible attractive colloid-solvent interactions we use attractive Lennard-Jones potentials given by Eq. (2.5). The implementation the colloid-solvent interactions with a potential concerns the solvent particles in the neighborhood of a colloid. These solvent particles update their positions considering MD instead of the streaming step. Besides the MD interaction all solvent particles are included in the collision step, while the colloids are excluded. Furthermore, since the colloid-solvent interactions are determined by central forces, the solvent particles do not experience any forces tangential to the colloid surface. This leads to slip boundary conditions and creates a friction coefficient, which is given by Eq. (1.23).

Attractive colloid-solvent interactions consider the experimental situation where the solvent molecules are attracted by the colloid surface. This can be due to chemical reasons in which the molecules on the colloid surface interact with the solvent molecules. One example are van der Waals forces. In other cases, the colloid surface is more complex and can have other materials attached (like poly-

mers) which may effectively induce soft repulsive or attractive interactions with the surrounding solvent. The attached substances can also screen interactions of the solvent with the colloid core. Generally, if we regard the colloid suspension as a model system for macromolecular solutions, there can be many more types of interactions that are attractive or repulsive for the solvent. So far we have not explicitly taken into account the ionic charges that are naturally present or intentionally added in experiments. These charges together with the charged surface of the colloid (which can not be avoided in many cases) can also lead to effective colloid-solvent interactions that might be comparable to the interactions that we have in our model system. In general the actual shape of the potential that describes the interaction might not be important, but rather the range and strength of the potential as has been already seen in simulations of concentrated systems. The potentials used in our simulations study the effects of repulsion or attraction with different ranges and strengths which mimic effective colloid-solvent interactions. In chemical terms this is often referred to as "good" or "bad" solvent.

5.2.2 Hard colloid-solvent interactions

In contrast with previous soft colloid-solvent interactions other MPC models [83, 82] describe the colloids as hard spheres with different ways to reflect the fluid particles at the surface.

A simple way is to apply specular reflection. In this model the velocity components of colloid and fluid particle at the time of impact are changed as in an elastic collision. In this collision the velocity components tangential to the surface remain unchanged, which leads to slip boundary conditions. The total momentum and energy are not altered. The momentum transfer during the collision time can be regarded as a force that acts between colloid and fluid particle. In this sense the model is similar to the one of a steep repulsive potential in which the trajectories are computed by MD. However, there is a difference between these two models that arises from the softness of the potential. In the picture of a mean force acting on the fluid with a continuous density there are additional repulsive interactions which are not present in a hard sphere model that only considers the momentum transfer between fluid and colloid.

In a more commonly used model, the reflection at the surface is considered with a "bounce back" operation [59]. This results in no-slip boundary con-

ditions. This method can be used in combination with virtual particles (see chapter. 2) in order to fully remove slip at the surface. Virtual particles are drawn from a Maxwell-Boltzmann distribution with a certain temperature. In systems with homogeneous temperature this is the average temperature. In our case, where the temperature is inhomogeneous, the temperature of the virtual particles would have to be the local temperature. This temperature can be either computed from the imposed temperature profile or measured from the local kinetic energy. Both methods are not optimal. The local temperatures have to be determined for the collision cells adjacent to the surface of the colloid, which introduces a discreteness of the temperature profile. Additionally the use of the imposed temperature neglects spatial and temperoral temperature fluctuations which are important in thermal diffusion processes. In the case of measurements of the local temperature, additional computational effort is required. For the above mentioned reasons we dispense with using this method. Another way to apply no-slip boundary conditions uses stochastic reflections from the surface, which also requires the local temperature since this method also uses of Maxwell-Boltzmann distributed velocities. A recent work on fluid-solid boundary conditions, that discusses the implementation of slip, partial slip and stick boundary conditions is found in [117].

5.2.3 Single Particle Thermodiffusion Algorithm

In a recent study of thermodiffusion of nano-particles by G. Galliero and S. Volz [34] a method has been introduced to study Soret coefficients for dilute suspensions, named single particle thermodiffusion algorithm (SPTA). In this study molecular dynamics simulations have been performed with suspensions of nano-particles to investigate effects of particle size and solvent properties on the Soret coefficient. The use of the standard definition of the Soret coefficient Eq. (1.20) which depends on the mass fraction profile is not of use in this case, since to obtain a concentration profile with a single particle is difficult due to bad statistics. A different way of computing the Soret coefficient makes use of the thermophoretic force. The thermophoretic force is the effective force that the colloids experience due to the presence of the temperature gradient. The thermophoretic force is related to the temperature gradient by $\boldsymbol{F}_T = -S_T k_B T \nabla T$ as is derived in section (5.1.2).

The idea of the SPTA is to measure the thermophoretic force by confining

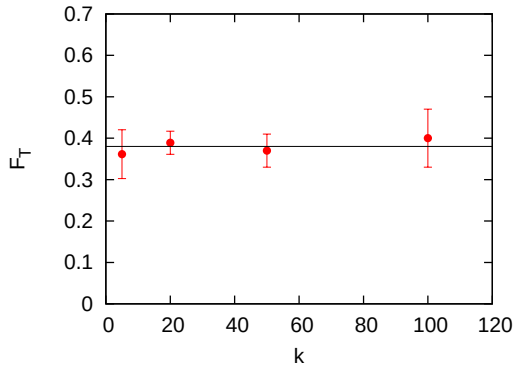

Figure 5.3: Thermophoretic force measured with the SPTA, as a function of the harmonic constant k. Line is a guide to the eye.

the colloid with a harmonic potential acting in all three spatial dimensions (also referred to as harmonic spring). The average deviation from the neutral position can then be used to obtain the force exerted by the solvent on the colloid. In this case the thermophoretic force is counterbalanced by the harmonic force $\boldsymbol{F}_T = k(\boldsymbol{r} - \boldsymbol{r}_0)$, where k is the harmonic constant and $\boldsymbol{r} - \boldsymbol{r}_0$ the deviation of the colloid from the neutral position. We implemented this method with the colloid in the MPC solvent and checked if the confinement of the colloid with the harmonic potential affects the thermophoretic force by using different harmonic constants. This is shown in Fig. 5.3 and it can be seen that the thermophoretic force is constant within the tested range of k.

We also checked the relation of the force and the temperature gradient as shown in Fig. 5.4. The results prove that the system is within the linear response regime in all employed temperature gradients. This is in contrast with simulations of polymers in a Lennard-Jones fluid [131] where the measured Soret coefficient was dependent on the temperature difference.

5.2.4 Simulation setup

For studying the thermophoretic force as described in Sect. 5.2.3 we use a simulation box with periodic boundary conditions as shown in chapter 4 which consists of two half boxes. In each of the half boxes one colloid is placed in the center and attached to a spring with a spring constant k. We use the same simulation box for studying the drift velocity which has been described in Sect. 5.1.2. In this case the colloids are not attached to a harmonic spring, but can move freely. In

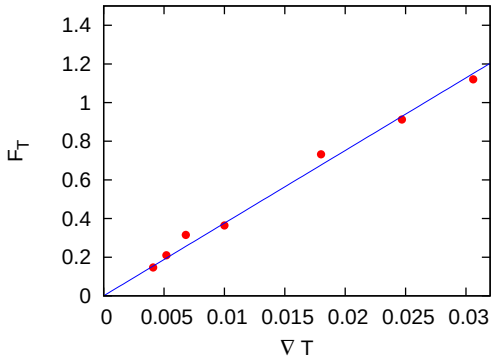

Figure 5.4: Dependence of the thermophoretic force measured with SPTA on the temperature gradient. Line corresponds to a linear fit.

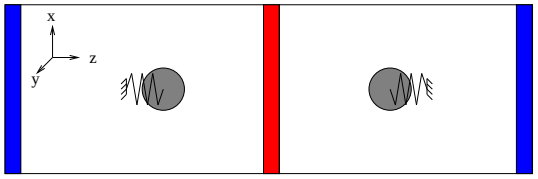

Figure 5.5: Simulation setup for measuring thermophoretic force in harmonic potential with velocity exchange algorithm.

both cases, the system it is made sure that the solvent surrounding the colloid is in its stationary state, before starting to measure the thermophoretic force or drift velocity.

The effective size of the colloids is determined by the parameters of the colloid-solvent interaction potential. The solvent particles interact with the colloid within the cut-off radius of the potential.

We use a method to reduce the computational effort required for the colloid-solvent interactions that is described in the appendix 7.1. Due to this method only solvent particles in a shell around the colloid have to be considered for computing the force in the MD part of the program, similar to a Verlet list. The solvent-solvent interactions are described by standard MPC dynamics to obtain the hydrodynamics of the colloid and include its thermal fluctuations. We use random shift of the collision grid which is performed in every MPC step. All collision cells within the system are considered equally in the MPC part, including the partially filled ones next to the colloid.

The solvent is implemented with the MPC parameters $h = 0.1$, $\alpha = 120°$, $\rho = 10$ and $m_f = 1.0$. The mass density of the colloid is the same as the mass

density of the solvent, namely $\rho_{m,coll} = \rho\ m_f$. Then the mass of the colloid is given by $m_{coll} = \rho_{m,coll}\ \mathrm{V}_{coll}$. The colloid volume for a colloid with diameter d is $\mathrm{V}_{coll} = 4/3\pi(d/2)^3$. With the above number density $\rho = 10$ of the solvent, mass values for range from $m_{coll} = 42$ for $d/2 = \sigma_{cs} = 1$ up to $m_{coll} = 5236$ for $d/2 = \sigma_{cs} = 5$. The timestep of the MD is $\Delta t_{MD} = 10^{-3}$, which corresponds to a ratio with the MPC collision time of $h/\Delta t_{MD} = 100$.

We express the Soret coefficient S_T obtained from Eq. (5.7) in units of 1/K by dividing the value obtained from Eq. (5.7) in our simulation units by a factor 120 K. This refers to taking the potential strength of Argon, which is $\epsilon_{Ar} = 999$ J/mol corresponding to $\epsilon_{Ar}/R = 120$ K, with $R = 8.314$ J/(K mol) the ideal gas constant.

5.2.5 Determination of the Soret coefficient

Example measurement of F_T

We measure the force parallel and perpendicular to the temperature gradient. The forces in the two directions perpendicular to the temperature gradient should be equal to zero on average, since there is no driving mechanism. This can be observed in Fig. 5.6 for the x- and y-direction. In the z-direction parallel to the temperature gradient a non-zero force is measured, which is the thermophoretic force. The data for the forces in Fig. 5.6 are the averaged over different individual simulations (runs) and over the number of timesteps of the simulation. The evolution of the averaged force over simulation time, denoted as $\langle \langle F \rangle_t \rangle_r (t)$, fluctuates around an average value. Averages over the number of runs are denoted by $\langle \rangle_r$ and averages over simulation time steps by $\langle \rangle_t$. It should be noted that the data for the force has a large noise amplitude. In the case of the example measurement with a colloidal particle of diameter $d = 6a$ (where a is the length of one MPC box) the forces have a maximum amplitude of about $\pm$ 20. The value of the average force in this case is $F = 0.74$. This is a signal to noise ratio of about factor 30, such that a large amount of statistics is required. Fig. 5.7 a) shows that the time average $\langle F \rangle_t$ of the individual runs fluctuates strongly. These fluctuations can be decreased by using larger number of simulation time steps, which implies longer run times. The better choice is the use of more simultaneous independent runs. The convergence to a final force value can be seen in Fig. 5.7 b) in which the dependence of the force average on the number of runs is $\langle \langle F \rangle_t \rangle_r (N_r)$ is plotted. The dashed lines in Fig. 5.7

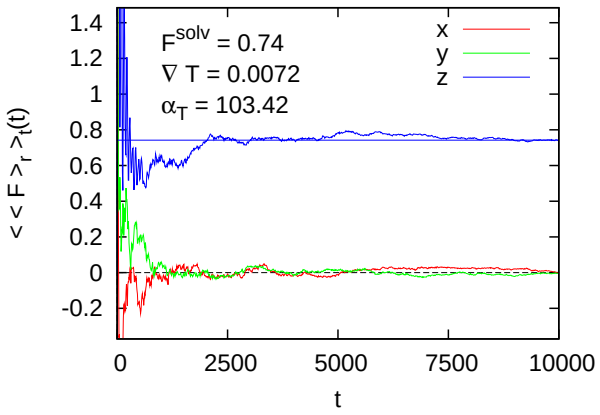

Figure 5.6: Example measurement of the thermophoretic force as a function of time. Repulsive LJ 12-6 potential with strength $\epsilon = 1$ and colloid diameter $d = 6$. System size $L_x = L_y = L_z/2 = 42$.

a) show the asymptotic standard error. The scattering of the individual runs is relatively large. The standart error (corresponding to the variance of a normal distribution of very large numbers of runs) is still very large and not shown here. The data does not include the error from the averaging over the simulation time steps, which has not been measured.

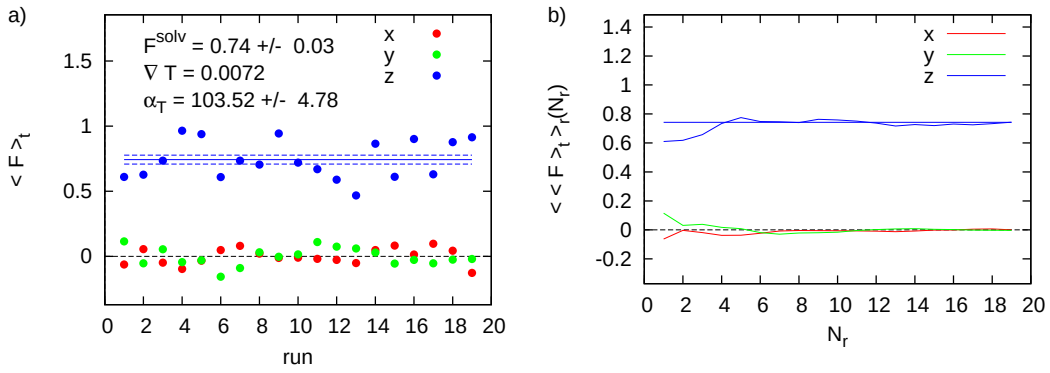

Figure 5.7: a) measurement of the thermophoretic force in different independent runs. b) convergence of the average force with number of runs.

Fig. 5.7 b) shows that the final value fluctuates only little after 4 runs, which is supposed to be sufficient to study effects where the Soret coefficients are clearly separated for different simulation parameters, like for expample the colloid size or the average temperature. Therefore, we typically use 4 to 8 runs to obtain

reliable values of the Soret coefficient. But, for example the study of finite size effects requires a high precision of the individual measurements, since there are large fluctuations of measurements for a fixed particle size in different system sizes (can be seen in section 5.2.6 in Fig. 5.9).

Example measurement of the drift velocity

Note that the drift velocity in Eq. (5.4) and Eq. (5.6) refers to the average of a diffusive motion. In order to measure this drift velocity consider one free colloid in each of the two halves of the simulation box, and observe the average displacement from the original positions and their averaged velocities. Initially the colloids are placed in the center of the two half boxes. The number of simulation steps is chosen small enough that the displacement of the colloid is still far away from the boundaries of the simulation box. Because of the short observation times of the colloid trajectories, a large number of individual runs is required in order to obtain the average displacement and drift velocity. For the smallest colloids with a radius of $\sigma_{cs} = 1$ the number of runs is in the order of at least 50000 and for the largest colloid with $\sigma_{cs} = 4$ ca. 1000 have been performed.

The average displacement of the colloid is shown in Fig. 5.8 a), in which a simulation time of t has been used. In principle the drift velocity can be determined from the slope of the displacement. But since the colloid is at rest at the beginning and is accelerated, it is not known *a priori* after which time it moves with a constant drift velocity. Alternatively we measure the drift velocity from the average of the instantaneous colloid velocities that are know during the simulation. These are shown in Fig. 5.8 b). The typical exponential increase towards the asymptotic drift velocity can be seen.

5.2.6 Finite-size effects

Finite size effects for the thermal diffusion factor $\alpha_T = T_0 S_T$ can arise from interaction of the colloid with its periodic images perpendicular to the temperature gradient and from interactions with the colloid in the other half box of the simulation system. In order to determine the finite size effect for α_T we measured the thermophoretic force for a fixed particle size and different simulation box sizes $L = L_x = L_y = L_z/2$. Fig. 5.9 shows the dependence of α_T on the

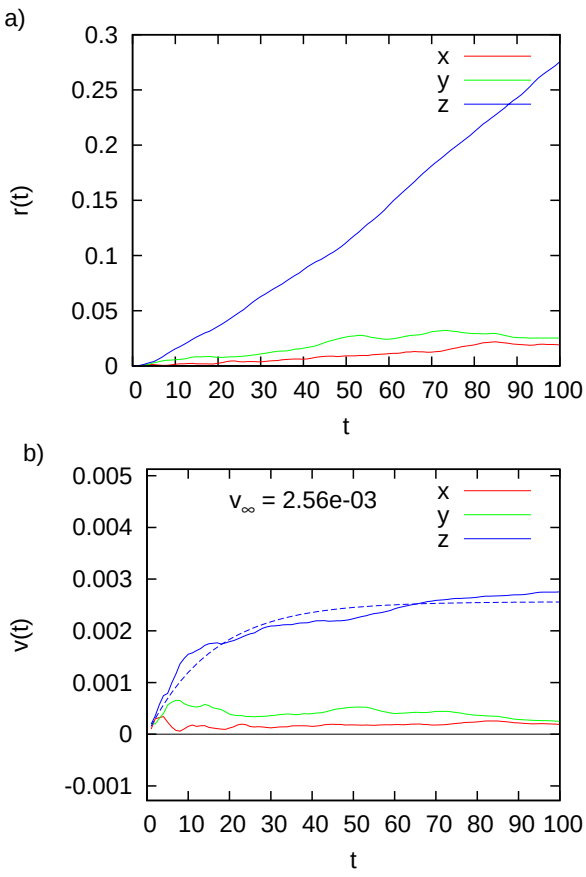

Figure 5.8: Example measurement of colloid displacement and drift velocity as a function of time. The particle radius is $\sigma_{cs} = 3$ and the colloid-solvent interaction is a repulsive rLJ 12-6 potential and the mean temperature is $T_0 = 1.0$. Average of ca. 2000 runs. Dashed line shows an exponential asymptotic fit $v(t) = v_\infty(1 - \exp(-t/\tau))$, with the relaxation time τ.

ratio of particle size to system size σ_{cs}/L characterized by the scaling relation

$$\alpha_T = \alpha_T^\infty \left(1 + \lambda_{fs} \frac{\sigma_{cs}}{L}\right), \tag{5.8}$$

where α_T^∞ is the thermal diffusion factor for an infinitely large system and λ_{fs} the scaling factor. The datapoints for each system size have been obtained from at least 16 independent runs except for the two largest systems which have been performed with 8 runs. The smallest system is 4 times larger than the diameter of the colloid and the largest system is 10 times larger. The scaling factor for the finite size effect $\lambda_{fs} = 4.5 \pm 1.1$.

We use this scaling factor for other simulations with different colloid-solvent

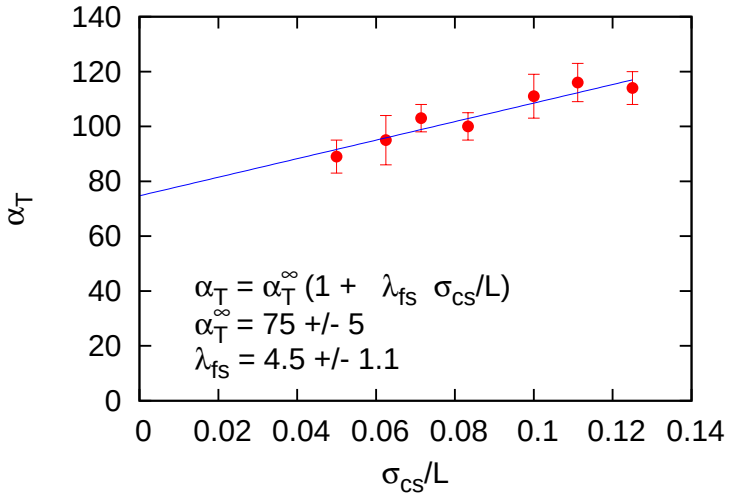

Figure 5.9: Finite size effect of the thermal diffusion coefficient, which is plotted against the ratio of particle over system size. The value α_T^∞ corresponds to an extrapolation for an infinitely large system. The simulations have been performed with a rLJ 12-6 interaction potential with strength $\epsilon_{cs} = 1.0$, particle size parameter $\sigma_{cs} = 3.0$ at temperature $T_0 = 1.0$ with a temperature gradient $\nabla T = 0.007$.

interactions and particle sizes for quantitative comparisons to analytical expression of the Soret coefficient in sections 5.3.6 and 5.3.7. This might not be fully correct, but at this point we have no precise data for other colloid-solvent interactions. The trend of a decrease of the thermophoretic force with system size is found in simulations with repulsive colloid solvent interactions as well. However, we did not study finite size effects in systems with attractive colloid-solvent interactions.

A higher precision of the scaling factor can be achieved by more precise measurements for the different system sizes. But since the asymptotic standard error with decreases with $1/\sqrt{N_r}$ the precision of the measurement increases only slowly in spite the large amount of computational effort.

The origin of the finite-size effect for the thermophoretic force has not been studied in detail. The thermophoretic force can be affected by interactions with the periodic images of the simulation box or by direct interactions between the two colloids in the their half boxes. It was found that changes of the system size in the z-dimension (along the temperature gradient) affect the thermophoretic

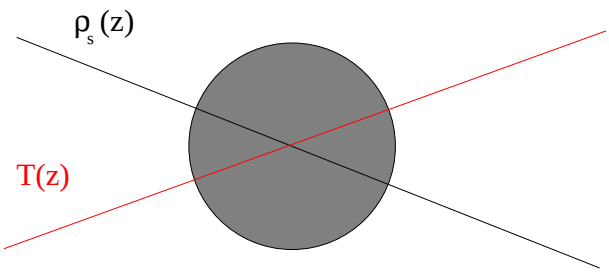

Figure 5.10: Diagram of a colloid with its surrounding MPC solvent density in the presence of a temperature gradient.

force similar as changes of the whole system size, which indicates a direct interaction between the two colloids. However, it has not been analyzed how changes of L_x and L_y by keeping L_z constant influence the thermophoretic force. One reason for interactions between the colloids might stem from an induced stationary flow field around the colloids.

5.3 Simulation results

The main objective of this chapter is the characterization of the size and temperature dependence of a single colloidal particle with regard to different colloid-solvent interactions. These are the most important factors that influence the single-particle thermophoretic force and the resulting thermal diffusion factor.

5.3.1 Attractive vs. repulsive colloid-solvent interactions

As a first observation it is found that colloids with repulsive colloid-solvent interactions respond differently to the temperature gradient than colloids with attractive interactions. It is observed that colloids with repulsive colloid-solvent interactions are generally driven to the hot side of the system, this is they display a negative single particle Soret coefficient. In contrast, the Soret coefficient can be positive or negative for attractive colloid-solvent interactions, depending on the system temperature.

The thermophoretic force on a colloid in a MPC fluid is governed by an interplay of the temperature and density gradient of the solvent as sketched in Fig. 5.10. Particles with higher temperatures penetrate further into the repulsive part of the potential, such that in a temperature gradient particles in the

hot side will *push* the colloid to the cold side. On the other hand, due to the thermal expansion of the solvent there are more particles interacting with the colloid on its cold side. This will imply that for attractive interactions the colloid is *pulled* to the cold side and for repulsive interaction ones the colloid is *pushed* to the hot side. This effect can explain that colloids with repulsive colloid-solvent interactions display negative Soret coefficient, while colloids with attractive interactions a positive one. With increasing temperature, the repulsive part of the attractive LJ potential becomes more important what can explain a sign change of S_T.

5.3.2 Size dependence of the Soret coefficient

We investigate the size dependence of the Soret coefficient for colloids with diameters ranging from $d = 2a$ to $d = 10a$, where a is the length of one MPC collision cell. Diameters which are in the order of one collision cell size or less are not suitable for MPC simulations since hydrodynamic interactions and energy conservation are not ensured for scales smaller than the collision cell size. Larger diameters have not been investigated because of the large computational effort, arising mainly from the large number of colloid-solvent interaction pairs. The size of the colloid is determined by its repulsive core potential, given by σ_{cs} in Eq. (2.4) and Eq. (2.5). Then the diameter of the colloid is $d = 2\sigma_{cs}$.

It is expected that the thermal diffusion coefficient of a single colloid which is mainly determined by colloid-solvent interactions depends on the form of the potential that we apply. We have used purely repulsive and attractive potentials in which we vary the strength and range. We compare our results for the size dependence of the Soret coefficient with those found in the experiments (see Fig. 5.2) in which the controversial results of a linear and quadratic power law have been observed. Therefore a special interest regards the exponent of the power law that we use to fit our data.

The functional form of the thermal diffusion factor $\alpha_T = T_0 S_T$ is

$$\alpha_T = \alpha_T^0(\epsilon, n, k_B T, \Sigma) \left(\frac{d}{a}\right)^b , \tag{5.9}$$

where Σ is a set of parameters that refer to the solvent on which the thermal diffusion factor can possibly depend. This can be for example the density ρ of the fluid or the shear viscosity ν.

Repulsive potentials

First we analyze the size dependence for a purely repulsive potential. The colloids modeled in this way can be regarded as colloids with a soft repulsive core. The steepness of the core is varied by changing the exponent and the strength parameter ϵ of the repulsive Lennard-Jones potential (given by Eq. (2.4)) that we apply.

Fig. 5.11 a) and Fig. 5.11 b) show the results for different colloid-solvent interactions defined by different repulsive Lennard-Jones potentials. The exponents

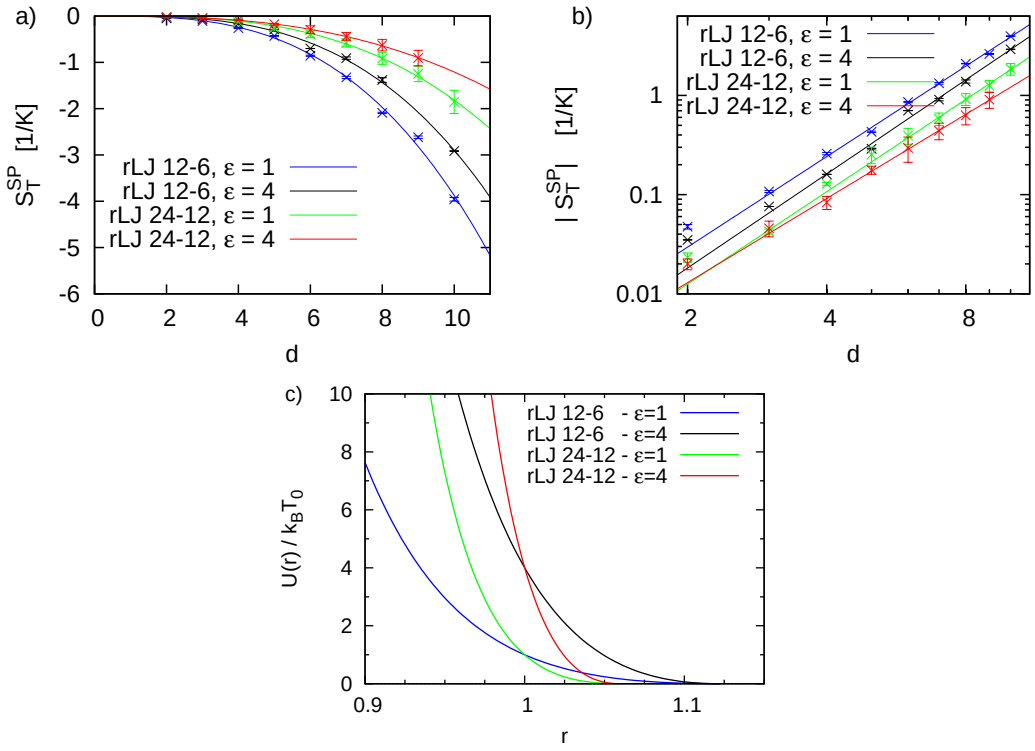

Figure 5.11: a) dependence of the single particle Soret coefficient on the particle size for different repulsive Lennard-Jones potential. The average temperature is $T_0 = 1.0$. b) double logarithmic plot of the data, cubic power law dependence c) steepness of the different potentials. Simulations with fixed $\sigma_{cs}/L = 1/12$ ratio.

b of the power law and its prefactors α_T^0 are summarized in Table 5.1. It can observed that the power law is almost cubic in all cases. This observation is in contradiction to what has been observed in experiments. However, this can be explained by the nature of the colloid-solvent interaction potential that we use.

	b	α_T^0
rLJ 12-6, $\epsilon = 1.0$	3.0	-0.0036
rLJ 12-6, $\epsilon = 4.0$	3.1	-0.0022
rLJ 24-12, $\epsilon = 1.0$	3.1	-0.0015
rLJ 24-12, $\epsilon = 4.0$	2.8	-0.0016

Table 5.1: Size dependence of the thermal diffusion factor for different repulsive potentials. Fits to the simulation data with the powerlaw in Eq. (5.9).

Due to the form of the potential an increase of the particle size does not only increase the surface of the colloid but also the range of the interaction. To be more precise the width of the layer in which the solvent particles interact with the colloid. That means in total an increase of the colloid diameter increases the "interaction volume" in which the number of interacting fluid particles scales as σ_{cs}^3 (see also end of Section 5.3.7 Fig. 5.23).

The steepness of the potential (which corresponds to the slope, i.e. force) is proportional to ϵn and thus changes in the strength ϵ and exponent n have similar effects as can be seen in Fig. 5.11 c). It is observed that with an increase of ϵ and n the thermal diffusion factor $\alpha_T = T_0 S_T$ decreases. That means that for a softer repulsive core potential the colloid experiences a larger thermophoretic force. A possible explanation is that for softer potentials the solvent particles can penetrate the interaction region more deeply, resulting in a larger number of particles in the interaction region and a larger total force between colloid and solvent.

Attractive potentials

The size dependence of the Soret coefficient is studied for different types of attractive Lennard-Jones potentials. For attractive colloid-solvent interactions the Soret coefficient is positive if the temperature to strength ratio is $T_0/\epsilon \lesssim 10$ and negative otherwise. This clearly indicates that the thermophoretic force is strongly influenced by the nature of the colloid-solvent interactions, as one has a very different behavior when the interactions are purely repulsive. It also supports the aforementioned explanation that the total force of the colloid results from the larger number of particles on the cold side which *pull* it to the cold side in the case of attractive interactions. In the case of repulsive interactions

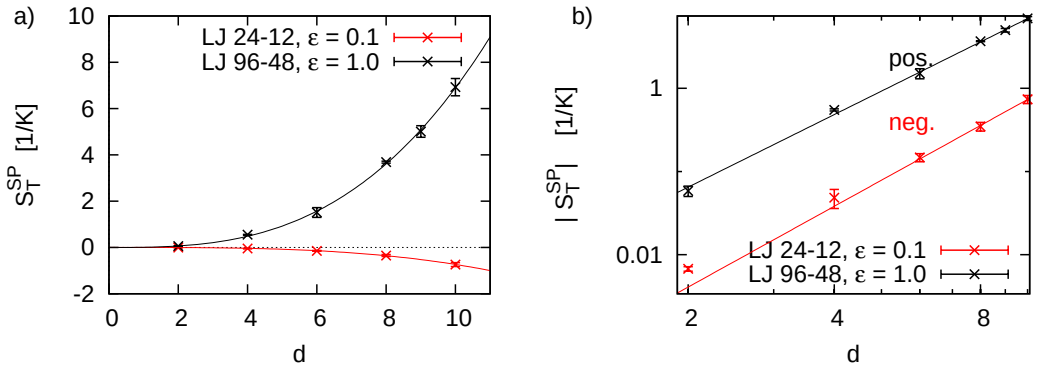

Figure 5.12: Dependence of the Soret coefficient on the particle size for different attractive Lennard-Jones potentials. The average temperature is $T = 1.0$. Simulations with fixed $\sigma_{cs}/L = 1/12$ ratio. a) data with power laws fits b) double logarithmic plot, cubic power law dependence

the colloid is *pushed* towards the hot side. However, in the case of attractive potentials the effect consists of a temperature-dependent interplay between the forces of the attractive region and the repulsive core. This will be discussed again in more detail in section 5.3.3.

Similar to the case of repulsive interactions the size dependence of the Soret coefficient is cubic. The reason is again that an increase of the particle size with the LJ parameter σ_{cs} increases the "interaction volume" around the colloid. The interaction volume increases similar to the case of a repulsive potential as σ_{cs}^3, since the width of the interaction volume increases with σ_{cs} and the surface area with σ_{cs}^2. Thus the number of particles interacting with the colloid and the resulting thermophoretic force increases as σ_{cs}^3. This will be discussed in more detail at the end of this chapter in section 5.3.6 and 5.3.7. The results

	b	α_T^0
LJ 24-12, $\epsilon = 0.1$	3.2	-0.00044
LJ 96-48, $\epsilon = 1.0$	2.9	0.0087

Table 5.2: Size dependence of the Soret coefficient for different attractive potentials. Fits to the simulation data with the powerlaw in Eq. (5.9).

presented in Fig. 5.12 and Table 5.2 have been obtained with an attractive

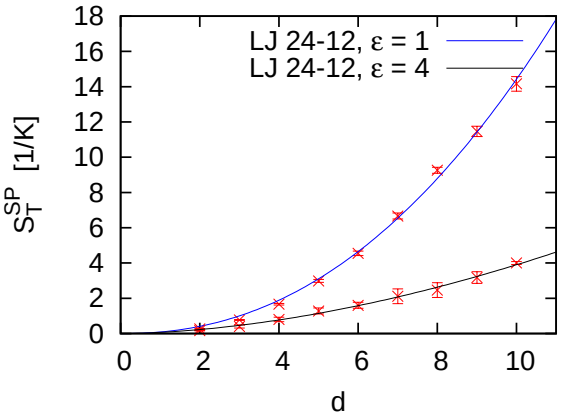

Figure 5.13: Dependence of the Soret coefficient on the particle size for different attractive Lennard-Jones potential. The average temperature is $T = 1.0$. Simulations with fixed $\sigma_{cs}/L = 1/12$ ratio.

LJ 24-12 potential with a strength of $\epsilon = 0.1$ and a LJ 96-48 potential with a strength of $\epsilon = 1.0$. The strength of the LJ 24-12 potential has been chosen very low because it is observed that due to the compressibility of the solvent and attraction of the colloid, there is an increased density of solvent around the colloid. The size dependence of the Soret coefficient is cubic in both cases. A quantitative description of the density close to the colloid surface is discussed in Sect. 5.3.6.

Further results with large potential strengths are shown in Fig. 5.13 and Table 5.3. The exponent of the powerlaw is quadratic in this case. The prefactor of the powerlaw of the thermophoretic diffusion factor $\alpha_T^0(\epsilon, n, k_B T, \Sigma)$ increases as ϵ decreases, which is again similar to the case of repulsive interactions, but might be of different origin here.

These results might not be representative for the size dependence of the Soret coefficient due to the increased density, which is up to 20 times the bulk value. It is not clear at the moment how the increased density affects the size dependence. But it can be noted that theoretical considerations show that the exponent of the power law is smaller when the colloid surface has stick instead of slip boundary conditions [71, 124]. It could be that due to the large density next to the solvent, the solvent particles that arrive from the bulk are somehow immobilized, leading to an effectively sticky surface. Whether this is true or other mechanisms are at work is not known presently.

	b	α_T^0
LJ 24-12, $\epsilon = 1.0$	2.2	0.087
LJ 24-12, $\epsilon = 4.0$	1.8	0.066

Table 5.3: Size dependence of the Soret coefficient for different attractive potentials. Fits to the simulation data with the powerlaw in Eq. (5.9).

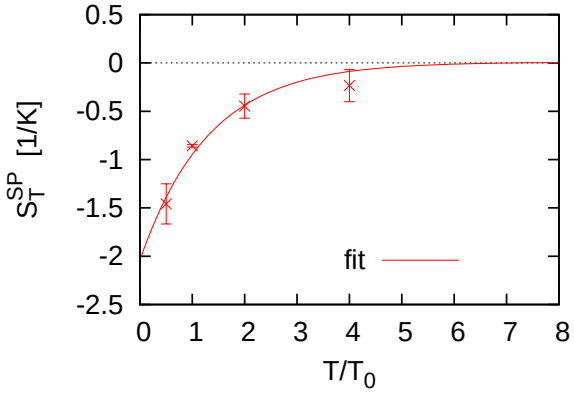

Figure 5.14: Dependence of the Soret coefficient on the temperature for repulsive LJ 12-6 with a strength $\epsilon = 1$ and particle radius $\sigma_{cs} = 3$.

5.3.3 Temperature dependence

The temperature dependence of the Soret coefficient in one case of repulsive colloid-solvent interactions can be seen in Fig. 5.14. The exponential behavior with an increase of the Soret coefficient with temperature towards a saturation value can be observed in simulation. This is shown by the exponential fit to the simulation data by means of Eq. (5.1). In contrast to experiments there is no sign change of the Soret coefficient with increasing temperature. In our simulations with repulsive LJ potentials the colloid always experiences a thermophoretic force towards the warm side of the system. The force and the corresponding Soret coefficient converge towards zero for large temperatures.

In Fig. 5.15, we show the temperature dependence of the Soret coefficient for one example of attractive colloid-solvent interactions. Here we find that at low temperatures the thermophoretic force drives the colloid towards the cold side. By increasing the temperature the Soret coefficient decreases and eventually changes its sign, so that the colloid is driven towards the warm side of the

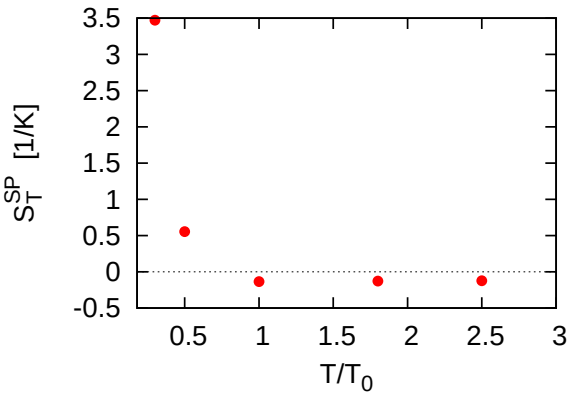

Figure 5.15: Dependence of the Soret coefficient on the temperature for attractive LJ 24-12 with $\epsilon = 0.1$ and $\sigma_{cs} = 3$.

system.

At low temperatures the thermophoretic force is dominated by the attractive forces, which drive the colloid downwards the temperature gradient, since there is a larger number of particles on the cold side of the colloid surface, than on its warm side. Forces that arise from the repulsive core dominate the thermophoretic force at high temperatures. In this case the solvent particles are distributed more closely to the repulsive core due to their larger kinetic energies and drive the colloid to the hot side.

5.3.4 Diffusion coefficient in a homogeneous fluid

The Soret coefficient of a single colloid is related to the thermophoretic mobility D_T and the self diffusion coefficient D_s by $S_T = D_T/D_s$. S_T can be determined by measurements of the thermophoretic force of a single colloid and D_T can be obtained from measuring the drift velocity of the colloid. These two independent measurements of thermophoretic quantities in temperature gradient systems can be compared when the self diffusion coefficient D_s is known.

The diffusion coefficient of a single colloidal particle is related to its friction coefficient by the Einstein relation Eq. (1.22). Together with the Stokes expression for the hydrodynamic friction coefficient this relation can be used to verify the correct hydrodynamic behavior for our model of the colloid and fluid. For a spherical particle with slip-boundary conditions the Stokes friction coefficient is given by Eq. (1.23)

The diffusion coefficient is determined from the mean square displacement of the colloid in a system with homogeneous temperature and density.

$$D_s = \frac{1}{6t} \left\langle (\boldsymbol{r}(t) - \boldsymbol{r}(t_0))^2 \right\rangle . \tag{5.10}$$

The self diffusion can be measured in equilibrium, since the employed temperature gradients are small enough to have linear response. Measurements of the

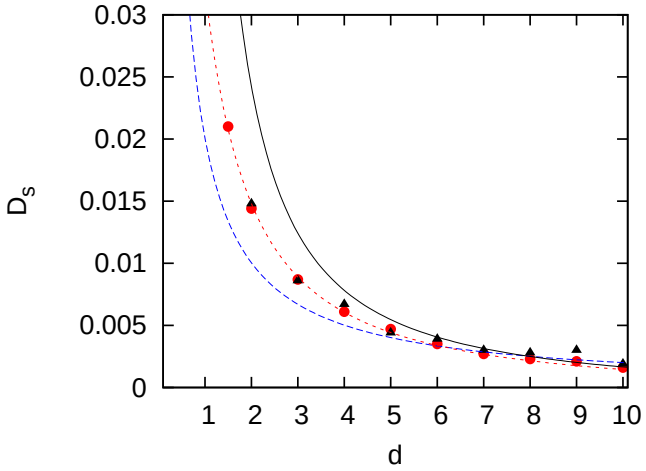

Figure 5.16: Self-diffusion coefficient vs. particle size for repulsive LJ colloid-solvent interactions. Symbols are simulation results, circles with fixed system size $L = 30$, and triangles with fixed ratio $\sigma/L = 1/12$. Lines correspond to the Einstein-relation in Eq. (5.14). The blue dashed line is the first term with Stokes friction (Eq. (1.23)) and the solid line corresponds to both terms in Eq. (5.14), including Enskog friction and the finite-size correction of the Stokes friction. The red dashed line is a fit to Eq. (5.14) with a colloid radius $R + \Delta R$, with $\Delta R = 0.35$.

self-diffusion coefficient for different colloid sizes are shown in Fig. 5.16. We have measured the self diffusion coefficient in a cubic system with fixed length $L = 30$ and with a fixed ratio $\sigma_{cs}/L = 1/12$. Both results differ only marginally. We compare the data to the theoretical Einstein relation Eq. (1.22), where the friction coefficient is given by the Stokes relation for slip boundary conditions Eq. (1.23).

The deviation of results from the Stokes-Einstein expression can be partially explained by Enskog friction and finite size effects. For the finite-size correction

of the Stokes friction $\xi_S = 4\pi\eta\sigma_{cs}$ we have used the relation

$$\xi'_S = \xi_S(1 - 2.837\frac{\sigma}{L}), \tag{5.11}$$

as given in [24, 64] and with the Stokes friction ξ_S given in Eq. (1.23). The finite-size correction results from long-ranged hydrodynamic interactions and decreases with increasing system size (i. e. small simulation boxes enhance the Stokes friction).

Furthermore, one has to take into account the additional Enskog contribution to the friction, arising from for local kinetic Brownian collisions. The Enskog friction is given by

$$\xi_E = \frac{8}{3}\sqrt{\frac{2\pi k_B T m_c m_f}{m_c + m_f}}\rho\sigma_{cs}^2 g(\rho), \tag{5.12}$$

as in ref. [43], where "the pair distribution at contact" $g(\rho)$ can be set to 1 as in [82]. The total friction is then obtained by

$$\frac{1}{\xi_t} = \frac{1}{\xi'_S} + \frac{1}{\xi_E}, \tag{5.13}$$

so that the one particle self diffusion coefficient is

$$D_s = \frac{k_B T}{\xi_t} = \frac{k_B T}{\xi'_S} + \frac{k_B T}{\xi_E}. \tag{5.14}$$

The Enskog friction is a local effect and is not affected by the finite size of the system [82]. Enskog friction is important when the granular nature of the solvent becomes important and can not be described as a continuous medium which is the case for small colloidal particles. In Fig. 5.16 the simulation results are compared to the Einstein relation in Eq. (5.14), where in one case only the Stokes friction is taken into account and in the other case the total friction including the finite size correction for the Stokes friction. It can be seen, that the simulation data lies in between both theoretical curves. The data in Fig. 5.16 can be fitted by using a free parameter for the colloid radius $R + \Delta R$ in Eq. (1.22). The fit result is then $\Delta R = 0.35$, which corresponds to an increased colloid radius.

5.3.5 Thermal diffusion coefficient from the drift velocity

In colloidal systems, the Soret coefficient can be determined from the drift velocity by rewriting Eq. (5.6) as

$$S_T = -D_s\frac{v_D}{\nabla_z T}. \tag{5.15}$$

This allows to compare the simulation results of S_T obtained from the drift velocity v_D with the previous results obtained from the thermophoretic force F_T.

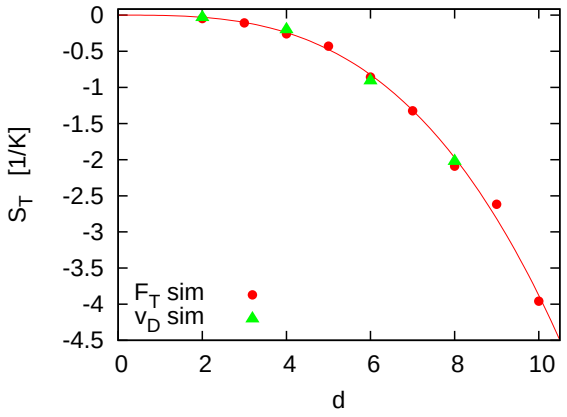

Figure 5.17: Size dependence of the Soret coefficient S_T. Comparison of results from "force measurement" and "drift velocity measurement". Repulsive 12-6 potential with strength $\epsilon = 1$ at temperature $T_0 = 1$ at constant ratio $\sigma_{cs}/L = 1/12$.

We use the case of repulsive colloid-solvent interactions with a repulsive Lennard-Jones 12-6 potential and a potential strength of $\epsilon = 1.0$. Fig. 5.17 shows that the results for the Soret coefficient determined from measurements of the drift velocity are in agreement with the results of the measurements of the thermophoretic F_T. Moreover, these results prove that confining the colloid with a harmonic potential is not relevant for the thermal diffusion coefficient.

In a complementary analysis, we want to check that the validity of the different expressions for the relation of the drift velocity and the thermophoretic mobility in Eq. (5.5) and Eq. (5.6). Reformulating Eq. (5.5) and using $S_T = D_T/D_s$ leads to

$$S_T = \frac{1}{D_s}\frac{\partial D_s}{\partial T} - \beta_T - \frac{1}{D_s}\frac{v_D}{dT/dz}. \tag{5.16}$$

The thermal expansion coefficient for the MPC solvent is known to be $\beta_T = 1/k_B T$. Since the simulations have been performed at temperature $T_0 = 1$, we have $\beta_T = 1$. The term $\partial D_s/\partial T$ is obtained from equilibrium measurements of D_s at different temperatures. From these measurements, which are shown in Fig. 5.18 it follows that $\partial D_s/\partial T = 0.0059$. The diffusion coefficient at T_0 is $D_s = 0.0065$. That means that the first two terms Eq. (5.16) are in the

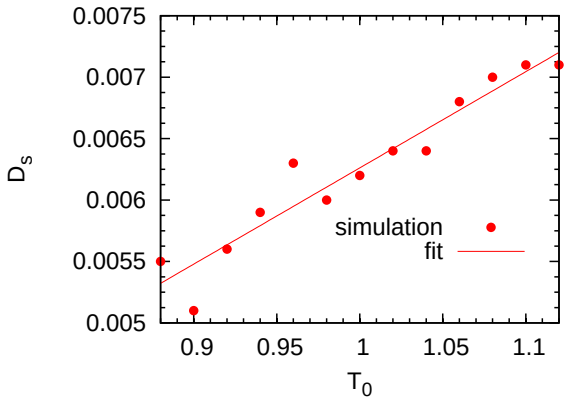

Figure 5.18: Temperature dependence of the self diffusion coefficient D_s from equilibrium measurements at different system temperatures T_0.

order of 1. The last term is can be estimated to be about 25, which is much larger than the first two terms. This quantitative analysis confirms that in the case of macroscopic colloids with Lennard-Jones colloid-solvent interactions the additional terms in Eq. (5.5) compared to Eq. (5.6) can indeed be neglected.

5.3.6 Analytical determination of the thermophoretic force

The total force of all fluid particles interacting with the colloid can be calculated analytically, by integrating over all interactions between colloid and solvent particles. The total force is

$$\boldsymbol{F}_{total} = \int_{\mathbb{R}^3} d^3r \rho(\boldsymbol{r}) \boldsymbol{f}_{cs}(\boldsymbol{r}), \tag{5.17}$$

where the center of the coordinate system is in the center of the colloid. Here $\boldsymbol{f}_{cs}(\boldsymbol{r})$ is the force density given by the colloid-solvent interaction potential

$$\boldsymbol{f}_{cs}(\boldsymbol{r}) = -\nabla U_{cs}(r). \tag{5.18}$$

The discrete solvent particles can be described by a continuous stationary density $\rho(\boldsymbol{r})$ which is understood as the average local density neglecting spatial and temporal fluctuations. Thus resulting total force $\boldsymbol{F}_{total}$ is the average force due to an average continuous density of solvent particles. On the basis of local equilibrium the density within the colloid-solvent interaction potential is given by

$$\rho(\boldsymbol{r}) = \rho_{bulk}(\boldsymbol{r}) \exp\left[-U_{cs}(r)/k_B T(\boldsymbol{r})\right], \tag{5.19}$$

where $\rho_{bulk}(\boldsymbol{r})$ is the bulk density of the solvent, which is given by the equation of state of the solvent (see chapter 3) and $T(\boldsymbol{r})$ is the temperature as given in Eq. (3.2). For small temperature gradients the bulk density can be approximated linearly by

$$\rho_{bulk}(\boldsymbol{r}) = \rho\left(1 - \beta_T \frac{\Delta T}{L_z} z\right), \tag{5.20}$$

where β_T is the thermal expansion coefficient of the solvent and $\Delta T = T_h - T_c$ the difference between the boundary temperatures.

A comparison of the density computed from Eq. (5.19) with simulation data can be seen in Fig. 5.19, for an attractive LJ 12-6 potential. In the region of the attractive part of the potential the solvent density increases with respect to the bulk value. The maximum value of the density is proportional to $\exp(\epsilon/k_B T)$, which can be inferred from Eq. (5.19). This means that for strong attractive potentials and low temperatures there is an largely enhanced surface density at the colloid. Within the repulsive part the density decays quickly. The decay is slower for higher temperatures and there is an asymmetry of the decay on the cold and hot side of the colloid which contributes to the total force F_{total}. For purely repulsive potentials the surface density of the solvent is similar except for the peak. Previous simulations of polymers that included attractive colloid-solvent interactions in a hybrid model of MPC and MD in polymer simulations have not reported a density increase [60].

Solving Eq. (5.17) shows (see appendix 7.2), that the only non-vanishing contribution is parallel to the temperature gradient whereas the perpendicular terms are zero. In the appendix 7.2 it is shown that Eq. (5.17) can be reduced to

$$F_{total} = \frac{4}{3}\pi \frac{\rho}{T_0}\frac{\Delta T}{L_z}\int_0^{r_c} dr\; r^3 \frac{\partial U_{cs}(r)}{\partial r}\left[\frac{U_{cs}(r)}{T_0} - T_0\beta_T\right]\exp\left[-\frac{U_{cs}(r)}{T_0}\right], \tag{5.21}$$

which can be solved numerically. This expression for the thermophoretic force can be used to calculate the Soret coefficient by means of Eq. (5.7). A comparison of the analytical and simulation results of the Soret coefficient is shown in Figs. 5.20 and 5.21, where we have obtained the simulation data of measurements of the thermophoretic force with the colloid confined in a harmonic potential. The simulation data have been rescaled by the finite size relation in described in section 5.2.6. Note that the finite size relation can be different for different potentials. We have not analyzed this with sufficiently precise data in simulations and assume here that the relation of section 5.2.6 can be used.

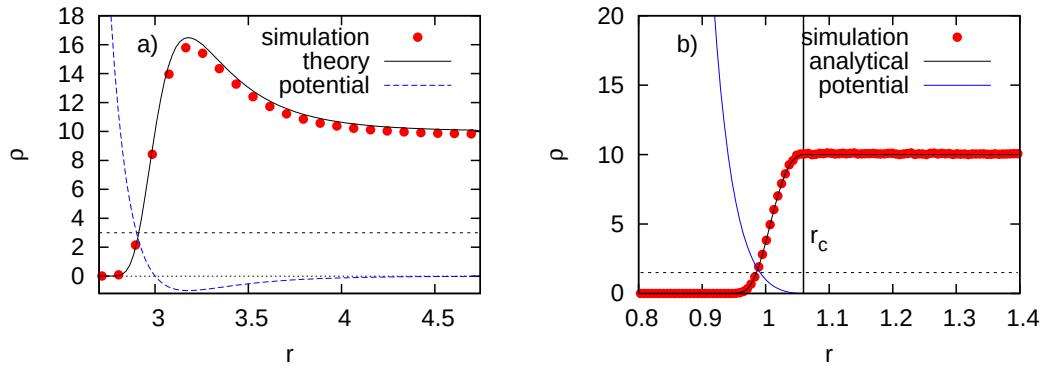

Figure 5.19: Local fluid density as a function of the distance from the center of the colloid. Symbols are the simulation data, the solid line is the analytical expression obtained with Eq. (5.19) and the dashed line is the employed potential. Average density $\rho = 10$. a) LJ 12-6 potential, strength $\epsilon = 1.0$, colloidal particle radius $\sigma_{cs} = 3.0$ and solvent temperature is $T = 2.0$. b) rLJ 12-6 potential, strength $\epsilon = 1.0$, colloidal particle radius $\sigma_{cs} = 1.0$ and solvent temperature is $T = 1.0$.

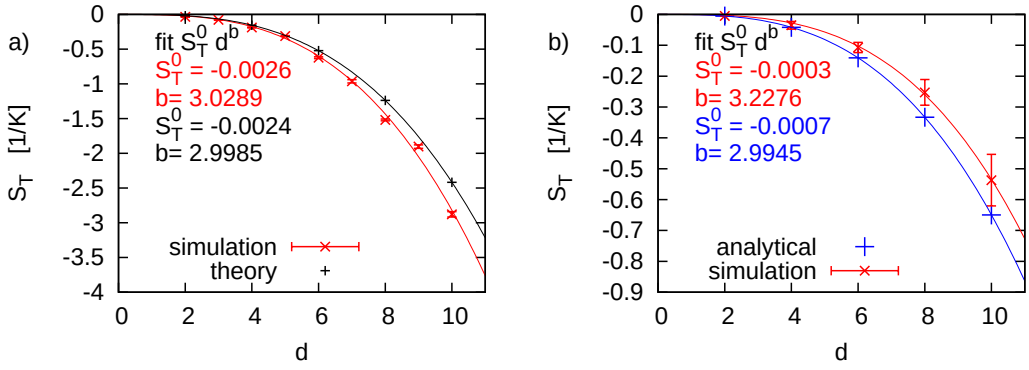

Figure 5.20: Dependence of the Soret coefficient on the particle size and comparison to analytical expression for a) repulsive LJ 12-6 with $\epsilon = 1$ and $T_0 = 1$ and b) LJ 24-12, $\epsilon = 0.1$ and $T_0 = 1$. Simulation data rescaled with finite size correction Eq. (5.8) (constant ratio $\sigma_{cs}/L = 1/12$) and theoretical values divided by factor 2.

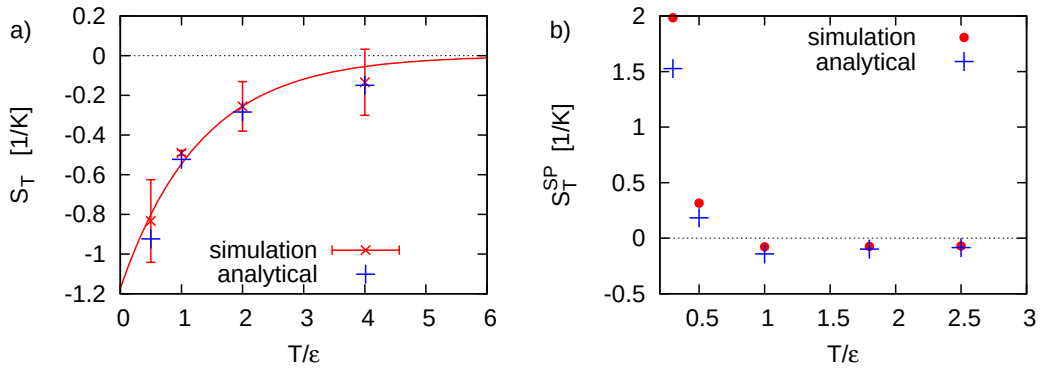

Figure 5.21: Dependence of the Soret coefficient on the temperature for a) repulsive LJ 12-6 with $\epsilon = 1$ and $\sigma_{cs} = 3$ and b) LJ 24-12 $\epsilon = 0.1$ and $\sigma_{cs} = 3$. Comparison to analytical expression. Simulation data rescaled with finite size correction Eq. (5.8) with $(\sigma/L = 1/12)$ and theoretical values divided by factor 2.

It can be shown that the total force F_{total} which qualitatively agrees with the simulated thermophoretic forces, apart from a systematic deviation of the results by a factor of about 2 (theory is larger than simulations by a factor 2). The analytical data in Figs. 5.20 and 5.21 is already rescaled by this factor. At the moment it is not clear where this deviation originates from. It is conspicuous that the deviation is systematic in all cases and is also not depending on the direction of the thermophoretic force. One reason might be that there is an additional contribution to the thermophoretic force which is related to momentum exchange between solvent and colloid. Independently of these findings, it is observed that F_T is proportional to the number of particles within the cut-off radius of the potential. The volume in which the solvent particles interact with the colloid is proportional to the thickness of the interaction shell and the surface of the colloid. In the case of a normal Lennard-Jones potential the cut-off radius increases with the particle size, which means that the number of particles within the interaction shell increases proportional to σ_{cs}^3, which results in a cubic size dependence of the thermophoretic force and Soret coefficient.

5.3.7 Displaced Lennard Jones potential

With a LJ potential, in which the interaction shell thickness is kept constant, a quadratic behavior for the Soret coefficient can be expected since then the

number of solvent particles in the interaction shell is proportional to the surface of the colloid. This can be achieved with a Lennard-Jones potential by increasing the colloid size not by increasing σ, but instead by displacing the potential by the desired particle size and keeping σ constant. The displacement in $\boldsymbol{r}$-direction of the potential is a_d. Then the diameter of the colloid is the given by

$$d = 2(a_d + \sigma_{cs}) \tag{5.22}$$

and σ_{cs} can be used to modify the range of the potential. The displaced Lennard-Jones potential (see for example Ref. [79]) for repulsive interactions is given by

$$U^{rdLJ}(r_{ij}) = 4\epsilon \left[\left(\frac{\sigma_{cs}}{r_{ij} - a_d} \right)^{2n} - \left(\frac{\sigma_{cs}}{r_{ij} - a_d} \right)^{n} \right] + \epsilon, \quad r_{ij} < r_c \ , \tag{5.23}$$

where the cut-off radius is

$$r_c = a_d + 2^{\frac{1}{n}} \sigma_{cs}. \tag{5.24}$$

The displaced Lennard-Jones potential for attractive interactions is given by

$$U^{dLJ}(r_{ij}) = 4\epsilon \left[\left(\frac{\sigma_{cs}}{r_{ij} - a_d} \right)^{2n} - \left(\frac{\sigma_{cs}}{r_{ij} - a_d} \right)^{n} \right], \quad r_{ij} < r_c \ . \tag{5.25}$$

Here the cut-off radius is chosen with the reference of the value of the standard Lennard-Jones potential at $\tilde{r}_c = 2.5\sigma_{cs}$, denoted as $U^{12-6}_{\epsilon=1} = U^{12-6}_{\epsilon=1}(\tilde{r}_c)$, such that it can be estimated as

$$r_c = a_d + 2^{\frac{1}{n}} \left(\frac{1}{1 - \sqrt{1 + \frac{U^{12-6}_{\epsilon=1}}{\epsilon}}} \right)^{\frac{1}{n}} \sigma_{cs} \ . \tag{5.26}$$

The actual shape of the potential in case of attractive interactions is shown in Fig. 5.22 for different values of the diameter.

The number of solvent particles that interact with the colloid N_{int} can be calculated from

$$N_{int} = \int_{\{\boldsymbol{r} |\ \boldsymbol{r} \in \mathbb{R}^3, r \leq r_c\}} d^3 r \rho_{bulk}(\boldsymbol{r}) \exp\left[-U_{cs}(r)/k_B T(\boldsymbol{r})\right]. \tag{5.27}$$

In Fig. 5.23 it is shown that the number of solvent particles that interact with the colloid scales with the colloid diameter with a quadratic power law in the case of a displaced repulsive LJ potential and with a cubic power law in the case of a standard repulsive LJ potential. This is the same scaling that holds for the

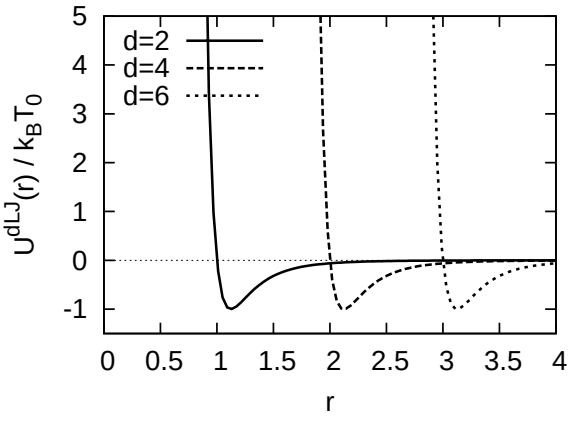

Figure 5.22: Attractive diplaced LJ potential in Eq. (5.25) for different colloid diameters. The range of interaction remains constant for all particle sizes.

thermophoretic force and thus the single particle Soret coefficient in our model. For attractive interactions the situation is similar. Note that the numbers of interacting particles are not rescaled by a factor two, as in the case of the Soret coefficients.

It can be observed in simulations that the size dependence of the Soret coefficient with a potential in which the range does not change with the particle size, is indeed quadratic. This is shown in Fig. 5.24 a) for a simulation with a repulsive displaced Lennard-Jones 12-6 potential with a strength of $\epsilon = 1.0$ at a mean temperature of $T_0 = 1.0$. Fig. 5.24 b) shows the numerical solutions of Eq. (5.21) for a displaced LJ 12-6 potential with strength $\epsilon = 1$ and range $\sigma_{cs} = 0.25$ at temperature $T_0 = 1.0$. The simulation data have been rescaled by the finite size relation described in section 5.2.6 for comparisons to the theoretical values.

Fig. 5.25 shows the a double logarithmic plot, to demonstrate the different power laws for the scaling of the Soret coefficient with particle size for the standard LJ potential and the displaced LJ potential.

Note that the displacement of the LJ potential must be considered in the integration range in Eq. (5.17) and Eq. (5.21) by integrating from a_d to r_c. Furthermore, it has been observed in the numerical solutions of Eq. (5.21), that eventually larger reference cut-off radii of the standart LJ potential in Eq. (5.26) are needed, like for example $\tilde{r}_c = 5.5\sigma_{cs}$ instead of $\tilde{r}_c = 2.5\sigma_{cs}$. Otherwise the potential is cut-off too early and the size scaling of the Soret coefficient deviates from a quadratic dependence (smaller exponent). This is more important when

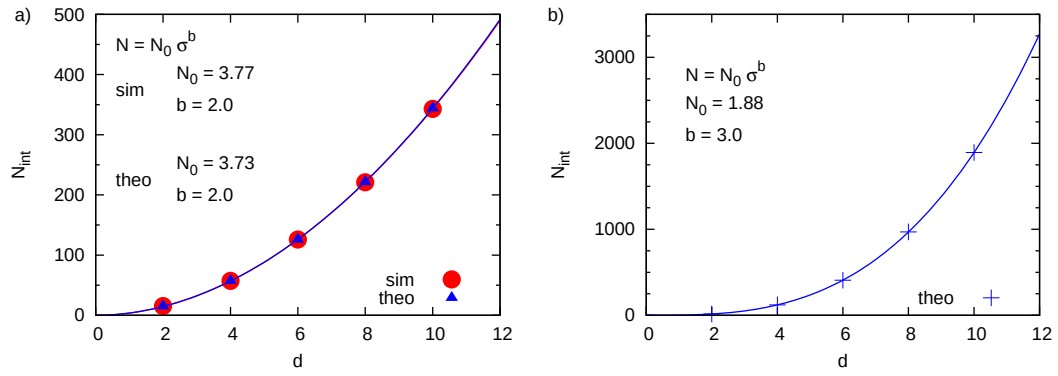

Figure 5.23: Number of interacting solvent particles with the colloid depending on the colloid size. Simulation results and theoretical analysis from Eq. (5.27). a) displaced repulsive LJ 12-6 potential with $\epsilon = 1.0$, $\sigma_{cs} = 1.0$, and $T_0 = 1.0$. Particle size changed displacing the LJ potential by a_d in Eq. (5.23) b) standard repulsive LJ 12-6 potential with $\epsilon = 1.0$ and $T_0 = 1.0$. Particle size changed by varying σ_{cs} Eq. (2.4).

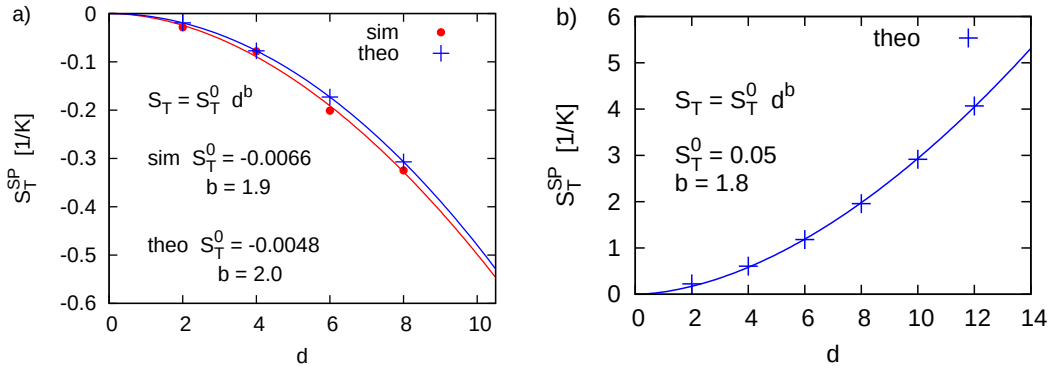

Figure 5.24: Dependence of the Soret coefficient on the particle size. Simulation results and theoretical analysis. a) displaced repulsive LJ 12-6 potential with $\epsilon = 1.0$, $\sigma_{cs} = 1.0$ and $T_0 = 1.0$. Simulation data rescaled with finite size correction Eq. (5.8) (constant ratio $\sigma_{cs}/L = 1/12$) and theoretical values from numerical evaluation of Eq. (5.21) divided by factor 2. b) displaced attractive LJ 12-6 potential, $\epsilon = 0.25$, $\sigma_{cs} = 1.0$ and $T_0 = 1.0$. Theoretical values from numerical evaluation of Eq. (5.21), Reference cut of in Eq. (5.26) $\tilde{r}_c = 5.5\sigma_{cs}$.

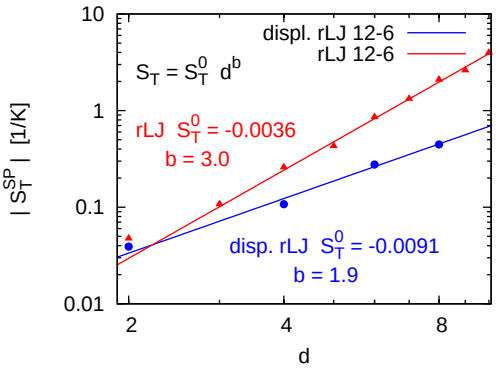

Figure 5.25: Dependence of the Soret coefficient on the particle size. Simulation results for different potentials with $\epsilon = 1.0$ and $T_0 = 1.0$, displaced repulsive LJ 12-6 potential with $\sigma_{cs} = 1.0$ and varying a_d and standard repulsive LJ 12-6 potential with varying σ_{cs}.

small potential strengths ϵ are used. The resulting cut of radii for the displaced LJ potential are still not much larger or even smaller than applying LJ potentials from Eq. (2.5). The computational effort should therefore be not larger. This has however, not been confirmed through simulations and tests (analytic and simulations) for appropriate cut-off radii in Eq. (5.25) would be needed.

5.4 Conclusions and outlook

Numerous experimental investigations have shown that the thermophoretic properties of a colloidal suspension in the limit of dilute solutions depend strongly on the particle size and on the average system temperature. These properties are determined by the specific interactions of the colloid with the surrounding solvent, which might depend on the nature of the system under study.

In this chapter a simulation study of the thermodiffusion properties of a colloidal system in the dilute regime is presented. The employed simulation model considers explicit potential interactions between the solvent particles and the colloid, allowing to investigate how different interactions vary the thermodiffusion properties of the solution. We study the influence of different factors, namely the attractive or repulsive character of the interaction, the average temperature of the system, the size of the colloidal particle, the softness of the repulsive interaction, and the strength, and the range of the attractive interactions.

Two different approaches to measure the Soret coefficient have been employed.

The first one consists in attaching the colloid to a harmonic spring. The average deformation of the spring can then be related with the thermophoretic force what quantifies the Soret coefficient. The second approach consists in measuring the drift velocity of the free colloid. Both methods can be compared by employing the corresponding self-diffusion coefficient. The good agreement of the measurements confirms the validity of the performed approximations. Furthermore, we propose an analytical determination of the Soret coefficient that explains quite satisfactory the obtained simulation results.

The thermophoretic behavior of one colloid in a solvent can be understood as the interplay of various effects. We consider first the variations of temperature and density around the colloid surface. Particles with higher temperatures penetrate further into the repulsive part of the potential than those with lower temperature. In a temperature gradient then, particles in the hot side will *push* the colloid to the cold side. Simultaneously though, the solvent equation of state translates into a larger number of particles interacting with the colloid on its cold side than on the warm side. This implies that when the interactions are attractive, the colloid is *pulled* to the cold side, while for repulsive interactions the colloid is *pushed* to the hot side. This effect can explain our results that show that colloids with repulsive colloid-solvent interactions display negative Soret coefficient (colloid goes to warm), while colloids with attractive interactions show a positive one (colloid goes to cold). With increasing temperature, the repulsive part of the employed potential becomes more important, what can explain a sign change of S_T from positive to negative.

Colloids with potentials with a softer repulsive core show to experience larger thermophoretic forces. The softer the repulsion, the higher the penetration of the solvent particles, what results on a higher number of particles in the interaction region and therefore larger forces. We investigate the dependence of the Soret coefficient as a function of the average temperature. Here the qualitative behavior is very different for colloids that have a certain attraction interaction range, or for those that are purely repulsive. Attractive interactions show a crossover from positive to negative S_T values, what can be justified with the above argument, as the increasing importance of the repulsive core. Purely repulsive interactions remain being negative, but with increasing value. Experimental observations report though a sign change from negative at low temperatures to positive at high ones, with a saturation value at very high temperature values. Our simulation with attractive interactions are therefore in

disagreement with this behavior, but not the simulations with purely repulsive interactions.

We further analyze the dependence of the Soret coefficient as a function of the colloid diameter, and we observe that in most of our results this dependence is cubic. This can be explained by the nature of the colloid-solvent interaction potential that we use, in which an increase of the colloid size increases also the interaction range. An increase of the colloid diameter increases then the "interaction volume" in which the number of interacting solvent particles scales with the cube of the colloid size. In order to check this argument, we employ a different type of potential in which the interaction range is constant with increasing colloid diameter what implies a quadratic increase of the "interaction volume". The resulting Soret coefficient shows, to a good approximation, to increase quadratically with the diameter. Note though that experimental results exhibit mostly a linear dependence with the exception of one group that observes a quadratic dependence. Another factor that has been reported to influence the thermophoretic properties of colloids is the coupling at the interface. The difference is if the solvent adapts to colloid by having the same velocity field at the surface (stick boundary conditions), or if there is a velocity difference between them (slip boundary conditions). The employed potential interactions in this work are central and therefore display slip boundary conditions. Additional simulations with a model that includes stick boundary conditions would clarify the influence of this contribution and if it will lead to a different size dependence.

Finally, it would also be interesting to extend the present study to understand the importance of the characteristics of the employed solvent. This could be done by modifying the MPC solvent such that its compressibility and thermal expansion would not be those of an ideal gas.

6 Conclusions

Thermodiffusion in colloidal suspensions includes hydrodynamic, diffusive and chemical effects. These are in general strongly influenced by interactions between colloids and the solvent and additionally by mutual colloid interactions.

We have used a mesoscopic simulation method to study suspensions of colloids with a temperature gradient. The method is known as multi-particle collision dynamics and has been used in many complex systems simulations, such as for example star polymers in shear flow or blood cells in capillary flow. The method bridges the time and length scale gap that arises from the suspended colloids and the fluid particles. The method locally conserves momentum and thus includes hydrodynamic interactions. Also, the method locally conserves energy and enables the transport of heat. Furthermore, thermal fluctuations are naturally included and diffuse behaviors are properly taken into account.

First we analyzed the properties of the MPC solvent in the presence of a temperature gradient in detail. We investigate different implementations regarding systems in confinement or in bulk. In confinement, hard walls are used as boundary conditions and the temperature gradients are imposed in two ways. Thermostats are applied in the boundary layers in which the kinetic energies of the solvent particles are rescaled. Second we consider the effect of virtual particles placed at the walls, what means that the walls act as thermal baths that we can fix at different temperatures. A third model accounts for the solvent with open boundaries and does not impose boundary temperatures, but a heat flux which leads to a temperature gradient. For all of the investigated methods the temperature profile is linear in the bulk region for the range of temperature gradients that we used. All of the above methods can be applied as long as the solvent parameters are chosen such that the mean free path of the fluid particles corresponds to the liquid like regime. For larger mean free bath boundary effects occur and the temperature profile does not adapt well to the boundary temperatures. In simulations of the heat conductivity we obtain a reasonable agreement with existing analytic predictions. The solvent parameters determine

the viscosity and other hydrodynamic properties. With this mesoscopic implementation, we have investigated colloidal suspensions with different simulation models.

The thermophoretic properties of colloidal suspensions are determined by two types of effects. The collective effects due to the simultaneous presence of many colloids and their interactions; and single particle effects due to the interaction of the colloid surface and the surrounding solvent.

The first method that we used, included colloid-colloid interactions and has been used to study collective effects in concentrated systems. The coupling to the solvent has been included in the MPC collision step, where momentum between the particles is exchanged. This coupling has resulted in a small contribution to the Soret coefficient that was attributed to the thermodiffusive mass effect. This contribution was independent on the concentration within the investigated range. We studied the collective contribution with repulsive and attractive interaction potentials. Repulsive interactions disfavor an inhomogeneous distribution which results in increasing negative Soret coefficients with increasing volume fraction of colloids. Experiments, when analyzed with respect to the collective contribution, show a similar trend. Colloidal particles with attractive interactions facilitate an inhomogeneous distribution in the temperature gradient. They accumulate in the cold region with respect to the solvent at low average volume fractions of the suspension. Eventually, when repulsive overlap of the interaction potential dominates, they are driven more to the warm side. This results in positive Soret coefficients at low volume fractions and negative Soret coefficients a high volume fractions. This behavior is enhanced for longer attraction ranges and larger potential strengths.

The second simulation model focuses on the investigation of single particle effects and includes excluded volume colloid-solvent interactions in dilute suspensions. Dilute suspension are investigated with this model and the Soret coefficient is determined with two types of measurements. In the first the thermophoretic force is measured by confining the colloid with a harmonic potential. And in the second the drift velocity is calculated from the average displacement of free colloids. The agreement of both methods confirms their validity and shows that the confinement does affect the single colloid Soret coefficient. In order to study the effect of the coupling to the solvent, we applied different types of colloid-solvent interaction potentials. We used repulsive and attractive interactions, implemented with Lennard-Jones type potentials. From experiments it

is known that the single colloid properties have a large influence on the overall thermodiffusive properties of the suspension and that they strongly depend on the average suspension temperature and the size of the colloids.

The temperature dependence of the Soret coefficient of dilute colloidal systems is described by an empirical exponential law with an asymptotically saturating increase. At low average suspension temperatures (e. g. 5 ° C for polystyrene particles) the colloids have small or even negative Soret coefficient, which means that they experience a small driving force towards the cold side or they are even driven to the warm side of the system. At high temperatures (e. g. larger than 20 ° C for polystyrene particles) the colloids are driven to the cold side of the system. In our simulations we find that colloids with repulsive colloid-solvent interaction potentials are driven to the hot side of the system at all temperatures. We have attributed this effect to a counterplay between the density and temperature gradient in the MPC fluid, which is also related to the fact that we use soft potentials. Due to the density gradient of solvent particles, the repulsive forces on the cold side of the colloid are larger than on hot side, which effectively drives the colloid towards the hot side of the system. On the other hand, the temperature gradient has the reverse effect due to the non-uniform distribution of kinetic energies, which results in different penetration depths in the colloid-solvent interaction potential on either side of the colloid. In total, the force due to the density gradient is stronger and the colloid is effectively driven towards the hot side of the system. With increasing temperature the opposing forces compensate each other and the effective force, i. e. the resulting Soret coefficient, converges to zero. The overall behavior can be described by an exponential increase which saturates asymptotically as in the experiments, but a sign change with increasing temperature is not observed. If we apply attractive potentials the mechanism that determines the thermophoretic force is similar, but due to the attractive interactions there is an additional contribution to the thermophoretic force from the density gradient driving the colloid towards the cold side. Effectively the colloid is driven to the cold side of the system at low temperatures and to the hot side at high temperatures, when the contribution from the repulsive core dominates.

The size dependence of the Soret coefficient has been measured to be linear by various experimental groups and to be quadratic by one group. In our simulations we obtain a cubic size dependence with normal Lennard-Jones potentials, apart from two cases that might have been chosen with too large attraction

strengths for the compressible MPC solvent. Otherwise, the cubic size dependence is found for both, attractive and repulsive interactions. This has been attributed to the fact that the number of interacting solvent particles depends cubic on the colloid size. This number is proportional to the surface area and proportional to the layer thickness in which the solvent interacts with the colloid. In the case of standard LJ potentials this thickness increases linear with particle size, which leads to an overall cubic behavior. LJ potentials that increase the particle size not by the range, but by a radial displacement keep the interaction layer thickness constant. With these displaced LJ potentials we observed a quadratic size dependence.

We can describe our simulation results qualitatively from theoretical analysis, which considers local equilibrium. It was observed that local equilibrium is fullfilled by showing that the solvent particle velocities are locally Maxwell-Boltzmann distributed. The theory does not consider hydrodynamic effects, which can become especially important, when colloids with stick surface boundary conditions are considered. Stick boundary conditions can be an important factor that influences thermodiffusion of single colloids, because they exert tangential forces on the colloid, which can contribute to the thermophoretic force. The interactions that we applied, act with central forces which results in slip boundary conditions. Preliminary results with a model that includes stick boundary conditions seem to indicate that the Soret coefficient scales with a power law with an exponent 1.5 with the particle size. Further simulations would still be necessary to resolve the experimentally debated linear or quadratic exponent. Furthermore, an MPC solvent with a different thermal expansion coefficient would be an interesting subject of study. And finally, concentrated colloidal suspension with a combination of both of our model systems are the next goal, so that colloid-solvent and mutual colloid interactions are considered. In this respect one could elucidate, if the contributions to the Soret coefficient can be expressed as the sum of the contribution given by the limiting cases of the two models that we have studied or if additional effects appear. For example, the single particle contribution or equivalently the interaction of the solvent at the colloid surface can modify its value with increasing concentration due to the inter-colloidal interaction. Additionally, the presence of lubrication forces or an enhanced effect of hydrodynamic interactions may affect the Soret coefficient.

7 Appendix

7.1 Colloid-solvent interaction

The colloid-solvent (cs) interactions are computed by using a list in which the solvent particles close to the colloids are stored. More precisely these are particles which are within a certain distance r_{list} from the center of the respective colloid. This distance is chosen larger than the cut off radius of the colloid-solvent interaction potential r_c. The list is updated each MPC step and is kept for one whole MD cycle. Therefore it has to be ensured that no that no interactions are missed out and the radius r_{list} has to be chosen large enough. The additional distance $\Delta r = r_{list} - r_c$ has to be larger than hv_{max}, where v_{max} is the maximum relative velocity between colloid and solvent. From experience it was found that $v_{max} \approx 8$ to be on the safe side. So with a typical value for the collision time $h = 0.1$, one has to choose $\Delta r \geq 0.8$.

The list is constructed in the following way. In the MPC step all solvent particles are streamed by the distance hv_i. Then it is checked which particles are closer the r_{list} to the respective colloids and for each colloid the list is updated. Then before the following MD steps the particles within r_{list} are set back to their original positions and from there their positions are updated with MD. This procedure corresponds to Verlet lists which commonly used in MD simulations.

7.2 Thermophoretic force

The thermophoretic force can be calculated by summing all individual forces of each solvent particle with the colloid

$$\boldsymbol{F}_T = \sum_{i}^{N_{at\ coll}} \boldsymbol{F}_i, \tag{7.1}$$

where $N_{at\ coll}$ is the number of particles that interact with the colloid. Taking the averages over the simulation time and different runs, the discrete particle

positions can be described by a continuous density

$$< \sum_{i}^{N_{at\ coll}} \delta(\boldsymbol{r} - \boldsymbol{r}_i) > \widehat{=} \rho(\boldsymbol{r}). \tag{7.2}$$

Which means that the individual forces transform into an integral over the local force and density

$$\boldsymbol{F}_T = < \sum_{i}^{N_{at\ coll}} \boldsymbol{F}_i > \widehat{=} \int_{\mathbb{R}^3} d^3r \boldsymbol{f}(\boldsymbol{r})\rho(\boldsymbol{r}). \tag{7.3}$$

Since the forces perpendicular to the temperature gradient are zero, we can only consider the direction of the temperature gradient, which we apply in the z-direction.

On the basis of local equilibrium the fluid density in the presence of the interaction potential $U_{cs}(r)$ of the colloid is given by

$$\rho(\boldsymbol{r}) = \rho_{bulk}(\boldsymbol{r}) \exp\left[-U_{cs}(r)/k_B T(\boldsymbol{r})\right],$$

where $\rho_{bulk}(\boldsymbol{r})$ is the bulk density of the solvent, which is given by the equation of state of the solvent (see chapter 3) and the temperature is $T(\boldsymbol{r}) = T_0 + \frac{\Delta T}{L_z} z$. Here we have applied a coordinate system with the origin placed in the center of the colloid. For small temperature gradients the bulk density can be approximated linearly by

$$\rho_{bulk}(\boldsymbol{r}) = \rho_0 \left(1 - \beta_T \frac{\Delta T}{L_z} z\right),$$

where β_T is the thermal expansion coefficient of the solvent. Then the fluid density in spherical coordinates is

$$\rho(r,\theta) = \rho_0 \left[1 - \beta_T \frac{\Delta T}{L_z} r\cos(\theta)\right] \exp\left[-\frac{U(r)}{T_0 + \frac{\Delta T}{L_z} r\cos(\theta)}\right], \tag{7.4}$$

with the thermal expansion coefficient

$$\beta_T = -\frac{1}{\rho}\left(\frac{\partial \rho}{\partial T}\right)_p.$$

Then the the force is

$$\begin{aligned} F_T &= \int \boldsymbol{F}(r)\boldsymbol{e}_z \rho(r,\theta)\, d^3r \\ &= \int_0^{2\pi}\int_0^{\pi}\int_0^{r_c} r^2 \sin(\theta) \frac{\partial U(r)}{\partial r} \cos(\theta)\rho_0 \left[1 - \beta_T \frac{\Delta T}{L_z} r\cos(\theta)\right] \exp\left[-\frac{U(r)}{T_0 - \frac{\Delta T}{L_z} r\cos(\theta)}\right] d\phi\, d\theta\, dr. \end{aligned}$$

The exponential term contains the θ and r dependence of the temperature, which is difficult to handle in the following calculation of the thermophoretic force from the integral. Since the temperature difference ΔT is much smaller than the average temperature T_0, we can perform a Taylor expansion for small $\Delta T/T_0$. From the Taylor expansion one can obtain

$$\exp\left[-\frac{U(r)}{T_0(1+\frac{\Delta T}{T_0}\frac{r}{L_z}\cos(\theta))}\right] = \left[1+\frac{\Delta T}{T_0}\frac{U(r)}{T_0}\frac{r}{L_z}cos(\theta)\right]\exp\left[-\frac{U(r)}{T_0}\right]+\mathcal{O}\left[\left(\frac{\Delta T}{T_0}\right)^2\right]. \tag{7.5}$$

After solving the angular integrals, the final expression for the thermophoretic force is

$$F_T = \frac{4}{3}\pi\frac{\rho_0}{T_0}\frac{\Delta T}{L_z}\int_0^{r_c} r^3\left(\frac{U(r)}{T_0}-\beta_T T_0\right)\frac{\partial U(r)}{\partial r}\exp\left(-\frac{U(r)}{T_0}\right)\,dr.$$

In the case of a solvent with an ideal gas equation of state (like standart MPC) the thermal expansion coefficient is $\beta_T = 1/T_0$. Partial integration for $r_c \gg \sigma$ so that $U(r_c) \approx 0$ leads to

$$F_T = \frac{4}{3}\pi\frac{\rho_0}{T_0}\frac{\Delta T}{L_z}\int_0^{r_c} 3r^2U(r)\exp\left(-\frac{U(r)}{T_0}\right)\,dr. \tag{7.6}$$

Bibliography

[1] E. Allahyarov and G. Gompper. Mesoscopic solvent simulations: Multiparticle-collision dynamics of three-dimensional flows. *Phys. Rev. E*, 66:036702, 2002.

[2] M. P. Allen and D. J. Tildesley. *Computer Simulations in Liquids*. Clarendon, 1987.

[3] P. A. Artola and B. Rousseau. Microscopic interpretation of a pure chemical contribution to the soret effect. *Phys. Rev. Lett.*, 98:125901, 2007.

[4] J. Bonet Avalos and A. D. Mackie. Dissipative particle dynamics with energy conservation. *EPL (Europhysics Letters)*, 40(2):141, 1997.

[5] J. A. Barker and D. Henderson. What is "liquid"? understanding the states of matter. *Rev. Mod. Phys.*, 48(4):587–671, Oct 1976.

[6] Patrice Bordat, Dirk Reith, and Florian Müller-Plathe. The influence of interaction details on the thermal diffusion in binary lennard-jones liquids. *J. Chem. Phys.*, 115:8978–8982, 2001.

[7] M. Braibanti, D. Vigolo, and R. Piazza. Does thermophoretic mobility depend on particle size? *Phys. Rev. Lett.*, 100:108303, 2008.

[8] Howard Brenner. Elementary kinematical model of thermal diffusion in liquids and gases. *Phys. Rev. E*, 74(3):036306, Sep 2006.

[9] E. Bringuier. On the notion of thermophoretic velocity. *Philosophical Magazine*, 87:873–883(11), 2007.

[10] F. H. Busse. *Mantle Convection: Plate Tectonics and Global Dynamics*, page 23. London, 1989.

[11] Norman F. Carnahan and Kenneth E. Starling. Equation of state for nonattracting rigid spheres. *The Journal of Chemical Physics*, 51(2):635–636, 1969.

[12] Norman F. Carnahan and Kenneth E. Starling. *The Journal of Chemical Physics*, 53:600, 1970.

[13] S. Chapman. *Philos. Trans. R. Soc. London Ser. A*, 217:115, 1917.

[14] S. Chapman and T. G. Cowling. *The mathematical therory of non-uniform gases*. Cambridge University, 1952.

[15] S. Chapman and F. Dootson. *Philos. Mag.*, 33:248, 1917.

[16] Klaus Clusius and Gerhad Dickel. Neues verfahren zur gasentmischung und isotopentrennung. *Naturwissenschaften*, 26:546–546, 1938. 10.1007/BF01675498.

[17] Helmut Cölfen and Markus Antonietti. Field-flow fractionation techniques for polymer and colloid analysis. *Adv. Pol. Sci.*, 150:67–187, 2000.

[18] S. R. de Groot and P. Mazur. *Non-equilibrium Thermodynamics*. 1962.

[19] Jan K. G. Dhont. Thermodiffusion of interacting colloids. I. A statistical thermodynamics approach. *J. Chem. Phys.*, 120:1632–1641, 2004.

[20] Jan K. G. Dhont. Thermodiffusion of interacting colloids. II. A microscopic approach. *J. Chem. Phys.*, 120:1642–1653, 2004.

[21] Stefan Duhr and Dieter Braun. Optothermal molecule trapping by opposing fluid flow with thermophoretic drift. *Phys. Rev. Lett.*, 97:038103, 2006.

[22] Stefan Duhr and Dieter Braun. Thermophoretic depletion follows boltzmann distribution. *Phys. Rev. Lett.*, 96:168301, 2006.

[23] Stefan Duhr and Dieter Braun. Why molecules move along a temperature gradient. *Proc. Natl. Acad. Sci.*, 103:19678–19682, 2006.

[24] Burkhard Dünweg and Kurt Kremer. Molecular dynamics simulation of a polymer chain in solution. *The Journal of Chemical Physics*, 99(9):6983–6997, 1993.

[25] A. Einstein. Über die von der molekularkinetischen theorie der wärme geforderte bewegung von in ruhenden flüssigkeiten suspendierten teilchen. *Annalen der Physik*, 322:549–560, 1905.

[26] J. Elgeti and G. Gompper. Self-propelled rods near surfaces. *EPL*, 85(3):38002, 2009.

[27] Jens Elgeti, U. Benjamin Kaupp, and Gerhard Gompper. Hydrodynamics of sperm cells near surfaces. *Biophysical Journal*, 99(4):1018 – 1026, 2010.

[28] D. Enskog. *Ann. Phys.*, 36:731, 1912.

[29] P. Español and P. Warren. Statistical mechanics of dissipative particle dynamics. 30:191, 1995.

[30] Pep Español. Hydrodynamics from dissipative particle dynamics. *Phys. Rev. E*, 52(2):1734–1742, Aug 1995.

[31] Pep Español. Dissipative particle dynamics with energy conservation. *EPL (Europhysics Letters)*, 40(6):631, 1997.

[32] Denis J. Evans and David MacGowan. Addendum to "heat and matter transport in binary liquid mixtures". *Phys. Rev. A*, 36:948–950, 1987.

[33] G. Galliero, B. Duguay, J.-P. Caltagirone, and F. Montel. On thermal diffusion in binary and ternary lennard-jones mixtures by non-equilibrium molecular dynamics. *Philosophical Magazine*, 83:2097–2108(12), 2003.

[34] G. Galliéro and S. Volz. Thermodiffusion in model nanofluids by molecular dynamics computer simulations. *J. Chem. Phys.*, 128:064505, 2008.

[35] Guillaume Galliéro, Bernard Duguay, Jean-Paul Caltagirone, and François Montel. Thermal diffusion sensitivity to the molecular parameters of a binary equimolar mixture, a non-equilibrium molecular dynamics approach. *Fluid Phase Equilibria*, 208:171–188, 2003.

[36] G. Gompper, T. Ihle, D. Kroll, and R. Winkler. Multi-particle collision dynamics: A particle-based mesoscale simulation approach to the hydrodynamics of complex fluids. In Christian Holm and Kurt Kremer, editors, *Advanced Computer Simulation Approaches for Soft Matter Sciences III*,

volume 221 of *Advances in Polymer Science*, pages 1–87. Springer Berlin / Heidelberg, 2009.

[37] B. Hafskjold, T. Ikeshoji, and S. K. Ratkje. On the molecular mechanism of thermal diffusion in liquids. *Molecular Phys.*, 80:1389–1412, 1993.

[38] B Hafskjold, T Ikeshoji, and SK Ratkje. On the molecular mechanism of thermal diffusion in liquids. *Molecular Phys.*, 80(6):1389–1412, DEC 20 1993.

[39] Bjorn Hafskjold, Ichiro Fujihara, and Tamio Ikeshoji. A comparison of non-equilibrium molecular dynamics and npt monte carlo methods for mixing properties and partial molar. *Molecular Phys.*, 90:999 – 1006, 1997.

[40] Bjorn Hafskjold and Signe Kjelstrup Ratkje. Criteria dor local equilibrium in a system with transport of heat and mass. *J. Stat. Phys.*, 78:463–494, 1995.

[41] M. Hecht, J. Harting, T. Ihle, and H. J. Herrmann. Simulation of claylike colloids. *Phys. Rev. E*, 72:011408, 2005.

[42] P. J. Hoogerbrugge and J. M. V. A. Koelman. Simulating microscopic hydrodynamic phenomena with dissipative particle dynamics. *EPL*, 19(3):155, 1992.

[43] James T. Hynes, Raymond Kapral, and Michael Weinberg. Molecular theory of translational diffusion: Microscopic generalization of the normal velocity boundary condition. *The Journal of Chemical Physics*, 70(3):1456–1466, 1979.

[44] S. Iacopini and R. Piazza. Thermophoresis in protein solutions. *Europhys. Lett.*, 63:247, 2003.

[45] T. Ihle and D. M. Kroll. Stochastic rotation dynamics: A galilean-invariant mesoscopic model for fluid flow. *Phys. Rev. E*, 63:020201(R), 2001.

[46] T. Ihle and D. M. Kroll. Stochastic rotation dynamics I: Formalism, galilean invariance, green-kubo relations. *Phys. Rev. E*, 67:066705, 2003.

[47] T. Ihle and D. M. Kroll. Stochastic rotation dynamics II: Transport coefficients, numerics, long time tails. *Phys. Rev. E*, 67:066706, 2003.

[48] T. Ihle, E. Tüzel, and D. M. Kroll. Resummed green-kubo relations for a fluctuating fluid-particle model. *Phys. Rev. E*, 70:035701(R), 2004.

[49] T. Ihle, E. Tüzel, and D. M. Kroll. Equilibrium calculation of transport coefficients for a fluid-particle model. *Phys. Rev. E*, 72:046707, 2005.

[50] Y. Inoue, Y. Chen, and H. Ohashi. Developement of a simulation model for solids objects suspended in a fluctuating fluid. *J. Stat. Phys.*, 107:85–100, 2002.

[51] R. Clark Jones and W. H. Furry. The separation of isotopes by thermal diffusion. *Rev. Mod. Phys.*, 18(2):151–224, Apr 1946.

[52] N. G. Van Kampen. Diffusion in inhomogeneous media. *Journal of Physics and Chemistry of Solids*, 49(6):673 – 677, 1988.

[53] Raymond Kapral. pages 89–146. John Wiley & Sons, Inc., 2008.

[54] N. Kikuchi, C. M. Pooley, J. F. Ryder, and J. M. Yeomans. Transport coefficients of a mesoscopic fluid dynamics model. *J. Chem. Phys.*, 119:6388–6395, 2003.

[55] J.M. Kincaid and B. Hafskjold. Thermal diffusion factors for the lennard-jones/spline system. *Molecular Phys.*, 82:1099–1114, 1994.

[56] J.M. Kincaid and B. Hafskjold. Thermal diffusion factors for the lennard-jones/spline system. *Molecular Phys.*, 82:1099–1114, 1994.

[57] Anthony J. C. Ladd, Hu Gang, J. X. Zhu, and D. A. Weitz. Temporal and spatial dependence of hydrodynamic correlations: Simulation and experiment. *Phys. Rev. E*, 52(6):6550–6572, Dec 1995.

[58] A. Lamura and G. Gompper. Numerical study of the flow around a cylinder using multi-particle collision dynamics. *Eur. Phys. J. E*, 9:477–485, 2002.

[59] A. Lamura, G. Gompper, T. Ihle, and D. M. Kroll. Multiparticle collision dynamics: Flow around a circular and a square cylinder. *Europhys. Lett.*, 56:319–325, 2001.

[60] S. H. Lee and R. Kapral. Mesoscopic description of solvent effects on polymer dynamics. *J. Chem. Phys.*, 124:214901, 2006.

[61] J. E. Lennard Jones. *Physica*, 4:941, 1937.

[62] Erminia Leonardi, Bruno D'Aguanno, and Celestino Angeli. Influence of the interaction potential and of the temperature on the thermodiffusion (soret) coefficient in a model system. *J. Chem. Phys.*, 128:054507, 2008.

[63] M. P. Lettinga, J. K. G. Dhont, Z. Zhang, S. Messlinger, and G. Gompper. Hydrodynamic interactions in rod suspensions with orientational ordering. *Soft Matter*, 6:4556–4562, 2010.

[64] Vladimir Lobaskin and Burkhard Dnweg. A new model for simulating colloidal dynamics. *New Journal of Physics*, 6(1):54, 2004.

[65] C. Ludwig. ˙ *Sitzungsber. Preuss. Akad. Wiss., Phys. Math. Kl.*, 20:539, 1856.

[66] Jutta Luettmer-Strathmann. Two-chamber lattice model for thermodiffusion in polymer solutions. *J. Chem. Phys.*, 119:2892–2902, 2003.

[67] David MacGowan and Denis J. Evans. Heat and matter transport in binary liquid mixtures. *Phys. Rev. A*, 34(3):2133–2142, Sep 1986.

[68] A. Malevanets and R. Kapral. Mesoscopic model for solvent dynamics. *J. Chem. Phys.*, 110:8605–8613, 1999.

[69] A. Malevanets and R. Kapral. Solute molecular dynamics in a mesoscopic solvent. *J. Chem. Phys.*, 112:7260–7269, 2000.

[70] Paul Melby, Alexis Prevost, David A. Egolf, and Jeffrey S. Urbach. Depletion force in a bidisperse granular layer. *Phys. Rev. E*, 76(5):051307, Nov 2007.

[71] Julien Morthomas and Alois Würger. Thermophoresis at a charged surface: the role of hydrodynamic slip. *Journal of Physics: Condensed Matter*, 21(3):035103, 2009.

[72] Florian Müller-Plathe. A simple nonequilibrium molecular dynamics method for calculating the thermal conductivity. *J. Chem. Phys.*, 106:6082–6085, 1997.

[73] K. Mussawisade, M. Ripoll, R. G. Winkler, and G. Gompper. Polymer dynamics in a mesoscopic solvent. *J. Chem. Phys.*, 123:144905, 2005.

[74] C. L. M. H. Navier. *Memoires de l' Academie des Sciences de la France*, 7:375, 1827.

[75] Carlos Nieto-Draghi, Josep Bonet Avalos, and Bernard Rousseau. The role of molecular interactions in the change of sign of the soret coefficient. *Europhys. Lett.*, 67:976–982, 2004.

[76] Carlos Nieto-Draghi, Josep Bonet Avalos, and Bernard Rousseau. Computing the soret coefficient in aqueous mixtures using boundary driven nonequilibrium molecular dynamics. *J. Chem. Phys.*, 122:114503, 2005.

[77] Hui Ning, Johan Buitenhuis, Jan K. G. Dhont, and Simone Wiegand. Thermal diffusion behavior of hard-sphere suspensions. *J. Chem. Phys.*, 125:204911, 2006.

[78] Hui Ning, Rio Kita, Hartmut Kriegs, Jutta Luettmer-Strathmann, and Simone Wiegand. Thermal diffusion behavior of nonionic surfactants in water. *J. Phys. Chem. B*, 110:10746–10756, 2006.

[79] María J. Nuevo, Juan J. Morales, and David M. Heyes. Self-diffusion coefficients and shear viscosity of model nanocolloidal dispersions by molecular dynamics simulation. *Phys. Rev. E*, 58(5):5845–5854, Nov 1998.

[80] Lars Onsager. Reciprocal relations in irreversible processes. i. *Phys. Rev.*, 37(4):405–426, Feb 1931.

[81] Lars Onsager. Reciprocal relations in irreversible processes. ii. *Phys. Rev.*, 38(12):2265–2279, Dec 1931.

[82] J. T. Padding and A. A. Louis. Hydrodynamic interactions and brownian forces in colloidal suspensions: Coarse-graining over time and lengthscales. *Phys. Rev. E*, 93:031402, 2006.

[83] J T Padding, A Wysocki, H Lwen, and A A Louis. Stick boundary conditions and rotational velocity auto-correlation functions for colloidal particles in a coarse-grained representation of the solvent. *Journal of Physics: Condensed Matter*, 17(45):S3393, 2005.

[84] R. Piazza and A. Parola. Thermophoresis in colloidal suspensions. *J. Phys.: Condens. Matter*, 20:153102, 2008.

[85] Roberto Piazza. 'Thermal forces': colloids in temperature gradients. *J. Phys.: Condens. Matter*, 16:S4195–S4211, 2004.

[86] Roberto Piazza and Andrea Guarino. Soret effect in interacting micellar solutions. *Phys. Rev. Lett.*, 88:208302, 2002.

[87] Pavel Polyakov, , Florian Müller-Plathe, and Simone Wiegand. Reverse nonequilibrium molecular dynamics calculation of the soret coefficient in liquid heptane/benzene mixtures. *J. Phys. Chem. B*, 112:14999–15004, 2008.

[88] Pavel Polyakov, Meimei Zhang, Florian Müller-Plathe, and Simone Wiegand. Thermal diffusion measurements and simulations of binary mixtures of spherical molecules. *The Journal of Chemical Physics*, 127(1):014502, 2007.

[89] C. M. Pooley and J. M. Yeomans. Kinetic theory derivation of the transport coefficients of stochastic rotation dynamics. *J.Phys. Chem.B*, 109:6505–6513, 2005.

[90] I. Prigogine, L. De Brouckere, and R. Amand. Recherches sur la thermodiffusion en phase liquide : (premire communication). *Physica*, 16(7-8):577 – 598, 1950.

[91] Shawn A. Putnam, David G. Cahill, and Gerard C. L. Wong. Temperature dependence of thermodiffusion in aqueous suspensions of charged nanoparticles. *Langmuir*, 23(18):9221–9228, 2007.

[92] S. K. Ratanathanawongs and D. Lee. Field-flow fractionation of proteins, polysaccharides, synthetic polymers, and supramolecular assemblies. *J. Separ. Sci.*, 29:1720–1732, 2006.

[93] J. Rauch, M. Hartung, A. F. Privalov, and W. Köhler. Correlation between thermal diffusion and solvent self-diffusion in semidilute and concentrated polymer solutions. *J. Chem. Phys.*, 126:214901, 2007.

[94] J. Rauch and W. Köhler. Diffusion and thermal diffusion of semidilute to concentrated solutions of polystyrene in toluene in the vicinity of the glass transition. *Phys. Rev. Lett.*, 88:185901, 2002.

[95] J. Rauch and W. Köhler. On the molar mass dependence of the thermal diffusion coefficient of polymer solutions. *Macromolecules*, 38:3571–3573, 2005.

[96] Dirk Reith and Florian Müller-Plathe. On the nature of thermal diffusion in binary lennard-jones liquids. *J. Chem. Phys.*, 112:2436–2443, 2000.

[97] M. Ripoll, P. Español, and M. H. Ernst. Dissipative particle dynamics with energy conservation: Heat conduction. *Int. J. of Mod. Phys. C*, 9:1329, 1998.

[98] M. Ripoll, P. Holmqvist, R. G. Winkler, G. Gompper, J. K. G. Dhont, and M. P. Lettinga. Attractive colloidal rods in shear flow. *Phys. Rev. Lett.*, 101(16):168302, Oct 2008.

[99] M. Ripoll, K. Mussawisade, R. G. Winkler, and G. Gompper. Low-reynolds-number hydrodynamics of complex fluids by multi-particle collision dynamics. *Europhys. Lett.*, 68:106–112, 2004.

[100] M. Ripoll, K. Mussawisade, R. G. Winkler, and G. Gompper. Dynamic regimes of fluids simulated by multiparticle-collision dynamics. *Phys. Rev. E*, 72:016701, 2005.

[101] M. Ripoll, R. G. Winkler, and G. Gompper. Star polymers in shear flow. *Phys. Rev. Lett.*, 96:188302, 2006.

[102] M. Ripoll, R. G. Winkler, and G. Gompper. Hydrodynamic screening of star polymers in shear flow. *Eur. Phys. J. E*, 23:249–354, 2007.

[103] M. Ripoll, R. G. Winkler, K. Mussawisade, and G. Gompper. Mesoscale hydrodynamics simulations of attractive rod-like colloids in shear flow. *J. Phys.: Condens. Matter*, 20:404209, 2008.

[104] M. E. Schimpf and J. C. Giddings. Characterization of thermal diffusion in polymer solutions by thermal field-flow fractionation: Dependence on polymer and solvent parameters. *J. Polym. Sci. B: Polym. Phys.*, 27:1317, 1989.

[105] J. Schnakenberg. *Thermodynamik und Statistische Physik*. Carl Grossmann, 2000.

[106] P. M. Shiundu and J.C. Giddings. Influence of bulk and surface composition on the retention of colloidal particles in thermal field-flow fractionation. *J. Chromatogr. A*, 715:117–126, 1995.

[107] P. M. Shiundu, P. S. Williams, and J.C. Giddings. Magnitude and direction of thermal diffusion of colloidal particles measured by thermal filed-flow fractionation. *J. Colloid and Interface Science*, 266:366–376, 2003.

[108] C. Soret. *Arch. Sci. Phys. Nat.*, 3:48, 1879.

[109] C. Soret. *C. R. Acad. Sci.*, 91:289, 1880.

[110] C. Soret. *Ann. Chim. Phys.*, 22:293, 1881.

[111] E. Tüzel, T. Ihle, and D. M. Kroll. Dynamic correlations in stochastic rotation dynamics. *Phys. Rev. E*, 74:056702, 2006.

[112] E. Tüzel, M Strauss, T. Ihle, and D. M. Kroll. Transport coefficients for stochastic rotation dynamics in three dimensions. *Phys. Rev. E*, 68:036701, 2003.

[113] Daniele Vigolo, Giovanni Brambilla, and Roberto Piazza. Thermophoresis of microemulsion droplets: Size dependence of the soret effect. *Phys. Rev. E*, 75(4):040401, Apr 2007.

[114] Mihail Vladkov and Jean-Louis Barrat. Modeling transient absorption and thermal conductivity in a simple nanofluid. *Nano Lett.*, 6:1224–1228, 2006.

[115] G. A. Vliegenthart, J. F. M. Lodge, and H. N. W. Lekkerkerker. Strong weak and metastable liquids structural and dynamical aspects of the liquid state. *Physica A: Statistical Mechanics and its Applications*, 263(1-4):378 – 388, 1999. Proceedings of the 20th IUPAP International Conference on Statistical Physics.

[116] John D. Weeks, David Chandler, and Hans C. Andersen. Role of repulsive forces in determining the equilibrium structure of simple liquids. *The Journal of Chemical Physics*, 54(12):5237–5247, 1971.

[117] Jonathan K Whitmer and Erik Luijten. Fluid-solid boundary conditions for multiparticle collision dynamics. *Journal of Physics: Condensed Matter*, 22(10):104106, 2010.

[118] Simone Wiegand. Thermal diffusion in liquid mixtures and polymer solutions. *J. Phys.: Condens. Matter*, 16:R357–R379, 2004.

[119] E. Wilhelm. Thermomechanische eigenschaften eines systems harter kugeln mit temperaturabhängigem, effektiven durchmesser. *Monatshefte für Chemie*, 105:291–301, 1974.

[120] R. G. Winkler and C. C. Huang. Stress tensors of multiparticle collision dynamics fluids. *J. Chem. Phys.*, 130:074907, 2009.

[121] R. G. Winkler, K. Mussawisade, M. Ripoll, and G. Gompper. Rodlike colloids and polymers in shear flow: A multi-particle collision dynamics study. *J. Phys.: Condens. Matter*, 16:S3941–S3954, 2004.

[122] R. G. Winkler, M. Ripoll, K. Mussawisade, and G. Gompper. Simulation of complex fluids by multi-particle-collision dynamics. *Comput. Phys. Commun.*, 169:326–330, 2005.

[123] J. K. Platten; M. M. Bou-Ali; P. Costeseque; J. F. Dutrieux; W. Köhler; C. Leppla; S. Wiegand; G. Wittko. Benchmark values for the soret, thermal diffusion and diffusion coefficients of three binary organic liquid mixtures. *Philosophical Magazine*, 83(17-18):1965–1971, 2003.

[124] Alois Würger. Transport in charged colloids driven by thermoelectricity. *Phys. Rev. Lett.*, 101(10):108302, Sep 2008.

[125] Alois Würger. Thermal non-equilibrium transport in colloids. *Reports on Progress in Physics*, 73(12):126601, 2010.

[126] Mingcheng Yang and Marisol Ripoll. Particle drift velocity and driving forces in inhomogeneous systems. 2011. (preprint).

[127] Yingzi Yang, Jens Elgeti, and Gerhard Gompper. Cooperation of sperm in two dimensions: Synchronization, attraction, and aggregation through hydrodynamic interactions. *Phys. Rev. E*, 78(6):061903, Dec 2008.

[128] z. Water and its structure, http://www.chem1.com/acad/sci/aboutwater.html.

[129] Meimei Zhang. *Thermal Diffusion in Liquid Mixtures and Polymer Solutions by Molecular Dynamics Simulations.* PhD thesis, Fachbereich Chemie der Technischen Universität Darmstadt, 2006.

[130] Meimei Zhang and Florian Müller-Plathe. Reverse nonequilibrium molecular-dynamics calculation of the soret coefficient in liquid benzene/cyclohexane mixtures. *J. Chem. Phys.*, 123:124502, 2005.

[131] Meimei Zhang and Florian Müller-Plathe. The soret coefficient in dilute solutions: Influence of chain length, chain stiffness and solvent quality. *J. Chem. Phys.*, 125:124903, 2006.

Acknowledgements

First I would like to thank Dr. Marisol Ripoll and Prof. Dr. Gompper for giving me the opportunity of doing this work. It has been, and continuously is, very interesting to work in this field of research and it has created a lot of interest for further studies. The atmosphere in this group with lots of opportunities to actively get to know the world of Biophysics and Softmatter in conferences and many other occasions has been very helpful for my research.

Especially, I would like to thank Dr. Marisol Ripoll for being the supervisor of this work. I am very grateful for taking the time for lots of valuable discussions and for the careful proofreading of my thesis. I greatly appreciate all the support within the last three years.

I highly appreciate the help Prof. Dr. Gerhard Gompper for giving me important advice and discussions for completing this work.

Special thanks are dedicated to Prof. Dr. Joachim Krug, who is the second referee of this thesis.

I would like to thank my colleague Dr. Mingchen Yang for lots of interesting and very helpful discussions and for good times in the office and in conferences in Toulouse and Granada.

I would like to thank Dr. Thorsten Auth for the opportunity of giving a talk in the Biosoft lectures of the International Helmholtz Research School. And I would like to thank all my colleagues at the ICS (former IFF-2) for all the small (or not so small), but important advices and discussions that make your work much easier. Fruitful discussions with Dr. Ingo Götze have been very helpful for a general understanding of the method and special thanks also go to Dr. Jens Elgeti and Dr. Sebastian Messlinger for their help at the beginning of my studies, which I had a lot of benefit from.

I also would like to thank Dr. Simone Wiegand, Prof. Dr. Jan Dhont and Bastian Arlt for personal discussions, and for fruitful discussions with the *young investigators group* of Dr. Marisol Ripoll.

I would like to thank Josef Heinen, Dorothea Henkel and Elmar Westphal

for the computational support in ICS. It was a pleasure to have computational resources that one can rely on.

Moreover, a great thank you goes to Helga Paffen for supporting me with everything that takes a lot of time, not knowing how to do it.

And I would like to thank Dr. Julia Fornleitner for valuable and interesting discussions, not only regarding this work, and for being the person that you are.

Last but not least I would like to thank my family for supporting me throughout my whole life on my way to become a scientist. And I would like to thank my friends from the Cologne area and my friends who I got to know in Aachen for the long time knowing each other before and during my studies, and for everything that made the time out of research much more worthwhile, and everything that helped me completing this work.

Kurzzusammenfassung

Ein Temperaturgradient in einem fluiden System erzeugt nicht nur einen Wärme- sondern auch einen Massenstrom. Dieser induzierte Massentransport ist bekannt als Thermodiffusion bzw. Soret-Effekt. Der Effekt wurde vor etwas mehr als 150 Jahren in Natriumsulfatlösungen entdeckt. Dabei wurde bei ungleichmässiger Erwärmung eine Erhöhung der Salzkonzentration auf der kalten Seite beobachtet und es wurde erkannt, dass dieser Vorgang durch Diffusion verursacht wird. Dieser Nicht-Gleichgewichtseffekt wird durch den Soret-Koeffizienten beschrieben, welcher phänomenologisch definiert ist als das Verhältnis der durch Temperaturgradienten und Konzentrationsgradienten verursachten Massenströme. Unterschiedliche Substanzen können zur kalten oder warmen Seite driften und Gemische können höhere Konzentrationen auf einer der beiden Seiten aufweisen. Eine allgemeine theoretische Beschreibung mit quantitativen Vorhersagen des Soret-Koeffizienten in flüssigen Systemen oder komplexen Fluiden war bisher noch nicht möglich und wird derzeit stark diskutiert. Industrielle Anwendungen der Thermodiffusion reichen von Rohölraffinierung bis hin zu Mikrofluidanwendungen wie DNA-Sequenzierung.

In dieser Arbeit untersuchen wir Thermodiffusion in Kolloidlösungen, auch als Thermophorese bekannt. Kolloide umfassen eine große Klasse von Partikeln oder Makromolekülen, welche klein genug sind, um im Lösungsmittel zu diffundieren und andererseits groß genug sind, um die Trägerflüssigkeit als kontinuierliches Medium zu erfahren. Beispiele für Kolloide sind sphärische Partikel, Polymere, Proteine oder Vesikel, wie sie in einer Vielzahl biologischer und technischer Anwendungen vorkommen. Das Verhalten von Kolloidlösungen in einem Temperaturgradienten ist eine besondere Herausforderung auf Grund des reichen Spektrums an möglichen Wechselwirkungen zwischen Kolloidteilchen bzw. Kolloiden und dem Lösungsmittel, welche einen großen Einfluss auf die thermophoretischen Eigenschaften haben.

Unsere Forschungsarbeit basiert auf einer mesoskopischen, state-of-the-art Simulationsmethode, bekannt als Multi-Particle Collision dynamics (MPC). Bei

dieser Methode sind die Masse, der Impuls und die Energie lokal erhalten. Zudem beinhaltet die Methode thermische Fluktuationen. Daher werden hydrodynamische Wechselwirkungen, Temperaturinhomogenitäten und Diffusion korrekt beschrieben.

Wir haben zunächst die Eigenschaften des MPC-Fluids unter Einbeziehung von Temperaturgradienten untersucht. Dabei wurden sowohl periodische Randbedinungen, als auch Systeme mit harten Wände untersucht. Liegen die Simulationsparameter in einem zur Beschreibung von Flüssigkeiten geeignetem Bereich, stellt sich zwischen den an den Systemgrenzen vorgegebenen Temperaturen ein lineares Temperaturprofil ein. Die dabei gemessene Wärmeleitung stimmt mit analytischen Ausdrücken überein.

Das thermophoretische Verhalten von Kolloidlösungen hat zwei hauptsächliche Beiträge: dies sind kollektive Einflüsse und Beiträge die von den Eigenschaften der einzelnen Kolloide abhängen. Die kollektiven Einflüsse haben wir in konzentrierten Lösungen im Hinblick auf unterschiedliche Wechselwirkungen zwischen den Kolloiden untersucht. Die Konzentrationsabhängigkeit des Soret-Koeffizienten in unseren Simulationen stimmt qualitativ mit experimentellen Ergebissen überein. Mit zunehmender Konzentration der Lösung sind die Kolloide effektiv höher auf der warmen Seite des Systems konzentriert. Zudem zeigt sich, dass sich die Kolloide mit zunehmender attraktiver Wechselwirkung zwischen den Kolloiden effektiver auf der kalten Seite akkumulieren. Dies gilt sowohl für stärkere, als auch für langreichweitigere attraktive Wechselwirkungen.

Effekte, die durch die Eigenschaften der einzelnen Kolloide beeinflusst werden, haben wir in verdünnten Lösungen untersucht. Dabei haben wir die Wechselwirkungen zwischen Kolloiden und Lösungsmittel variiert. Bei repulsiven Wechselwirkungen diffundieren die Kolloide zur warmen Seite, wobei dieser Effekt mit zunehmender Temperatur der Lösung schwächer wird. Bei attraktiven Wechselwirkungen diffundieren die Kolloide bei niedriger Lösungstemperatur zur kalten Seite. Überschreitet die Temperatur einen gewissen Wert, ändert sich die Diffusionsrichtung und die Kolloide bewegen sich zur warmen Seite. Unsere Simulationsbefunde stimmen qualitativ mit denen durch eine theoretische Beschreibung gewonnenen Ergebnisse überein. Vergleiche mit Experimenten zeigen z.T. tendenzielle Übereinstimmungen, jedoch sind die Ursachen für die auftretenden Abweichungen zwischen Simulationen und Experimenten noch zu klären.

Erklärung

Ich versichere, da ich die von mir vorgelegte Dissertation selbständig angefertigt, die benutzten Quellen und Hilfsmittel vollständig angegeben und die Stellen der Arbeit - einschlielich Tabellen, Karten und Abbildungen -, die anderen Werken im Wortlaut oder dem Sinn nach entnommen sind, in jedem Einzelfall als Entlehnung kenntlich gemacht habe; da diese Dissertation noch keiner anderen Fakultät oder Universität zur Prüfung vorgelegen hat; da sie - abgesehen von unten angegebenen Teilpublikationen - noch nicht veröffentlicht worden ist sowie, da ich eine solche Veröffentlichung vor Abschluß des Promotionsverfahrens nicht vornehmen werde. Die Bestimmungen dieser Promotionsordnung sind mir bekannt. Die von mir vorgelegte Dissertation ist von Prof. Dr. G. Gompper betreut worden.